POLITECNICO DI TORINO

Faculty of Engineering

Master of Science in Aerospace Engineering

Master Thesis

Inflatable Structures for space applications

Advisors
Prof. Erasmo Carrera
Prof. Alfonso Pagani

Candidate:
Leonardo Urbinati

2020

Contents

List of Figures

Chapter 1

Introduction

Inflatable structures are flexible structures in which membranes are widely used. A membrane implies high thinness and a capability of creating complex shaped volumes after the deployment.
The interest in inflatable space structures rose in 50s and in the decades to follow significant technology developments focused on the demonstration of their potential. They represent a new possibility and a better alternative to classic rigid space structures thanks to their low costs and low masses. Indeed they are lightweight and can be packaged into small volumes: smaller launch veichles can be used so as to reduce mission costs. Flexible composite structures tend to be more damage tolerant and lower in manufacturing costs than rigid ones [11] [16] [92].

1.1 Historical review of principal missions and design concepts

The first example of inflatable structure space mission is the Echo-1 communication balloon satellite, launched by NASA in 1960. It was a 150 pounds, 30 meters diameter passive satellite that reflected radio and radar waves back to Earth (reflector). A blower was connected to the Echo-1 through a hose in order to inflate the balloon directly in space. It didn't have a rigid skin and its surface was made of mylar plastic covered smoothly with vapor-deposited aluminum. A make-up gas system was present in the satellite to keep the balloon inflated even after meteorite punctures. Inflation rate has to be slow to ensure the integrity of the surface [28] [1].

In the following years, after the Echo Balloon, other inflatable devices, such as Goodyear Antennas in the 60s and Contraves antennas and sunshades in the 70s, were flown into space despite the still immaturity of this technology: at that time, launch vehicle dimensions were too small and inflatables were the only possible option to carry out certain types of missions. When larger launch vehicles were built,

the interest in inflatable structures was put aside in favour of the improvement of classical mechanically deployed structures. The interest in inflatables rose again in the nineties in conjunction with the need to reduce costs and weights [92] [14].

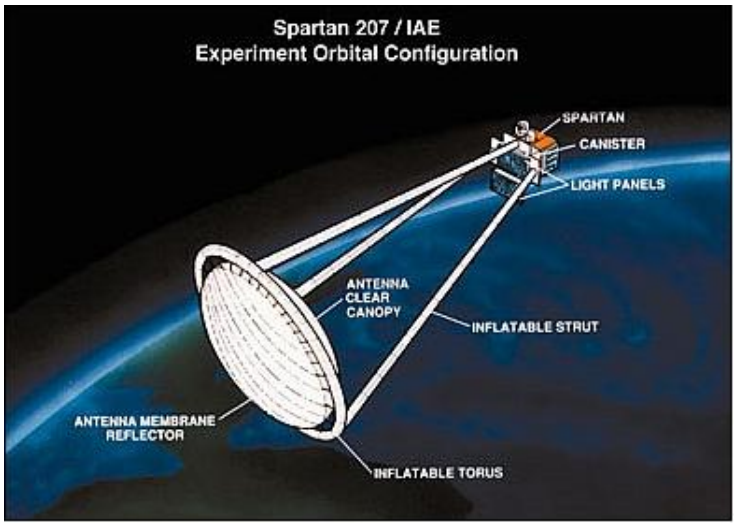

Figure 1.1. L'Garde IAE configuration during flight

In the nineties lots of representative projects were made by L'Garde Inc, a company with a long history in inflatable structure matters. L'Garde Inc designed and realized an inflatable deployable antenna that was then selected in 1996 by NASA for a flight experiment: the IAE (Inflatable Antenna Experiment) was the most significant demonstration of this type of technology of the 20th century (figure 1.1). The IAE objectives were: to validate the deployment of a 14 meter-diameter inflatable reflector antenna, to verify the effectiveness low costs and light weights of large inflatable structures, to demonstrate that high surface precision and high packing efficiency were possible. The experiment succeed in that [17] [91].

Inflatable structure applications are very wide: in addiction to balloons and antennas previously described, inflatable were also thought to be used for solar arrays, sunshields, reflectors and re-entry and landing systems.

One of the most important recent applications includes the Inflatable Re-entry and Descent Technology (IRDT). Compared to classical heat shield and parachute systems it represents an innovative lightweight and lowcost technology. Another advantage is the wide application versatility: small capsules, ISS download system for Automated Transfer Vehicle (ATV) and planetary missions. The IRDT unifies the classical elements of a re-entry vehicle into a single system, indeed it consisted of a reentry thermal protection, a parachute system and a landing system. The first demonstration mission was launched in 2000 in order to demonstrate the feasibility

of the technology. A second demonstration mission was performed in 2002 to verify the improvements effectiveness after the first mission [66] [67].

All the structures described above belong to the unmanned class: human presence is not considered in them. In the last two decades the increasing interest in human exploration of Mars and Moon led to the study of manned inflatable structures. A launch vehicle can't stow a classical rigid space habitat in its payload bay, so the only way to design an extraterrestrial base is using inflatables.
Manned structures are more challenging than unmanned ones. In addiction to thermal insulation and micrometeorites protection (that are equally important in unmanned inflatables), they need radiation protection, hermetic sealing and mechanical resistance [52].

The ISS TransHab, developed by NASA in 1997, is the largest manned inflatable structure program of the last decades. It was thougth as a four levels inflatable module for the ISS and had an hybrid structure: an hard central core with an inflatable exterior shell. A pressurized tunnel was placed in the fourth level of the structure, in corrispondence to the space station attachment (figure 1.2).

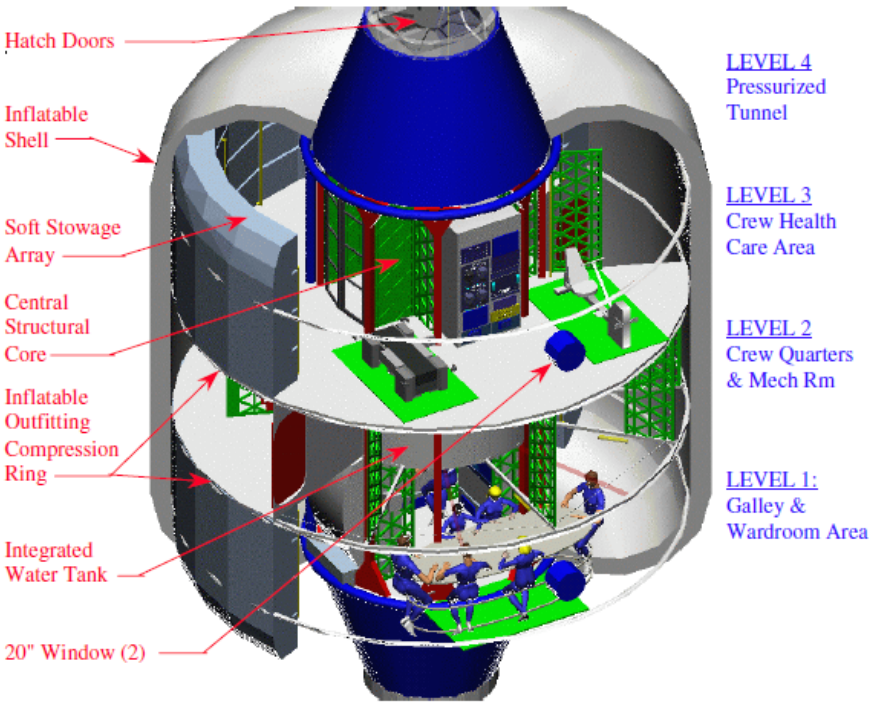

Figure 1.2. TransHab Internal View

The inflation system was incorporated in the first level of the structure in corrispondence to an unpressurized tunnel. The inflatable shell was composed of four

layers: the inner scuff barrier and pressure bladder, the structural restraint layer, the MMOD shield and the outer thermal protection blanket.
Altough NASA never canceled the project in 2000, this program led to breakthrough in the state of the art of manned inflatable structures, in particular with regard to the multi-layered shell [48] [60].

In 2006 Bigelow Aerospace took over the fundamentals of the Transhab program and launched the first ever inflatable space habitat, the Genesis I inflatable module. The main objective was to test and validate inflation and deployment technologies. The mission was a complete success. Following the success of the previous mission, Bigelow launched the Genesis II mission in 2007 and then began collaborating with NASA on the Bigelow Expandable Activity Module (BEAM) project in 2012 (figure 1.3). The BEAM, launched and installed on the ISS in 2016, is the first ever human occupied space inflatable module.

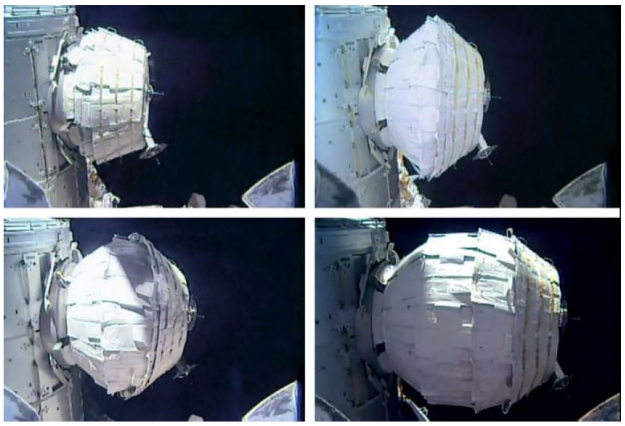

Figure 1.3. BEAM module progressive inflation

The demonstration proved the feasibility of inflatable habitats and paved the way to possible future applications such as creating outposts to explore Moon and Mars surface. The habitat could be packaged and then inflated once on the ground, eventually in a hole or underground tunnel in order to protect it from radiation. NASA is currently working under the NextSTEP-2 program to develop habitat and airlock systems for future lunar and Mars missions.

Other advanced concepts concerning human exploration of Titan and Venus are in development. The high altitude Venus Operation Concept (HAVOC) involves the use of an airship with an habitable inflatable gondola to explore Venus atmosphere (figure 1.4). A blimptype vehicle is being studied for Titan exploration. It is characterized by an inflatable wheel at the bottom whose purpose is to cushion an eventual landing or act as a floatation device. Other concepts involve the use of

inflatable wheels, used as rover, for surface exploration.

Figure 1.4. Titan aerover with inflatable wheels (left), inflatable rover concept vehicle (right)

Altough most of the proposed inflatable configurations have only reached the conceptual stage, they have shown that inflatables can be adapted to a wide variety of space applications and provide a unique solution to the volume and mass costraints required by space exploration [90] [60].

Chapter 2

Manned Configurations

Classical rigid modules for the ISS or habitats for Lunar and Mars exploration can't be stowed in the launch vehicle due to their large size. In this scenario, inflatable structures come into play to provide larger habitats needed for equipment and to support the life of the crew.
The major challenge for an inflatable habitat is the harsh environment it has to withstand, that is composed of micrometeoroids, extreme thermal gradients, radiations and atomic oxygen. In addiction to dangers already mentioned, the habitat will face additional environmental challenges according to the site of the mission: for example, for a lunar surface mission, the major danger is lunar dust. Conversely, a Mars habitat doesn't need a MMOD shield thanks to its, albeit thin, atmosphere. Furthermore, inflatable habitats have to face extremely high loads due to size and internal pressure [49].

In this section, it will be first described the difficulties related to the space environment and the materials used for space applications, for then move on to the analysis of the various inflatable manned configurations.

2.1 Space environment

Even before designing an inflatable manned space structure (habitats, modules or airlocks), a deep understanding of the space environment is needed.
First of all, the vacuum environment makes many materials unstable, so an accurate evaluation of materials used is needed. The structure must protect the crew from a very harsh environment ruled by radiations (solar wind, solar cosmic rays and galactic cosmic rays), meteoroid impacts and large variations in temperature (from -213.9 to 111.1 °C). In addition to that, an air pressurization of the manned structure is needed. Altough the optimum habitat pressure is Earth's atmospheric pressure (101.325 kPa), actual studies involve the use of a pressure of 69 kPa: an excessive

pressure differential between the structure and the extravehicular activity (EVA) suits is dangerous for human body.
For lunar missions, another danger is represented by lunar dust since it sticks to all surfaces and is highly abrasive. Furthermore, inflatable structures are also subject to pressure losses due to gas diffusion or puncture: an abrasion resistant and a pressure containment structure is needed [79].

2.1.1 Environmental shielding and materials used

In order to shield the structures from the harsh space environment, it was thought to use a multi-layered flexible structure consisting of the following components: the bladder, the restraint, the thermal cover and the micrometeoroid cover (figure 2.1). Each layer should be optimized for a particular function.
The main features of space application materials appear to be high strength, ductility, durability, stiffness, puncture resistance, low thermal expansion and low leakage. Moreover, all the materials chosen have to be stable in vacuum environment. The advent of flexible polymers and high strenght fibers such as Kevlar, Vectran and Spectra helped the development of inflatable structures from a densely packed state. Those materials have an high strength to weight ratio, abrasion and thermal exposure resistance.

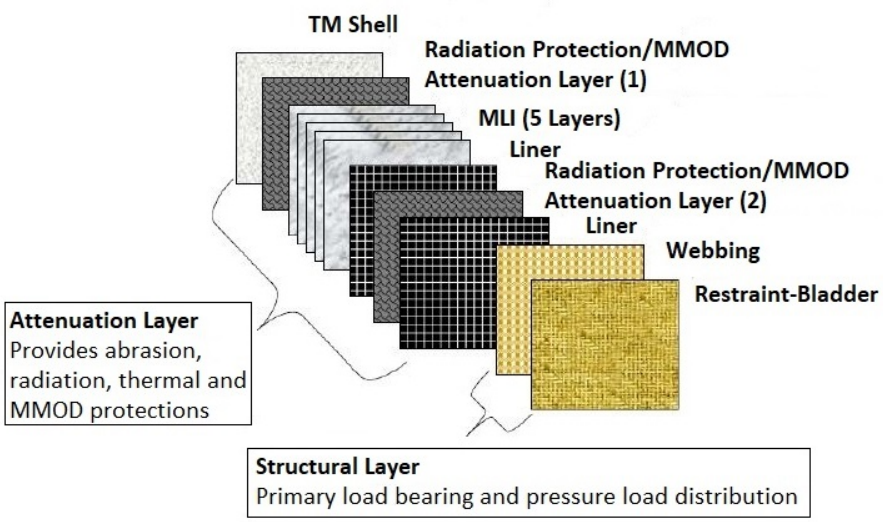

Figure 2.1. Wall layers for an inflatable manned structure

Going back to talking about layers, the restraint one is used to handle internal pressure loads, while the bladder one is used to retain eventual gas leakage.
As concerns the former, a combination of a webbing restraint and a coated fabric is often used. The most used material for both the webbing and the fabric is Vectran.

As for the bladder layer, a coated fabric system is often chosen. There are two ways of gas output: diffusion and effusion. Diffusion regards the leakage through the material, while effusion regards the leakage through punctures. The fabric system gives strenght to the bladder without affecting the diffusion properties of the material chosen. The fabric can be coated on both sides to reduce diffusion, even if that entails an increase in mass. As for the restraint, also for the bladder the most used material is Vectran. A secondary redundant bladder layer could be added to increase safety in the case of puncture.
The thermal cover usually involves a multi-layer insulation (MLI) with five to seven layers and a spacing between them to reduce heat transfer.
The MMOD layer break apart the debris that impact on the structure and subsequently have a foam absorb the vapor.
In addiction to these layers, an outer cover is required to reflect radiation and to resist abrasion due to external cuts. For lunar missions, a layer of compacted lunar regolith can be placed atop the structure as outer cover: it works as a shield against meteorites and radiation. In addiction, the regolith protects the structure from extreme temperature cycles [38] [11] [79].

2.1.2 InFlex program

Since 2005, several materials and laminates for inflatable habitats, modules, space suits and airlocks have been tested and developed under the InFlex program.
The aim is to increase performance of inflatable structures providing intelligence to the system. The main objectives are: to develop a flexible health monitoring system (HMS) that identify penetrations and quantify material degradation over time; to develop self-healing materials that can repair penetrations below 2mm; to develop new flexible low permeation and radiation protective materials.
A central monitoring system (CMS), thanks to the continuous communication with the health monitoring system, will alert the crew about penetrations and degradation of the structure over time. Safety, reliability and probability of mission success will be improved.
A simultaneous optimization of all the layers (bladder, restraint, MMOD layer, ecc) is studied. The most challenging aspect is where to place the new technologies and modifications within the layers: technologies must be positioned in such a way as not to have a loss of funcionality when combining them.
Self-healing materials are used in corrispondence of the bladder layer. Radiation protective materials are spread within all layers. To maintain the HMS and the CMS, a power system has been developed: the flexible photovoltaics are thought to be applied externally, while flexible batteries, needing thermal insulation, are located internally. The HMS has several duties: to determine if a penetration greater than 2mm occurred within the bladder, to locate it in the structure and to notificate the damage to the crew; to determine if a penetration occurred within

the restraint, thermal protection layer or MMOD layer, to quantify and locate the relative damage.

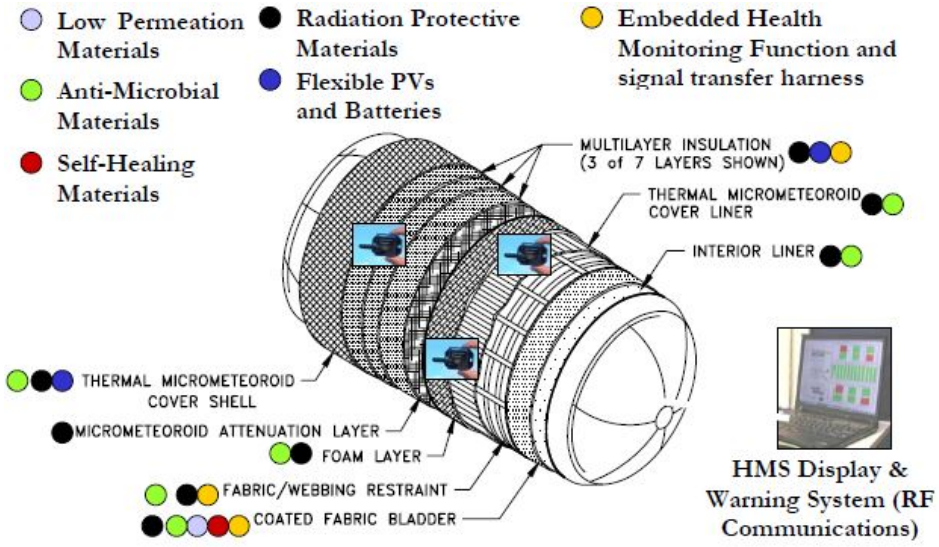

Figure 2.2. Insertion points for InFlex Technologies

Several self-healing materials and passive methods are studied (figure 2.3). All aspects of the life of the materials are considered: manufacturing, ground test, packing, deployment.
The most efficient methods seem to be the ones that add material laterally in order to fill the hole. Viscoelastic gels, filled hollow rods with polyurethane reactants and macroencapsulation can fulfill their task with the least mass.

As concerns low permeation materials studied for the bladder layer, the most performing polymers are shown in figure 2.4.
The figure shows the rate of permeation for several materials: the lower the permeation rate, the lower the diffusion losses. A layer of aluminium can be applied to give zero permeation to the membrane, however it can affects charge transfer and can cause radio frequency blockage.
As regards radiation protective materials, the InFlex program established that the most effective one is polyethylene, thanks to its high hydrogen content. It is a polymer that can be modified in several forms, such as film or textile. The most tenacious form is the Ultra-high molecular weight polyethylene (UHMWPE). Materials such as Spectra and Dyneema are part of the UHWPE. [12]

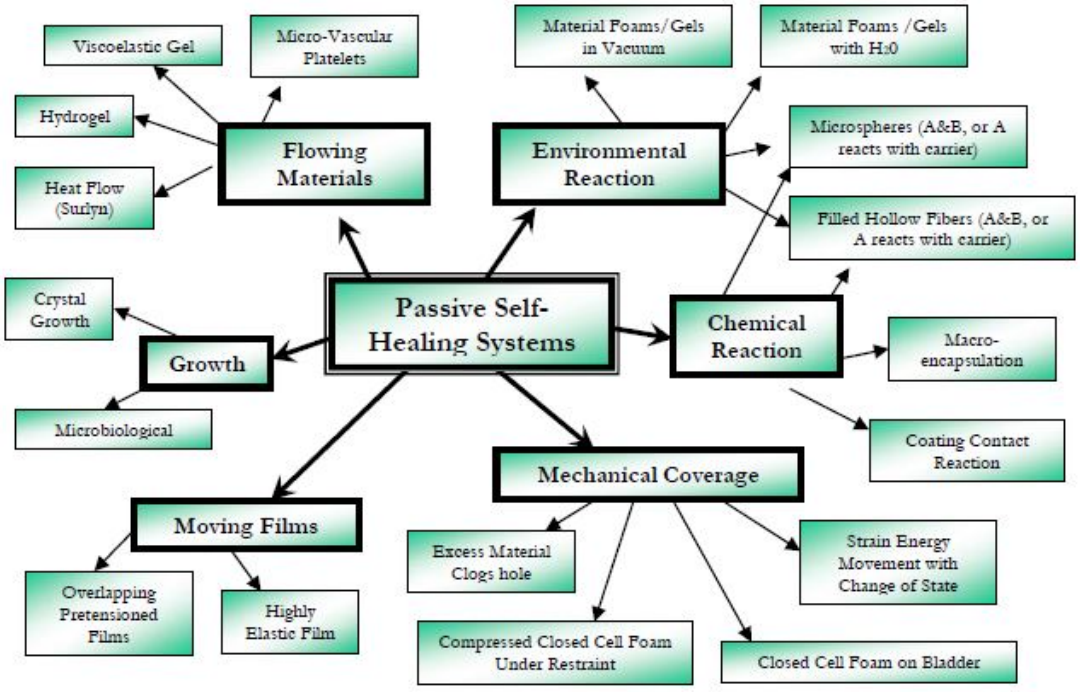

Figure 2.3. Self-healing materials considered in InFlex for space inflatable applications

Material	Oxygen Transmission Rate @25C & 0%RH	Nitrogen Transmission Rate @25C & 0%RH	Water Vapor Transmission @38C 90%RH
Units	cc.25u/m2*24hr*atm	cc.25u/m2*24hr*atm	g/m2/24hr/atm
Polyurethane	800-1500	600-1200	400-600
Polyethylene (HD)	2325-4448	650	7-10
EVOH	3-5	No data	16-18
Polyamide	40	14	84-3100
Aluminum Foil	0	0	0

Figure 2.4. Best polymers for the bladder layer

2.1.3 Protection against space debris

The increasing number of space debris, due to recent intensive use of space, leads to necessity of constructing protective shield for inflatable modules attached to the ISS. Many of those debris have a sufficient velocity and mass to penetrate inflatable modules. The consequences of an impact would be catastrophic for both the module and the ISS: depressurization of the module, cracks, atypical loading conditions and damages to the control system in addition to the death of the crew.
For modules attacched to the ISS, the MMOD shield must withstand the impact

of particles with a speed of 7km/s and a diameter up to 10mm.

The main parameter that indicates the robustness of the protection system is the Ballistic Limiting Dependence (BLD). It represents the capability of the high speed debris (or MMOD) to penetrate the shield. In other words, when the relationship between the velocity and the size (diameter) of the debris is over a certain BLD value, the particle can penetrate the shield (figure 2.5).

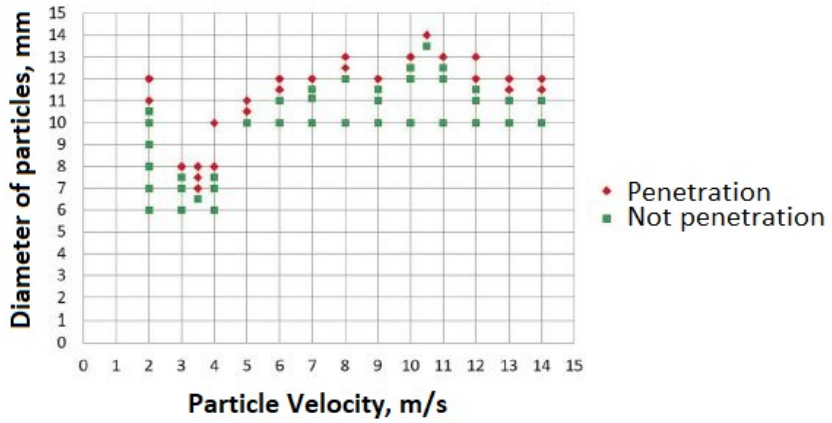

Figure 2.5. BLD for the protection of an inflatable module

Most protective shields are based on the concept of destroying the MMODs or debris reducing them into small, non-dangerous fragments ("whipple shield"). An example of the interaction between the shield and the particle is shown in figure 2.6.

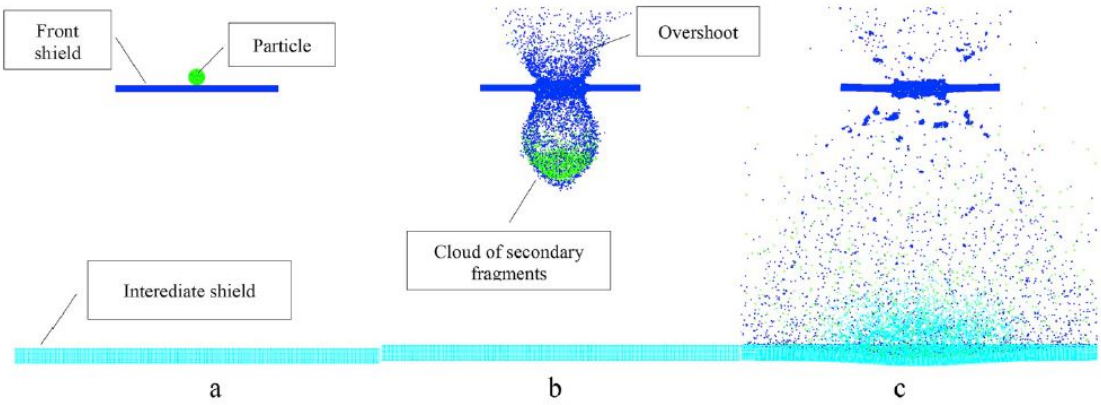

Figure 2.6. Interaction between an high-speed particle and the protective shield

A typical debris protection is made of multiple separated shields in series (multilayer), as shown in figure 2.7. The debris, beating on the shield, breaks into fragments and loses much of its initial kinetic energy. The foam spacing layers are very important: they allow the particles to disperse into a cone or plume fashion until they hit the next surface. The more spacing between the layers, the grater the dispersion.

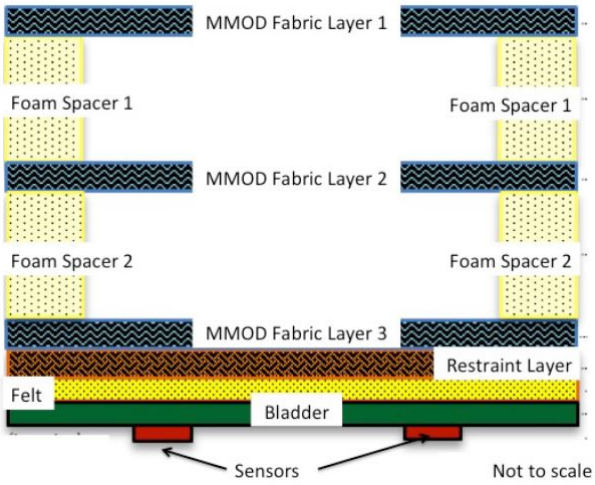

Figure 2.7. 2-D lineup of a protection shield

In the past, shield was made of metal, usually aluminum. However, they were very heavy and expensive. Lightweight and flexible polymer such as Kevlar, Nextel cermic fiber cloth, beta cloth and carbon fibers are now used as shielding materials. The flexibility of those materials allows to fold them in the launcher, together with the inflatable module the has to shield.
A numerical simulation is needed to evaluate the effectiveness of the shield. The numerical simulations obtained through a finite element method consist of two steps. The first step consists on the simulation of the impact on the multilayered shield. This analysis allows to calculate the loading generated by the debris fragments on the inflatable module. The second step, consists on calculating the strains of the inflatable module subjected to the debris fragments loads
. During tests, a Distributed Impact Detection System (DIDS) is placed at the end of the multilayer shield. The DIDS consists of a series of accelerometers connected to a processer that are used to evaluate the the place of impacts [9] [7] [62].

2.1.4 Creep testing

The long-term behaviour of inflatable structures under pressure and thermal loads has to be studied in order to mitigate risk of material degradations.

Polymer fibers used for the restraint layer of an inflatable module/habitat, such as Kevlar of Vectran, are viscoelastic materials. Viscoelastic materials have a non-linear behaviour over time and thus are subject to creep (progressive deformations of the material under constant loads). Furthermore, those materials, unlike metallic materials, don't have fixed properties. The high variability in the ultime tensile strength (UTS) and a non-uniform load distribution in the restraint layer can lead to a reduction in the creep time to failure (TTF). A long-term deformation study is needed to avoid creep.

NASA studied and tested several samples of Kevlar and Vectran webbings in different loading conditions in order to determine which material was less prone to creep. The materials tested were Kevlar rated for 4,000 lbs/inch (4K), 6,000 lbs/inch (6K) and 12,500 lbs/inch (12.5K) and Vectran rated for 6,000 lbs/inch and 12,500 lbs/inch.
Firstly, the UTS variations of the samples have to be studied: the greater the percentage change in the UTS, the shorter the creep life. The Kevlar samples have a lower, but still high, UTS variation in both 12.5K and 6K cases.

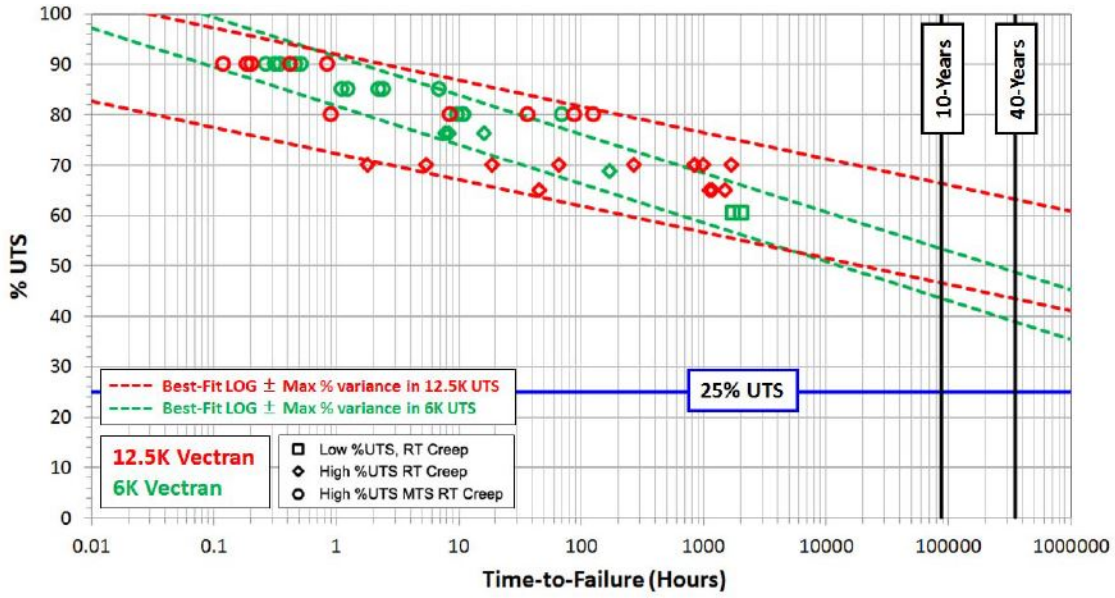

Figure 2.8. % UTS as function of Creep life TTF for 6K and 12.5K Vectran

Subsequently the Kevlar and Vectran samples are loaded with a load corrisponding to a certain percentage of the UTS value: the relationship between displacement and time and between strain and time have to be studied. The current safety factor for space inflatable applications is set to 4, so inflatable structures have to bear at least 25% of the UTS for a long time period. However, during tests, the samples

are always loaded with an higher percentage of the UTS value.
The test results for 6K Vectran and 12.5K Vectran are shown in figure 2.8. The two red and green boundlines are due to UTS variations in the different samples taken into account. This graph demonstrates that both 6K and 12.5K Vectran can bear pressure loads for over 40 years without incurring in creep: the % UTS nedeed to cause a failure before 40 years is well over the 25% determined by the safety factor. NASA tests demonstrated that 6K Vectran webbings can bear higher loads than 6K Kevlar webbings over extended period times. Furthermore 4K Kevlar webbings showed a long (twenty-one months) creep life, while both 12.5K Kevlar and Vectran showed a short creep life (eight month). The greater the constant load applied and the shorter the creep life seems [90] [50] [82].

2.2 Inflatable modules

The first ever revolutionary inflatable space habitat concept, developed in 2000 and conceived as a living module for the ISS, is the Transit Habitation Vehicle, also called TransHab.
It was a cylindrical module consisting of four levels that could accomodate six crew members for a mission duration of approximately 15 years. It ensured a living space larger than $300m^3$ and was pressurized to a pressure of 14,7psia. The first three levels could be used for housing purposes, while the fourth level was a pressurized tunnel consisting of two hatches and was used as transition to the ISS. The inflation system was located in a unpressurized tunnel, in opposite side to the transition tunnel (level 0). The Transhab had an hybrid structure consisting of an aluminum and graphite-composite stiff core sorrounded by an inflatable shell. This hybrid configuration allowed the structure both to be ligthweight and easily packable (lateral inflatable) and to carry higher loads (central core). The central core was composed of eight longerons that guaranteed the absorption of pressure loads and shear loads (launch configuration).

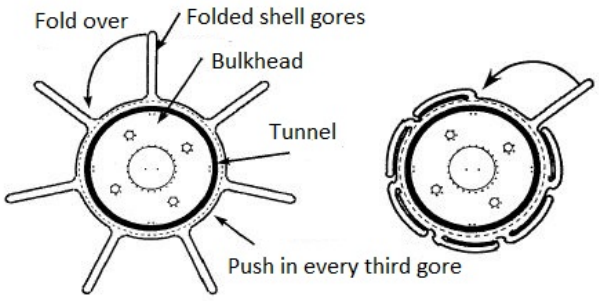

Figure 2.9. TransHab deployment method

A deployment system, shown in figure 2.9, integrated to the external inflatable shell and based on straps, was chosen for the TransHab. In the folded configuration, the gores were pushed towards the central core. Despite the Transhab project was abandoned, it represented a big step towards the inflatable modules state-of-the-art [48] [47].

In 2006, taking up the concept of Transhab, the Genesis 1 inflatable module was launched. It was the first ever space habitat launched into space. It was thought for a mission duration of six months, but it survived the harsh space environment for two years. In 2007 Bigelow Aerospace launched Genesis 2, an improvement of the inflatable habitat launched the previous year. The system reliability was increased through a multi-tank inflation system rather than the single-tank of Genesis 1: this allowed a more efficient and stable inflation process. Additional protective layers were added to the Genesis 2 outer shield in order to provide better thermal and MMOD protection.

In 2016 the Bigelow Expandable Activity Module (BEAM), consisting of two metal bulkheads, an aluminum structure and a multilayered soft facbric, was put into orbit and attacched to the Tranquillity Node of the ISS. It was the first ever inflatable module attacched to the ISS. The success of the mission brought the technology readiness level of inflatable manned modules to TRL-9.
For the duration of the mission the crew has to take measurements and monitors several performances such as radiations, temperature changes, modal tests and MMOD impact detections in order to verify the correspondence with the tests carried out on the ground. For this reason, several sensors are placed in the BEAM: Distributed Impact Detection System (DIDS) for detecting structural impacts, Deployment Dynamic Sensors (DDS) for recording acceleration loads during inflation, Wireless Temperature Sensors (WTS) for monitoring surface temperatures, Radiation Environment Monitor (REM) and Radiation Area Monitor (RAM) for monitoring internal radiations.
The DDS system detected higher temperatures than expected ones during initial inflation: new models for evaluating MLI blankets performances and convective heat transfer have to be developed. Furthermore modal tests found out that the first three modes were higher to those predicted by ground tests: the lateral bending mode was 10% higher, while the torsion mode was 28% higher. Future studies involving the interaction between MMOD layer and restraint layer will have to be done to make a better model.

Although some on orbit test results didn't coincide with the results of ground tests, the BEAM was a complete success: the initial two-years mission has been extended. Further on orbit experiments and data collection will be conducted to improve the reliability of inflatable modules for space applications [89] [44].

2.3 Inflatable space stations

In recent years, after the success of the BEAM module, Bigelow Aerospace has been developing a new space inflatable module called B330 (figure 2.10). Compared to the BEAM, the B330 module has a very large size: it offers $330m^3$ of habitable volume, about a third of the living space of the ISS. The module can accomodate up to six people and its folded configuration can be get to space in a single launch. The module consists of an inflatable cylinder, two large solar arrays and two thermal radiator arrays in order to dissipate heat. The cylinder consists of a classical multilayered structure, similar to that of the NASA Transhab. Furthermore, two docking nodes are placed on opposite sides of the cylinder: a node is designed to be docked to another B330 or the ISS; the other node is designed to be docked to visiting vehicle, such as space capsules (Space X's Dragon, Russian Soyuz, Boeing's CST-100 Starliner or NASA's Orion).

The B330 can be used as a commercial habitat to be anchored to the ISS (X-BASE concept) or as a stand-alone space station. A long-term goal is to use them for deep space missions, such as exploration of Mars and the Moon.

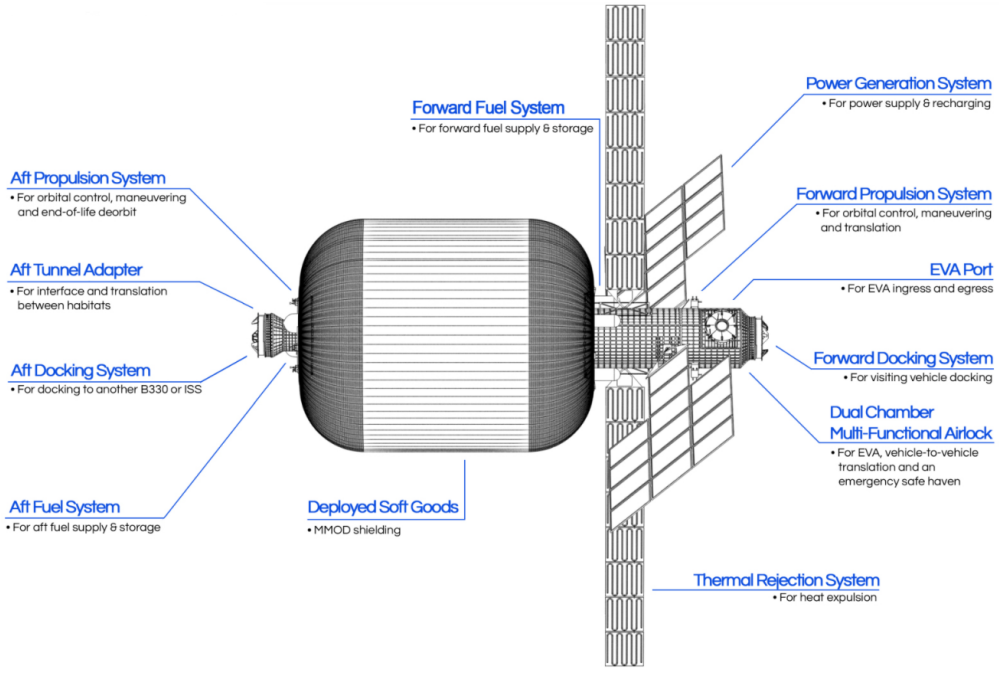

Figure 2.10. B330 module design

In 2021 Bigelow aerospace will launch two B330 capsules that will be ganged together in order to form the Alpha Station (figure 2.11). The modules can work separately and are attached through docking nodes.

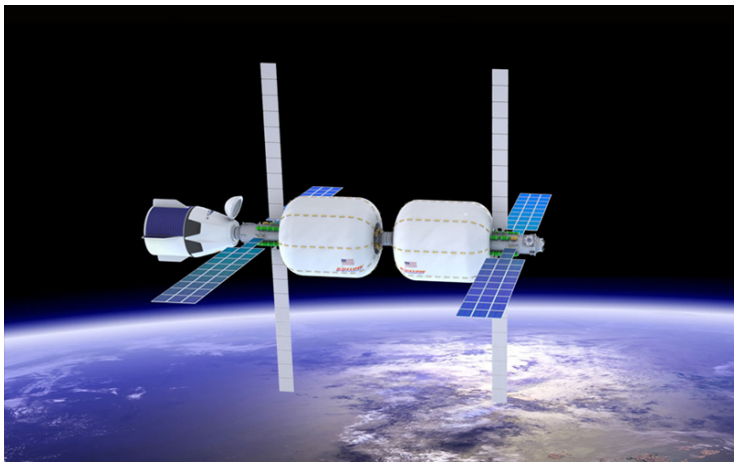

Figure 2.11. Alpha Station Design concept

2.4 Inflatable airlocks

The airlock is a device that allows the passage between two environments at different pressures. Its development is of primary importance for crew Extra Vehicular activities (EVA) such as maintenance and outer human exploration of planets.
It is often composed of a central volume enclosed by two hatches. If both hatches (intravehicular and extravehicular) are closed, the air can be pressurized or depressurized in case respectively of ingress or egress without air losses.
There are two classes of airlocks: single-chamber and dual-chamber. In the former all the EVA subsystems are included in a single volume. The latter is composed of a Crew Lock, through which the crew enters or exits, and an Equipment Lock where the EVA subsystems are located. The Equipment Lock is used as redundancy chamber during EVA in case of Crew Lock fail. For all future applications, a dual-chamber redundant inflatable airlock is requested.
In order to reduce launch costs, weights and stowage volume, several inflatable airlock concepts have begun being developed since early 2000. They are often composed of high strenght fabric flexible materials and, as opposed to their rigid counterpart, can be adapted for a large variety of uses.
However, altough several advantages, an inflatable airlock isn't usable until fully pressurized: in situ hardware mounting and outfitting after deployment is needed. Advanced packing and deployment techniques have to be determined in order not to damage the flexible materials.
As for the inflatable space modules, the major requirements for an airlock are: pressure containment, leak reduction, capability to endure space environment and, in addiction, withstand the depressurization cycles due to EVA. For planets surface missions, additional protective layers for dusts should be included.

2.4.1 Design concepts

Volga is the first inflatable airlock made in history (1965). It was used for the russian Voskhod-2 mission. It was a cylinder made of 36 inflatable air booms that were used to maintain rigidity. A fabric tube was used as restraint layer in order to bear loads. No radiation shielding was used since the mission duration was very short [58].

Another important inflatable airlock concept, which dates back to early 2000, is the Advanced Inflatable Airlock (AIA). In the stowed configuration it was similar to a compressed bellows. Once inflated it assumed a spheroidal shape with a diameter of 7 meters and a legth of 8 meters. In order to maintain the shape after a depressurization cycle (during EVA), the AIA was supported by air beams. Furthermore, pneumatic muscles were added to improve the folding. The three main elements (internal volume, air beams and pneumatic muscles) were pressurized at three different pressure levels through three different inflation subsystems.
An elliptical hatch was chosen for the AIA concept. It had a dual function: it could be used both as interior hatch for launch vehicle and as exterior hatch for deep space. The AIA was made of a classical multayered structure, taken from Transhab concept:

- an ortho fabric layer was chosen for MMOD tear protection
- 5 layers of MLI with scrim were chosen for thermal protection
- a Nextel layer was chosen for MMOD attenuation
- a Vectran layer was chosen as pressure containment (restraint layer)
- woven PFTE was chosen as slip layer in order to reduce friction between the bladder and the restraint layer
- silicon impregnated nylon was chosen as containing air layer (bladder layer)
- a scuff barrier was included as protection against internal damages

The restraint layer was made of a braided tube to bear hoop loads and 48 axial webbings to bear meridional loads.
A comparison between classical rigid airlocks and AIA is shown in figure 2.12. AIA stowed configuration is three times smaller than ISS Crewlock and Shuttle Airlock. Furthermore AIA is two times lighter than Shuttle Airlock. Altough the AIA is developed only as preliminary concept, the advantages of an inflatable airlock are unequivocal [13].

In 2001 NASA developed the Dual-Chamber Inflatable Suitlock (DCIS) thought for both planetary surface applications and deep space applications (figure 2.13).

Characteristics	Inflatable Airlock	Shuttle Airlock	ISS Crewlock
Dimensions:			
Volume:	8' x 7' dia	7' x 5.25' dia	9' x 5' dia
Deployed:	226 ft^3	150 ft^3	177 ft^3
Stowed:	56 ft^3	150 ft^3	177 ft^3
Weight:	1064 lbs (1)	2171 lbs (2)	13368 lbs (3)
Material:	Various fabrics and Aluminum	Aluminum	Aluminum
Number of Crew Supported:	2	2	2

Figure 2.12. Comparison between AIA and classical rigid airlocks

Being originally intended for a lunar surface application, unlike the structures previously exposed, the DCIS had an integrated dust protection system.
A secondary structure made of inflatable tubes and pneumatic beams were used to rigidize the airlock.
The DCIS consisted of two cylindrical membrane volumes separated by three bulkheads. The inner compartment was continuosly pressurized while the outer one remained unpressurized. This allowed faster entry and exit operations since the crew didn't need to wait for the compartment depressurization.
The DCIS has two operational modes: an EVA suitport mode and an EVA airlock mode. In airlock mode the middle bulkhead is removed [39].

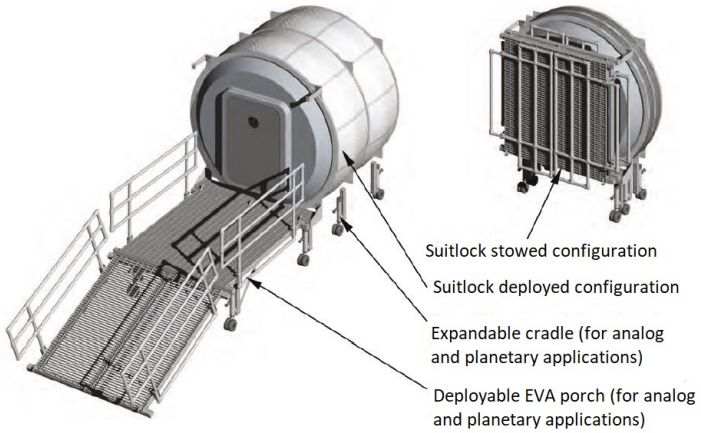

Figure 2.13. DCIS in deployed and stowed configurations

In 2014 a new and revolutionary inflatable airlock design was studied: the Non-Axisymmetric Inflatable Pressure Structure (NAIPS), an inflatable structure with

weakly stressed areas along a principal axis (figure 2.14).

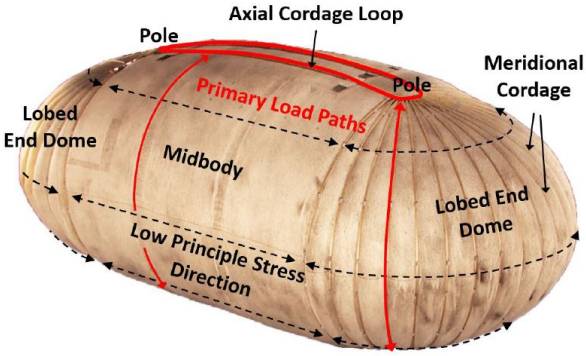

Figure 2.14. NAIPS design with stress directions

Thanks to these areas, it was possible to replace the classical rigid metallic hatch with a flexible seal: the system mass resulted to be greatly reduced, as well as the package efficiency resulted to be improved. Furthermore, the difficulties related to interactions between inflatable and rigid structures could be overcome. The NAIPS was made of a central body with two end lobe-shaped domes. The end domes beared primary loads through meridional cords that run towards two larger axial cordage loops, placed in the central body. Those loops beared axial loads and provided areas of low stress. Several areas of low stress, perpendicular to the primary load paths, were found.

A typical NAIPS configuration is made of an internal urethane coated Nylon bladder and a series of Vectran cordage and fabric acting as structural restraint layer. Vectran is chosen thanks to its high specific strenght. The restraint layer is sized according to the internal pressure loads that are beared by meridional cords in the lobes and are transferred to the central body through the cordage loops. In that way the lobes have to bear only low hoop loads.
Both tests and FEA non-linear analysis, that are then compared, has to be performed in order to size the airlock and verify the feasibility of the concept.

Tests carried out on Vectran meridional cords showed that the breaking strenght was 11.6% higher than expected. Furthermore, it was found that the lenght of the meridional cords doesn't influence the failure loads (figure 2.15) [27] [83].

Nasa, in collaboration with LaRC, developed the Minimalistic Advanced Softgoods Hatch (MASH), based on the NAIPS concept.
Another NAIPS-like concept called LISA (Lightweight Inflatable Structural Airlock) was developed between 2016 and 2018 by Nasa LaARC. LISA bladder was

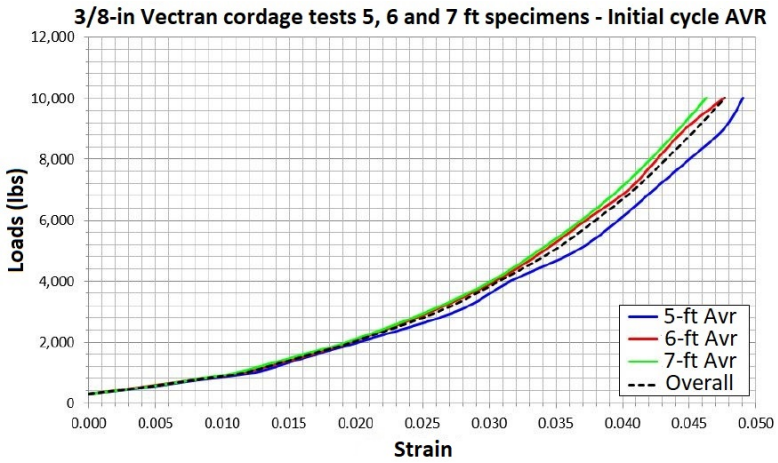

Figure 2.15. Meridional cordage loads as function of displacements for different lengths

composed of a removable urethane coated nylon fabric bladder and of a Kevlar fabric and Vectran cordage restraint layer. Carbon fiber rod should be placed directly by the crew in order to hold the structure after depressurization.

In 2017 NASA JSC began to develop the Lightweight External Inflatable Airlock, also called LEIA (figure 2.16). It was an hybrid microgravity airlock thought for Lunar Gateway mission. It was composed of a central rigid metallic Equipment Lock with two inflatable Crew Locks placed on opposite ports.

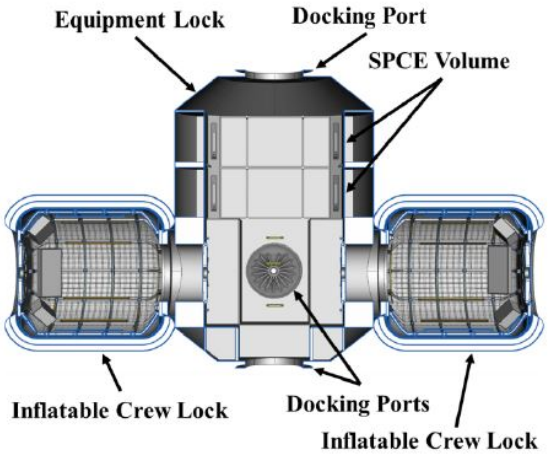

Figure 2.16. Design of LEIA airlock

This configuration provided an efficient redundance in case of failure of one of

the two Crew Locks. The Crew Lock was an inflatable cylinder enclosed between two metallic bulkheads. The restraint layer was made of two Vectran sublayers: a webbing straps layer (capable to bear loads in both hoop and longitudinal directions) and a broadcloth, as shown in figure 2.17).

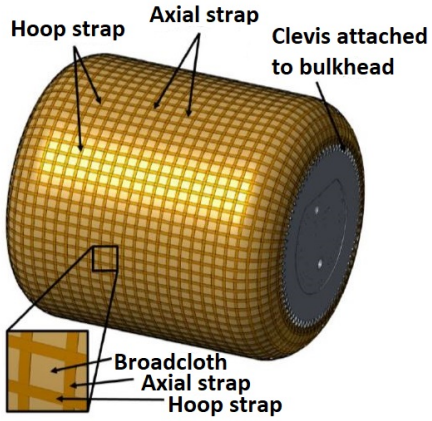

Figure 2.17. Design of LEIA restraint layer

Several secondary internal rigidizing structure concepts (needed during depressurization) were evaluated for the LEIA: a constructible truss, an inner inflatable wall or inflatable beam truss and a deployable mechanism (figure 2.18).
The constructible structure was composed of lightweight composite longerons and hoops connected through nodes. This structure would have been assembled by the crew after Crew Lock inflation.

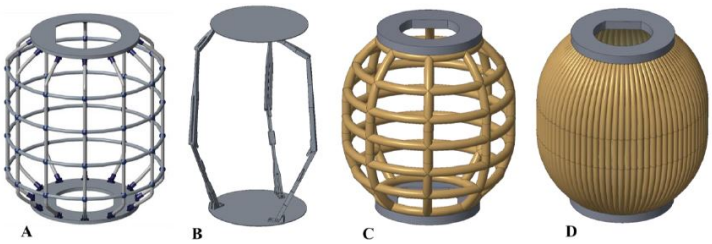

Figure 2.18. Designs of LEIA inner structure: A) Constructible truss, B) Deployable mechanism, C) Inflatable neam truss, D) Inner inflatable wall

Both the inflatable rigidizing structure concepts consisted of inflated fabric or graphite composite air beams. The unique difference between the two concepts was the number, location and size of the beams. The deployable mechanism consists of three metallic folding bars.
Altough the inflatable concepts were more lightweight and easy to package, the costructible truss concept was chosen due to an higher TRL [59].

2.5 Inflatable lunar habitats

Over time, all the space agencies have been trying to create a human habitat on the Moon. The main objectives of human presence on the Moon are the exploitation of the lunar surface resources, the possibility of conducting several research activities (in particular medical and biological), astronomy and mining. A human base on the Moon will also ease future missions to Mars since lunar based spacecraft can escape Moon's gravity with lower costs and masses: Moon's gravity is approximately six times lower than that of Earth. The Moon can be so used as an outpost to reach Mars. Besides, lunar inflatable habitat design can be also reused and adapted for Mars conditions, which are less critical than Moon's one: for example the presence of atmosphere on Mars removes the need of a micrometeoroid shield.
NASA has been interested in manned space exploration, including Lunar and Mars surface, since 1960s. At that time, costs for such types of missions were very high. The only way to have low masses and low costs was to study inflatable composite structures. Indeed, flexible deployable habitats are lower in weight, have less complexity and an higher realiability rather than mechanical one since minimal mechanical components are required for deployment. Moreover, inflatable habitats have reduced complexity rather than mechanical one.

2.5.1 Loading conditions

The loads that a lunar inflatable habitat have to withstand are divided into two major categories: internal and external.
External loads predominantly depend on lunar environmental conditions and micrometeoroid impacts. The most challenging external load is the extreme temperature gradient. A regolith shield on top of the structure can solve the MMOD problem and can reduce the temperature gradient.

Thickness of regolith cover (m)	Monthly variation and range (°C)							
	Permanently shadowed polar craters (Average T=233 °C)		Other polar areas (Average T=−53 °C)		Equatorial zone (Average T=−18 °C)		Midlatitudes (Average T=−35.5 °C)	
	Variation	Range	Variation	Range	Variation	Range	Variation	Range
0.0	0.0	−233	±10	−63 to −43	±140	−153 to 122	±50	−85.5 to 14.5
0.5	0.0	−233	±3.9	−56.9 to −49.1	±55.8	−73.8 to −37.8	±19.6	−55.1 to −15.9
1.0	0.0	−233	±1.2	−54.2 to −51.8	±16.6	−34.6 to −1.4	±5.8	−41.3 to −29.7
1.5	0.0	−233	±0.5	−53.5 to −52.5	±7.5	−25.5 to −10.5	±2.7	−38.2 to −32.8
2.0	0.0	−233	±0.3	−53.3 to −52.7	±4.3	−22.3 to −13.7	±1.5	−37.0 to −34.0
2.5	0.0	−233	±0.2	−53.2 to −52.8	±2.8	−20.8 to −15.2	±1.0	−36.5 to −34.5

Figure 2.19. Effect of regolith thickness on temperature ranges on Moon surface

Another possible solution to reduce extreme temperature changes is to place the structure at one of the lunar poles: since the Moon's axis of rotation is almost

perpendicular to the plane of the ecliptic, the sun always radiates the horizon at the poles.
The eventual presence of a regolith shield layer put on top of the structure represents an additional external load. The choice of the thickness of the regolith layer has to be a compromise: the greater the thickness, the greater the protection from MMOD and temperature gradient, but the greater the load that the structure must carry. Moreover the structure's material weight (dead load) has to be considered.
As concerns the internal loads, the most challenging is the pressurization one. The internal pressure is often set to 69KPa. From literature it is known that membrane stress created by the habitat internal pressure is directly proportional to the local radius of curvature ($\sigma = (p * r)/2$), so in large inflatables structural reinforcements have to be added. If the internal pressure load is designed correctly, it will induce only tensile stresses so as not to have problems related to stability. [80] [71]

Inflatable structures consist of membranes and membranes consist of thin sheets of materials, so they can only transmit loads through the plane. Any type of transverse load (bending or shear) is not allowed. Moreover membranes can't bear compressive stresses as wrinkles would begin to form. Wrinkles cause a loss of load carrying capacity in the membrane which leads the membrane to buckling. For those reasons an inflatable habitat has to be supported by rigidized colums and arches in order to stabilize the structure, support loads and limit the deformations. The structural response of the system must be studied under different loading conditions: for example structure fully pressurized with or without the regolith layer put on it or structure fully depressurized with regolith covering layer in place. In order to complete dynamic stresses and deformations analysis, a set of homogeneous coupled fourth order non linear partial differential equation with constant coefficient should be solved.
The stresses and deformations non-linearity occurs though the material used remains linear and elastic. Due to their strong non-linearity, only in very special cases a closed solution exist for membrane structures: numerical solutions such as FEM are needed.
In order to have a first calculation of stresses and deformations it is possible to study the structure steady-state behavior instead of the dynamic one. The linearization of membrane structure behavior is possible for small structures: this is why a modular structure is preferred rather than a single large one. [71] [72] [15]

2.5.2 Geometrical considerations

A lunar habitat has to meet numerous requirements: in addition to withstanding the harsh lunar environment and the different types of loads, they must respect the habitality rules.
Habitability is the set of qualities that make an environment a pleasant place to

live and a productive place to work. The NASA Man-System Integration Standards (NASASTD3000) established a minimum habitable volume to ensure the safety of the crew for long-duration missions. The minimum walkable floor area per person is set to $34.4m^2$. A floor height of 4.0 m seems to be most suitable. An additional area is required for equipments and stowage.
Inflatable structures provide large amounts of volume without affecting the transportation system.

Crew size	6	8	10	12
Habitable area [m^2]	206	275	343	412
+20% for equipment and stowage [m^2]	41	55	69	82
Total area (rounded up) [m^2]	250	320	415	500

Figure 2.20. Needed floor area according to crew members

Once the dimensions of the inflatable habitat have been established, it is important to choose a proper shape. Inflatables can take any shape, but there are simplier shapes that allow to avoid using reinforcing structural elements such as hoops or cables. The three simplest and most used shapes for an inflatable habitat application are the sphere, the cylinder and the torus (figure 2.21).

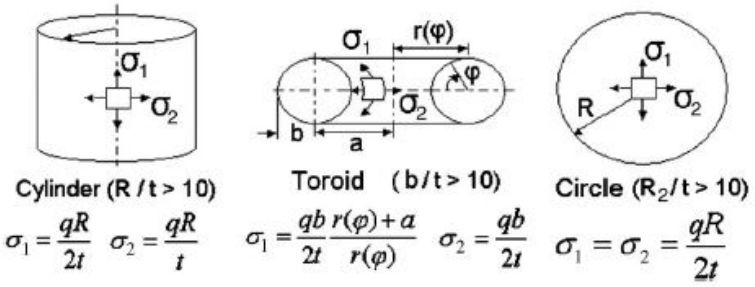

Figure 2.21. Stresses in different inflatable habitat shapes

As concerns the sphere, it is the most volumetrically efficient and, one the volume is assigned, has the least surface area and mass. Therefore, stress is almost uniform throughout the membrane. The sphere's biggest problem is the architectural inefficiency: most of the space is not used due to the double curvature of the wall. On the contrary, the cylinder shape is more efficient architecturally since the walls have curvatures in only one direction, however membrane stress and mass are higher. Finally, the torus configuration doesn't need endcaps, contrary to the case of the cylinder: this allows to save mass. However the torus shape has the same

curvature problems of the sphere. One way to solve this problem is to decrease the minor diameter as much as possible. [79] [78] [45]

2.5.3 Design Concepts

Over time, many inflatable lunar habitat concepts have been conceived. The first one was the NASA Lunar Stay Time Extension Module (STEM) in 1960s (figure 2.22).
The STEM consisted of an inflatable cylinder with hemispherical endcaps and an integrated airlock unit. The STEM was intended as an expandable shelter for Lunar stay extension, it could accomodate two crew members and was designed for a 30-days mission. Its configuration consisted of a pressurized habitable module and an airlock unit.

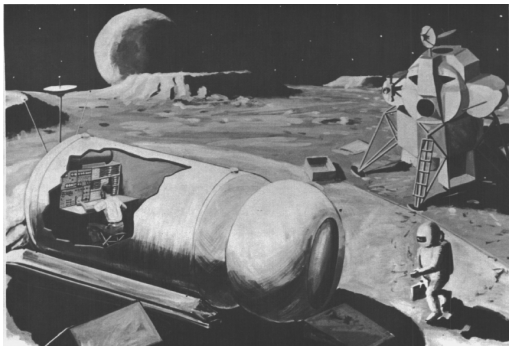

Figure 2.22. Concept of the STEM mission

In 1989 other important improvements in structural analysis, materials evaluation and pressure containment systems were made thanks to the Livemore Inflatable Habitat (LIH) project. The study of LIH foresaw the development of standard modules that could be assembled in order to create a larger lunar base.
LIH was thought as an hybrid structure: a combination of rigid metal elements and flexible membranes. The several compartments were separated by rigid composite end plates. The main LIH innovation was that the modules had a secondary pressure containment wall accomodating different pressurized compartments: in the event of loss of a compartiment, the rest of the module could continue to work safely.
Another configuration which involved an all flexible composite toroidal system has been proposed. The flexible portion of both concepts consisted of a bladder layer made of a Kevlar scrim reinforced with Tedlar film laminates and a restraint layer made of kevlar coated fabric with kevlar webbings. The all flexible concept was selected for further studies: despite the higher mass and the greater difficulty of pressure compartmentalization compared to hybrid concept, it showed a greater

usable volume and simplified packing and deployment.

In 1996 NASA Johnson Space Center (JSC) started to study a return mission to the Lunar surface. The lunar habitat concept (figure 2.23) involved a cylindrical structure with rigid endcaps and flexible mid-body that expanded once on the surface. The JSC structure needed to maintain structural geometry after ingress/egress depressurization, so a rigidization progess was studied. Rigidizable structures are flexible when packed and deployed and then are rigidized in their final configuration, acting like a rigid composite structure.[11] [37].

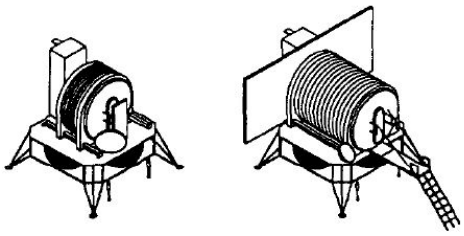

Figure 2.23. Stowed and Deployed JSC Lunar Habitat

Large space habitats are more complex and less reliable, so the most recent concepts foresee to build small modular inflatable habitats that can be shaped and assembled into larger and more complex structure. Moreover, smaller inflatable structure are easier to fold. A concept proposed by Vanderbilt, Criswell and Sadeh [71] for a modular inflatable lunar structure consists of four external wall membranes, a roof and a floor membrane, four inflatable columns with footings and four rigid arches. All the walls, roof and floor membranes had a radius of curvature in order to reduce stresses. Tha aim of colums and arches were to support the system in case of depressurization, stabilize the structure and limit roof deformations.

In the last two decades, also thanks to the advent of new materials and technologies, other important aspects were taken into consideration while developing an inflatable lunar habitat: stay-time and rapidity in the usability of the structure. In order to create an efficent human lunar settlment the structure must be designed in such way as to withstand the harsh lunar environment for long-term duration. In that way the crew is enabled to conduct in-situ research and explore the surrounding environment.

Most recent concept developed are the Thales Alenia Space IHAB inflatable habitation system (2008) and the ILC Dover X-HAB (2010).
The former (figure 2.24) was thought to provide an habitat for a crew of 4 to 6 people for a mission lasting about 12 months. The concept consist of a rigid core with side inflatable elements covered with lunar regolith to shield radiation.

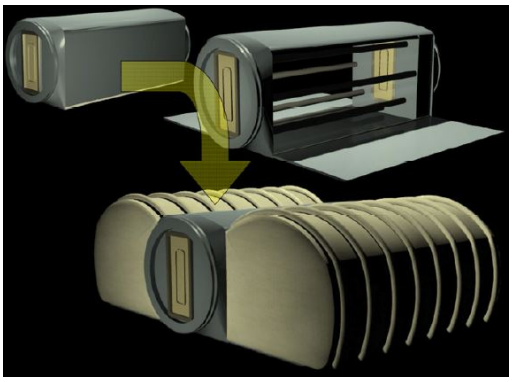

Figure 2.24. Preliminary concept of Thales IHAB

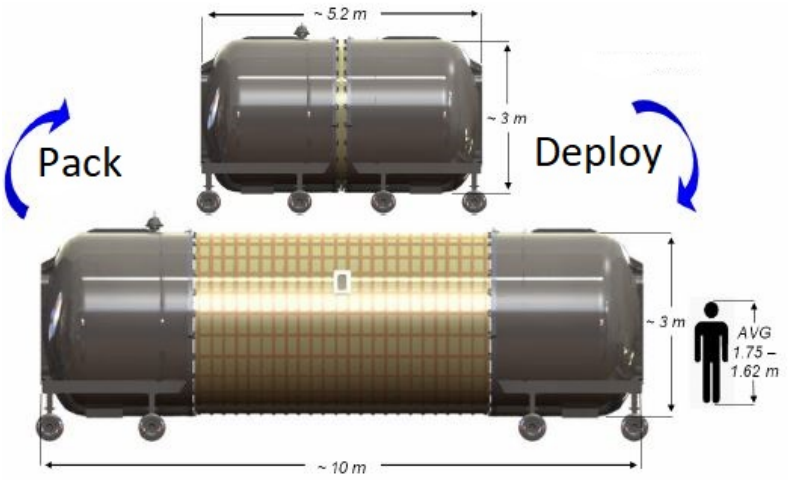

Figure 2.25. ILC Dover X-Hab lunar habitat concept

The latter (figure 2.25), resuming the previously described JSC habitat concept, consisted of a flexible middle segment between two rigid endcaps. The flexible segment was made of Vectran and the bladder is manufactured from a specialized coated fabric. The deployment of the structure occured along the longitudinal axis by inflation [37].

Chapter 3

Re-entry and descent inflatable technology

3.1 Advantages and disadvantages

The necessity to make re-entry and landing system less complex, less expensive, lower in storage volume and lightweight led to the development of inflatable systems. Those systems provide a large high-drag shape and can be stored in a small volume. Unlike rigid structures, inflatable ones will not require a backshell that wraps the payload. The backshell makes the Thermal Protection System (TPS) heavier and introduces potential heat penetration during re-entry phase due to its structural attachments and electric connections.
Unlike inflatable aeroshells, rigid ones need a removable door in order to access the payload: this leads to a large amount of testing that heavily increases the cost of the mission. Due to their high-effective insulation, rigid aeroshell can easily withstand re-entry heat, but, at the same time, are problematic for high-power payloads during interplanetary cruise: internal heat should be rejected by radiators in order not to damage the payload.
The problems listed above can be overcomed by the use of inflatable aeroshells. Thanks to their low ballistic coefficient, re-entry heat is lower than in the case of rigid stuctures.
The Ballistic Coefficient is defined as follows:

$$\sigma = \frac{m}{Cd * S}$$

where Cd is the drag coefficient, S is the reference aerodynamic surface area and m is the mass of the system.
This parameter defines deceleration and descent modes, dynamic pressure, g-load of the vehicle as well as heat fluxes caused by aerodynamic braking.
In inflatable aeroshell this parameter has a low value thanks to the large area and

light weight of the inflatable structure: this bring several advantages in aerodynamic heating reduction, as shown in figure 3.1.

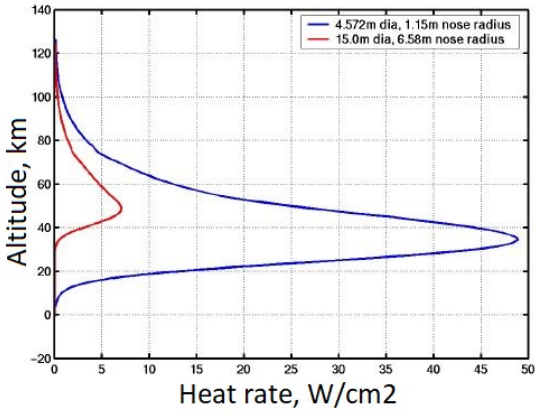

Figure 3.1. Convective heat rate comparison between rigid (blue) and inflatable (red) aeroshell

Furthermore low Ballistic Coefficient values imply greater deceleration in the atmosphere. In that way, inflatable aeroshell can be deployed and landed at an higher altitude.

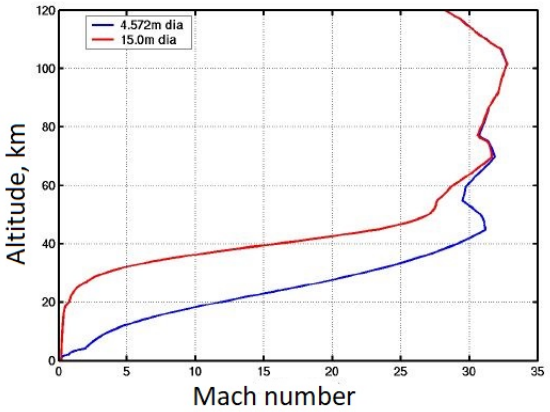

Figure 3.2. Mach number vs altitude between rigid (blue) and inflatable (red) aeroshell

Considering that the parachute deployment velocity is about M=2, the inflatable system allows deployment at an altitude of 20km greater than rigid one (figure 3.2). This is a great advantage in particular for Mars missions, since the most interesting landing sites seem to be at an altitude greater than 2km: it is hard to land on these sites with rigid aeroshells.

Despite the many advantages, several technical challenges need to be addressed in the development of an inflatable aeroshell. Indeed, flexible structures are subjected to unpredictable drag performance during re-entry and to aerostructural dynamic instability. The danger due to puncture is also to take into account [42] [46].

3.2 Design concepts

The inflatable aerodynamic decelerators (AID) are divided into two classes: supersonic IAD (SIAD) and hypersonic IAD (HIAD). SIAD are inflated at supersonic speed (M<5) while HIAD are inflated at hypersonic speed (M>5) or exoatmospherically. IAD entry systems are composed of two elements: the structure and the Thermal Protection System.
As concerns the TPS, its task is to protect the inflated structure from aerothermal re-entry environment. The TPS will be dealt with in a later paragraph paragraph.
As concern the structure, several trailing and attached geometries have been studied (figures 3.3 and 3.4).

Figure 3.3. Attached IAD configurations

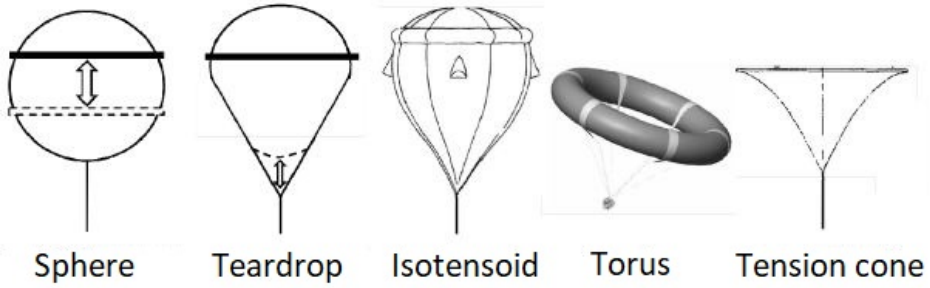

Figure 3.4. Trailing IAD configurations

The most permorming seem to be the trailing and attached isotensoid, the tension cone and the stacked toroid blunted cone.

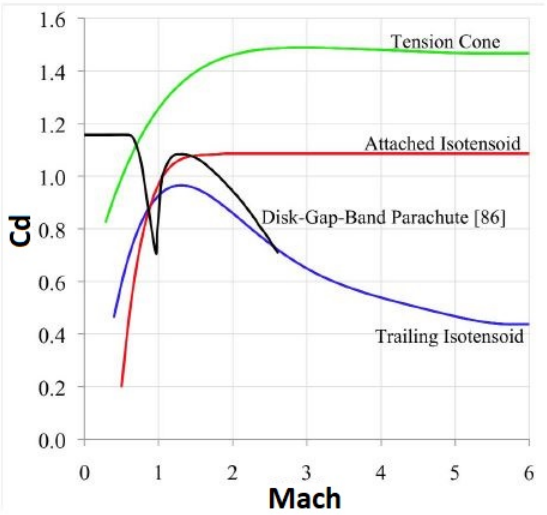

Figure 3.5. Drag comparison among different types of AID

Figure 3.5 shows the drag coefficient comparison between diffent AID geomentries as a function of the Mach number. The tension cone seems to be the most suitable in the hypersonic and supersonic regimes: it provides a higher drag coefficient than the other configurations [85].

The possible applications for inflatable aeroshells are very large: return of small orbiting vehicles, support to the ISS (download system) and to planetary missions. A potential application for an IAD is to carry robotic systems (such as rovers) to Mars surface. The use of inflatables offer mass benefits that are fundamental for interplanetary missions.
Preliminary design for Exomars mission proves the feasibility of this technology: an IAD with a diameter of $3m$ and a mass of about $450kg$ can withstand the heat flux of about $300KW/m^2$, due to entry conditions of $4800m/s$ and -13 degrees.
The Mars Aerocapture demonstrator (Aurora Program), an AID of $150kg$, succed in withstanding an heat flux of about $200KW/m^2$, due to entry conditions of $6000m/s$ and -9.2 degrees [98].

The main historical inflatable aeroshell applications are described below.
The first inflatable deceleration system concept dates back to 1970. It consisted of an inflatable Viton coated Nomex fabric canopy directly attached to a payload, thought for entering the Mars atmosphere.
In the late 80's Aerospace Recovery Systems Inc. developed the Inflatable Recovery Vehicle (IRV), a truncated cone with a small torus linked by inflatable cylindircal elements to a larger torus. In this case the canopy Kevlar fabric was coated with silicone, an insulating material [92].

The previous systems described had been developed only at conceptual level. The first real demonstration of a re-entry and descent inflatable technology happened in February 2000 with the IRDT (figures 3.6 and 3.7).

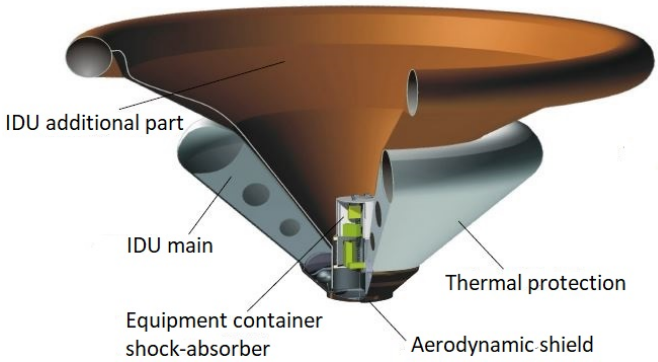

Figure 3.6. IRDT vehicle design

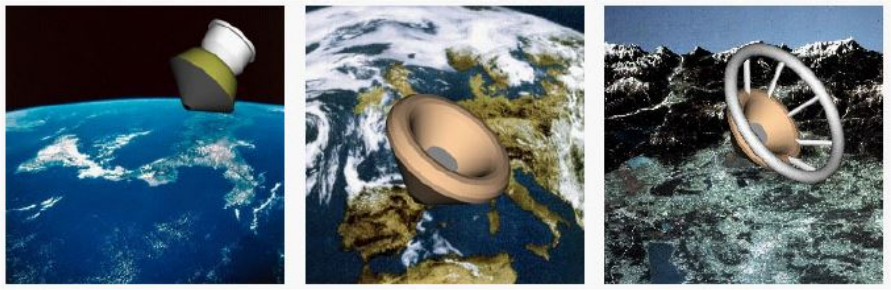

Figure 3.7. From the left: IRDT in orbital stored, re-entry and landing configuration

It combines the classical heatshield, parachute and landing systems into a single system in order to reduce mass and complexity. The main subsystems were: the re-entry thermal protection system, the parachute system for descent and the damping system for landing. It consisted of an ablative rigid nose shield and a conical inflatable envelope (called Inflatable Deceleration Unit, IDU) that inflated in two steps. The first step was an entry shield, while the second acted as a parachute system. The first inflation step increased the diameter from 0.8m to 2.3m. The second inflation step, which happens once subsonic speeds are reached, took it to 3.8m. The second step brings the landing speed at about 10 m/s. The inflatable entry shield (first inflation step) consisted of an internal network of rubber hoses pressurized with nitrogen. It was covered by an insulating layer protected in turn by a silica-based fabric impregnated with an ablative material. The ablative material

had the task of absorbing heat and then subsequently decomposing. In that way heat penetration into the inner layers was avoided.
Altough some damages caused by an heavy impact on the ground (estimated touch-down speed of 60 m/s), the IRDT mission was a step forward in the development of inflatable re-entry capsules. [65] [68] [99].

Other important recent improvements were made thanks to IRVE missions. The IRVE-1 (figure 3.8), launched in 2006, consisted of 3m, 60° half taper angle sphere cone. It is composed of a central body, containing electronics and inflation systems, and a multiple tori inflatable aeroshell.

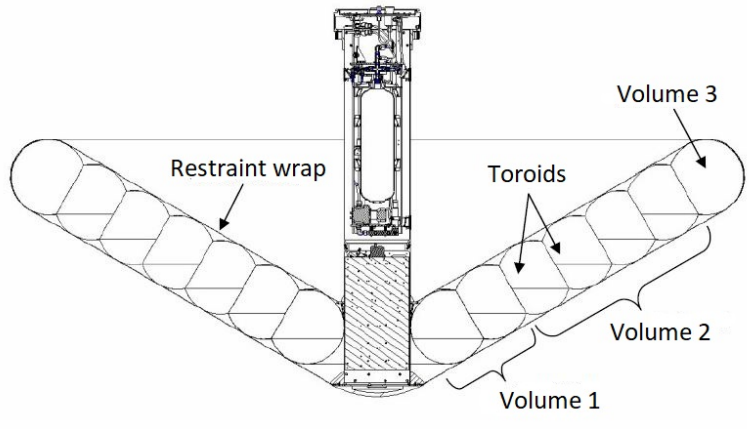

Figure 3.8. Concept of IRVE system

The central body is an aluminum cylinder with a Teflon nose cap. The inflatable aeroshell is packed around the cylinder during launch phase and then deployed. The cylinder has one upper attachment (interface ring) for the launch vehicle and two lower attach rings for the aeroshell.
The bladder is made of seven toroids divided into three separated volumes and linked together with a restraint wrap. Having separated volumes reduces the risk of failure in case of punctures. Any torus consisted of inflatable bladder, a structural restraint, a gas barrier and a thermal protection layer. The material used for the bladder is a silicone coated Kevlar fabric. The restraint wrap is made Nextel 312 for thermal protection and Kapton as gas barrier. A dry Kevlar fabric is used to absorb structural loads (figure 3.9) [42] [57].

Unfortunately the IRVE-1 mission didn't go well: launch vehicle failed to release payload. Based on the same mission concept of IRVE-1, IRVE-2 and IRVE-3 missions have been completed (respectively in 2009 and in 2012). Compared to the first mission, the leak rate of the aeroshell was reduced and structural straps were

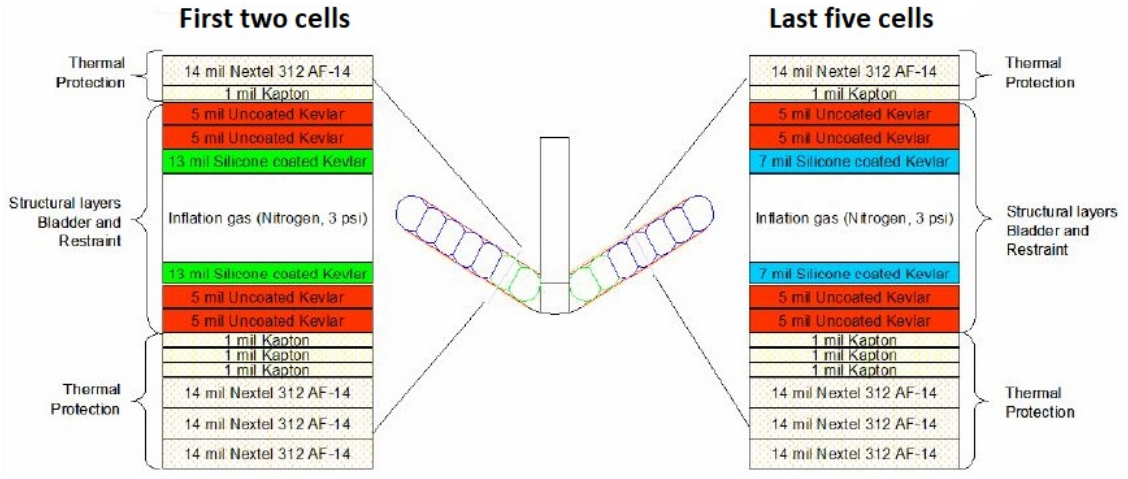

Figure 3.9. IRVE materials layup

added to connect the various toroids and the central body. A new TPS which allows protection of the rigid nose as well as the aeroshell was designed [26].

3.3 Flexible thermal protection system

The principal problem for a space re-entry vehicle that runs through a planet's atmosphere is extreme heating. Hence the need to design a proper Thermal Protection System (TPS). Generally, when external heat is lower (SIAD case), a classical heat shield is used. When the external heat reaches very high values (HIAD case), an heat protection ablative layer is needed. Furthermore the shape of the inflatable has a great impact in aerodynamic heating. As seen before, the configurations that ensure the lower heating are the attached isotensoid, tension cone and stacked toroid blunted cone.

3.3.1 Materials used

Materials for a flexible TPS system must comply with very stringent requirements. The main features are high thermal resistance, chemical stability in an oxidizing environment and strength retention under thermal loading. Furthermore materials should have low aerial weight and permeability while remaining malleable in order to maintain uniformity and homogeneity after packing.

In the past woven fabrics of synthetic fibers such as Nomex, Nylon and Dacron were widely used. Also filament materials (fabric of woven metal or ceramic strands) were studied. They resulted more performing than fibers (temperature resistance

up to 800K compared to 480k), but they have a very high cost.
In order to reduce porosity and increase thermal protection elastomeric (urethane and silicon) coatings were studied. In the last decades some studies highlighted the possibility to use ablative materials to increase thermal resistance.

Recent studies show that a multilayer layout seems to be the best choice for a flexible TPS. It consists of porous outer fabric layers (silicon carbide), porous middle insulation layers (carbon felt and aerogel) and an impermeable inner gas barrier layer (film material). A one-dimensional example of a multilayer layout is shown in figure 3.10.

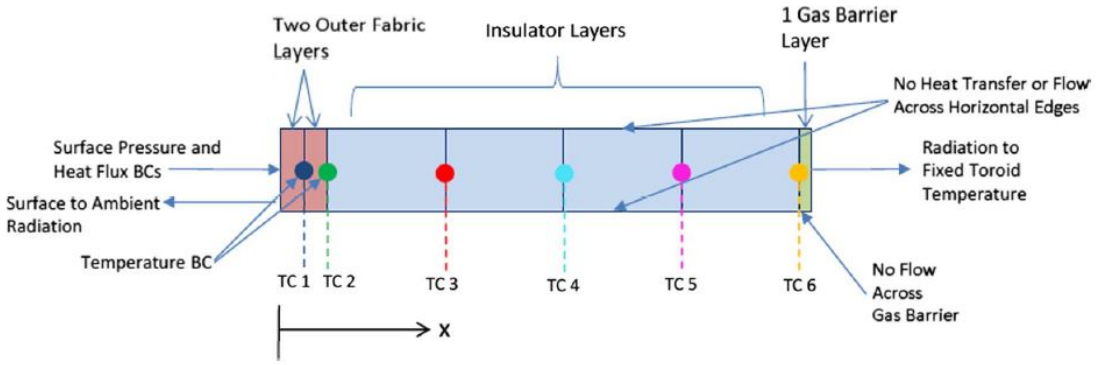

Figure 3.10. Example of a flexible TPS configuration

The task of the outer fabric is to protect the insulation material from external convective heat flux, aerodynamic forces and abrasion. Materials with high emissivity and low catalicity such as Nextel BF-20 and Nicalon (silicone carbide) seem to be the best choices. They can withstand heat fluxes respectively up to $30W/cm^2$ and $50W/cm^2$.
The task of insulator layers is to keep the TPS backside temperature within a maximum limit, so materials with low thermal transport are required. The most used materials are Pyrogel 3350, Pyrogel 2250 and Saffil. More generally, insulation materials are divided into three categories: fully insulative, transpiration-insulative and ablative.
The first class manages heat loads by conduction and radiation. Their effectiveness mostly depends on the thickness of the layer and can withstand heat pulses from 20 to 50 W/cm^2 for less than 200 seconds.
The transpiration class manages heat loads by conduction, radiation and endothermic processes (out-gassing). They are charactized by charring without surface recession and can withstand heat pulses from 30 to 100 W/cm^2 for less than 500 seconds.

The ablative class manages heat loads by pyrolisis. They are characterized by charring and recession and can withstand heat pulses from 75 to 150 W/cm^2 for a time greater than 500 seconds.
A first approximation calculation of the thickness of the ablative layer is derived from the heat transfer formula with constant wall temperature:

$$\frac{T_{(x,t)} - T_s}{T_i - T_s} = erf(\frac{\delta}{2\sqrt{\alpha t}})$$

Where α is the diffusion coefficient of the ablative material.
As concerns the gas barrier, the most used material is aluminized Kapton laminated to Kevlar (AKK or KKL). The Kapton Kevlar laminate is both an AID structural component and a TPS component. The Kapton, thanks to its impermeability, is used to avoid or reduce hot gas inflow through the TPS laminate. The Kevlar is used as mechanical interface in order to attack the TPS to the AID structure.
In recent years several tests that contributed to the development of flexible TPS materials were conducted. In figure 3.11 are shown some layouts tested in the Program to Advance Inflatable Decelerators for Atmospheric Entry (PAIDAE) conducted by NASA Langley Research Center [22] [3].

Layup #	Outer Fabrics	Insulators		Gas Barrier
L1	Nextel AF-14	Pyrogel 6650		2x Kapton
L2	Nextel BF-20	Pyrogel 6650		2x Kapton
L3	2x Nextel AF-14	2x Pyrogel 3350		2x Kapton
L4	2x Nextel BF-20	2x Pyrogel 3350		2x Kapton
L5	Refrasil UC100-28	KFA5	Pyrogel 3350	2x Upilex

Figure 3.11. TPS layouts tested in the PAIDAE

3.3.2 Heat transfer

Different heat transfer mode inside the TPS layers have to be considered: solid conduction, radiation, gas conduction and convection. The local energy and gas conservation equations (figure 3.12) are used to estimate the amount of heat and mass transfer through the layers.

The terms in the first equation represent (from left to right): the rate of energy storage in a control volume, the conduction heat flux, the advention (convention within porous materials) heat flux and the rate of energy generated or consumed after insulator decomposition reactions.
As concern the second equation, the first term is the rate of gas mass storage and the second term is the rate of change of mass. The term on the right-hand side is the rate of pyrolysis gas generated due to the insulator decomposition reactions.

$$\rho_s C_{ps} \frac{\partial T}{\partial t} - \frac{\partial}{\partial x}\left(k \frac{\partial T}{\partial x}\right) + \rho_g C_{pg} v_{gx} \frac{\partial T}{\partial x} + H_d \frac{\partial \rho_s}{\partial t} = 0$$

$$\phi \frac{\partial \rho_g}{\partial t} + \frac{\partial}{\partial x}(\rho_g v_{gx}) = -\frac{\partial \rho_s}{\partial t}$$

$$v_{gx} = -\frac{k_x}{\mu_g} \frac{\partial p}{\partial x}$$

Figure 3.12. Energy and gas conservation equations

Pyrolysis consists of oxidation and outgassing of the insulation material that occur at high temperature.
Another important phenomenon to take into account is the catalysis. It is caused by the air dissociation and ionization that occur at high temperatures. Recombination reactions can increase heating rates so, in the choice of materials, it is important to consider their catalytical efficiency [23] [8].

3.4 Load conditions

Re-entry and descent vehicles have to withstand an extreme hypersonic flight environment consisting of extreme heating, dynamic pressure, deceleration loads and impact absorbtion. In order to decelerate, the re-entry capsule exploits the surrounding air. The greater the diameter, the greater the deceleration caused by air resistance. The gas particles beating on the surface convert kinetic energy into heat. In order to decrease thermal loads on the surface and inside the capsule there is the need to develop a thermal protection, such as an ablative material layer. The greater the thickness of the ablative material,the greater the thermal protection. Geometry and trajectory of the aeroshell affect load conditions too.

An analytical method to predict aeroelastic behavior of an IAD is requested. Indeed, the structure changes with the flowfield and the flowfield consequently changes around the deformed structure. Aerodynamic and structural response (fluid-structure interaction) have to be studied simultaneously through FEA and CFD analysis.
Very big dangers for an inflatable re-entry vehicle are wrinkling and buckling. There is the need to find an optimized shape which makes the structure loaded in tension in both principal directions simultaneously, otherwise wrinkling or buckling occurs.

Wrinkling makes the behavior of the structure unpredictable and can lead to localized stress concentration, flutter and heating. In order to prevent wrinkling and buckling, a nonlinear finite element analysis is required [85].
Another primary problem is the impact load. In order to give to the system proper landing conditions, an inflatable impact attenuator is often used to absorb the kinetic energy of impact. Also a damping system may be added. The inflatable landing system has to decrease the speed of the system bringing it below 15 m/s in order to avoid strong impact loads [65].

3.4.1 Geometry and ballistics

Aerodynamic forces (and so heating loads), depends on parameters as aeroshell geometry and mission trajectory. The goal is to optimize those parameters in order to have lower aerodynamic and heat loads. Consequently the TPS will be less stressed.
The most important parameters for an inflatable aeroshell are the half taper angle θ, the nose radius R_c and the initial re-entry angle. The first two are shown in figure 3.13, together with other important geometric parameters: aeroshell diameter D, and the radius of blunt R_t.

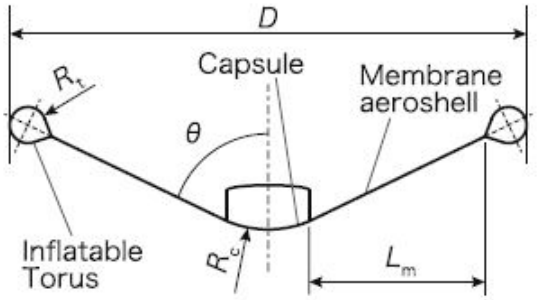

Figure 3.13. Design parameters for an inflatable aeroshell

In general, the bigger the nose radius R_c, the lower the heat rates. A first approximation relationship between the heating rate at stagnation point and the nose radius can be seen in the equation below:

$$q_s = k\sqrt{\frac{\rho_\infty}{R_c}}\left(\frac{V_\infty}{1000}\right)^3$$

Before dimensioning the thermal protection system, the ballistic trajectory of the inflatable aeroshell has to be determined.
As a first approximation, the two-dimensional system of equations, shown in figure 3.14, can be used to obtain the ballistic trajectory of the inflatable aeroshell: Θ is

the flight path angle, Θ_0 is the initial re-entry angle and β_e is the flight range angle. Once the drag coefficient C_d is obtained through CFD analysis, the ballistic trajectory can be calculated and so all aerodynamic and consequently heat loads conditions too.
Some tests for an Earth aeroshell application show that the half taper angle largely affects the drag coefficient but not much the drag acceleration during re-entry. Furthermore, as the half taper angle decrease, the heat flux seems to increase so as the height at which maximum heating occurs (figure 3.15).

$$\left.\begin{aligned} \frac{dv}{dt} &= -\frac{1}{2}\rho\left(\frac{C_D S}{m}\right)v^2 - g\sin\Theta \\ \frac{d\Theta}{dt} &= \left(\frac{v}{r} - \frac{g}{v}\right)\cos\Theta \\ \frac{dh}{dt} &= v\sin\Theta \\ \frac{d\beta_e}{dt} &= v\cos\Theta \end{aligned}\right\}$$

Figure 3.14. Ballistic trajectory equations

Half Taper Angle	Maximum Heat Flux (MW/m^2)	Heat absorption (MJ/m^2)	Maximum Deceleration	Reentry Time (s)	Landing velocity (m/s)
50°	2.14	256.3	-5.76g_0	1350.35	44.85
55°	2.01	239.8	-5.8g_0	1361.9	44.33
60°	1.92	231.5	-5.54g_0	1368.16	43.87
65°	1.84	224.6	-5.35g_0	1376.8	42.96

Figure 3.15. Effects of the half taper angle on ballistic parameters

In order to optimize the descent aerodynamic and heat loads, the influence of initial re-entry angle has to be considered. If the initial re-entry angle increase, the drag acceleration increases (in absolute value) , while the heat flux decreases (figure 3.16). Considering that for unmanned missions the maximum drag acceleration is set to $12g_0$ ($8g_0$ for manned missions), and since the maximum heat flux tolerable with current technology is around $2.5MW/m^2$, the feasible region of optimization can be found.

An half taper angle greater than 55° and an initial re-entry angle between -2.7° and -2° is recommended. In that way the TPS can work safely without failure [95] [3].

Initial Reentry Angle	Maximum Heat Flux (MW/m^2)	Heat absorption (MJ/m^2)	Maximum Deceleration	Reentry Time (s)	Landing velocity (m/s)
-1°	1.39	316.1	-2.98g_0	1702.05	43.88
-2°	1.92	231.5	-5.54g_0	1368.16	43.87
-3°	2.31	192.4	-8.01g_0	1202.85	43.87
-4°	2.64	168.6	-10.4g_0	1096.77	43.87
-5°	2.93	152.1	-12.8g_0	1020.02	43.87
-6°	3.18	139.7	-15.2g_0	960.429	43.86

Figure 3.16. Effects of the initial re-entry angle on ballistic parameters

3.4.2 External flux

Evaluating the heat transfer in the boundary layer is very complicated. A coupled approach about both computational fluid dynamics and structure analysis is required. A first approssimation calculation of the stagnation heat flux can be obtained with Tauber's model:

$$q_{w,tauber} = 1.35 * 10^{-4} * \sqrt{\frac{\rho_\infty}{R_n}} * U_\infty^{3.04} * (1 - \frac{h_w}{h})$$

This model can be applied to a sphere-shaped model, so the heat flux calculated through this equation will be conservative.
More generally the heat flux is obtained using the following equation:

$$q_j = \lambda_{trs}\frac{\delta T_{trs}}{\delta x_j} + \lambda_{rot}\frac{\delta T_{rot}}{\delta x_j} + \lambda_{vib}\frac{\delta T_{vib}}{\delta x_j} + \lambda_{ele}\frac{\delta T_{ele}}{\delta x_j} + \rho\Sigma_{s=1}^{ns} h_s D_s \frac{\delta X_s}{\delta x_j}$$

This equation considers energy transfer among the internal energy modes: translation, rotation, vibration and electron. Indeed, due to the high temperatures, the flow downstream of the shock layer is in a chimical nonequilibrium state: particles are characterized not only by classical translation and rotation modes, but also by dissociation and ionization processes. A very detailed and difficult chemical model is requested in order to make analytical calculations. [87] [2].
Once an estimate of the external heat flux has been calculated for different boundary conditions (representing the whole descent), the flexible TPS can be designed.

3.4.3 Static and modal analysis

Once established materials, ballistics, CFD and heat transfer models, in order to preserve the shape of the inflatable decelerator and to provide a safety design for the structure, a non-linear finite element analysis is requested.
An analysis of a stacked toroid blunted cone configuration, similar to that of IRVE

mission, which use a Kevlar fiber membrane, will be presented below. Even if the results vary from case to case, the method of approach used is similar for all inflatable aeroshell configurations.

Firstly a finite element static and modal analysis have to be performed: the static inflatable structure has to be analyzed to obtain the distribution of static stresses, natural frequencies and modal shapes.
The parameters that influence the most the static and modal analysis are the inflation pressure and the material film thickness.
The maximum static stress during atmospheric re-entry is approximately directly proportional to the inflation pressure and inversely proportional to the film thickness (figure 3.17).
The first natural frequency seems to increase with inflation pressure, while seems to decrease as the film thickness increase (figure 3.18).

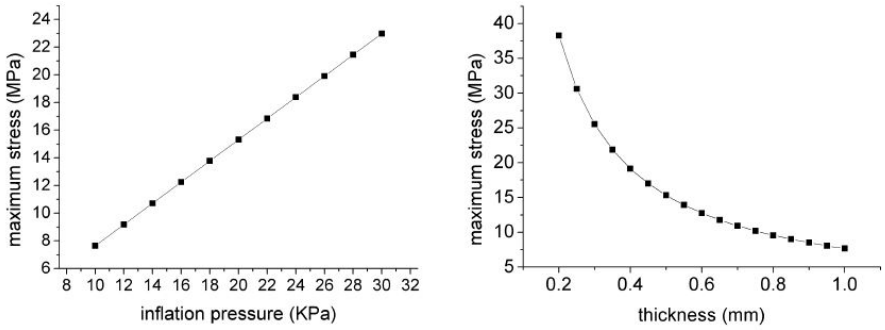

Figure 3.17. Maximum stress as a function of inflation pressure and thickness

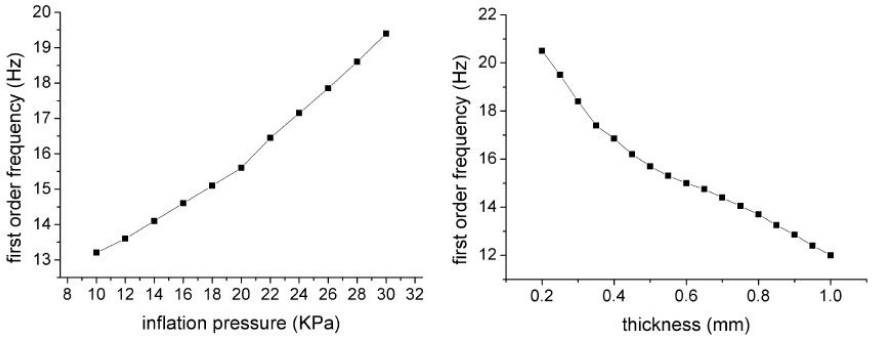

Figure 3.18. First order frequency as a function of inflation pressure and thickness

Static stresses, natural frequencies and modal shapes are affected by the hypersonic flow (aerodynamic pressure and aeroheating). For a complete analysis, the

hypersonic flow has to be studied, obtaining temperature and pressure distributions at different altitudes.
In this case study, the maximum aerodynamic pressure of the hypersonic flow tends to decrease with increasing altitude. On the contrary, the maximum aerodynamic temperature tends to increase with increasing altitude. Those results of the hypersonic flow analysis must be integrated with the previous results of the static analysis.
The aerodynamic pressures at different altitudes is interpolated and used as input for the dynamic analysis. The variations of maximum static stress and first natural frequency as function of the altitude, taking into account the contribution of aerodynamic pressure, are shown in figure 3.19.

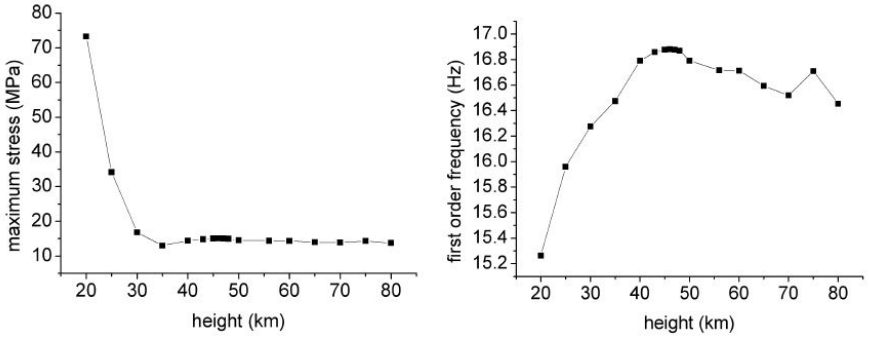

Figure 3.19. Maximum static stress and first order frequency considering aerodynamic pressure

Finally, for a complete study, aeroheating effects have to be studied. Aerodynamic temperatures at different altitudes are interpolated and used as input for the dynamic analysis.

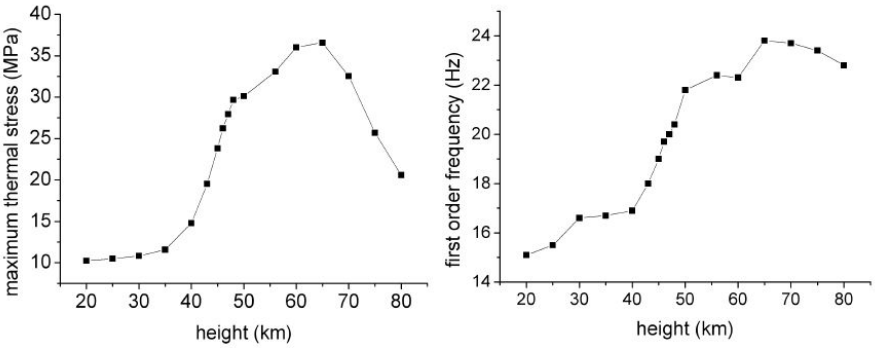

Figure 3.20. Maximum static stress and first order frequency considering aeroheating

Aeroheating causes a change in the inflation pressure value due to internal gas

expansion. Thermal stresses and deformations are influenced both from the temperature of the structure and the inner gas thermal expansion due to aeroheating. The variations of maximum static stress and first natural frequency as function of the altitude, taking into account the contribution of thermal loads caused by aeroheating, are shown in figure 3.20.

In conclusion, as concerns the static characteristics, the stacked toroid blunted cone configuration studied, seems to be most stressed by aerodynamic pressure when altitude is below 40km. The aeroheating effect turns out to be very decisive when the altitude is above 40km. Furthermore the first order frequency seems to be more influenced by aeroheating rather than aerodynamic pressure [101].

Chapter 4

Solar Arrays

Inflatable solar arrays have several advantages over their mechanical counterpart: higher specific power, low masses, low costs and reduced stowage volume. They are of fundamental importance for missions that require high power outputs with restriction dictated by the launch vehicle.
The greater complexities in the development of an inflatable solar array are rigidization and controlled deployment. Furthermore ,a rigidization method in order to avoid gas leakage is needed.

4.1 Design concepts

The JPL ST4 is one of the first satellite that mounts an inflatable solar array (1999). The mission involved a rendez-vous around the Temple-1 comet and then a landing on it. An output power of $12kW$ was requested to carry out the mission.
The inflatable solar array consisted of four subsystems: the solar array blanket, the structural support components, the controlled deployment system and the inflation system (figure 4.1).

The ST4 was a split blanket type. The deployment tube was positioned on the centerline. In the stowed configuration, the solar array modules were folded as an accordion. The building blocks of the DS4 consisted of rigid, high-efficiency silicon photovoltaic assemblies: flexible silicon thin film solar cells ensure masses and costs reduction. The structural support components included stowage panels, attacks for the launcher and the rigidizable inflatable beam. The latter had to support the solar array structure and to allow the deployment. The ST4 inflation system was a compressed gas type.

The teledesic mission (1997), that involved the launch of 288 satellites in LEO orbit, was thought it could be equipped with a $3mx10m$ rectangular inflatable solar array. The concept was similar to that of ST4 satellite, but the teledesic array had

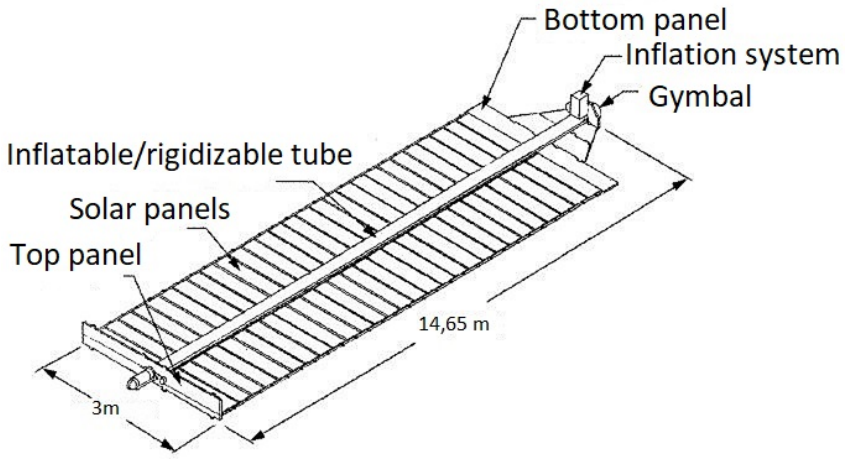

Figure 4.1. JPL ST4 inflatable solar array design

three inflatable tubes: a deployment tube that allowed the deployment of the array and of two rigidizable tubes used as structural support after deployment.

In the early 2000s L'Garde developed the Inflatable Torus Solar Array Technology (ITSAT) in order to provide power to small satellites (from 0.01 to 1.0kW). The initial prototype was a four-sided torus with corner joints folded into three panels along the axis of the array and then rolled up (unidirectional fold). A first phase of testing showed that the material had to be as thick as possible to facilitate packagability and that a sharp 90ř corner joint caused excessive stress concentrations. In the second and final prototype the corner joints were removed: the canister and its lid were two of the sides of the torus. The other two sides were made of two parallel booms. The blankets were attacched to the booms through cables in different place along the booms length. The folding direction of the booms was perpendicular to that of the blanket in such a way to reduce out-of-plane motion (figure 4.2).

The two inflatable booms were made of a three-layer aluminum laminate structure: an aluminum foil sadwiched between two layers of thin plastic (Kapton). The Kapton provided tear resistance during inflation. Thanks to the Kapton layers, once inflated, the two tubes allowed a permament rigidization: no make-up gas system was needed. Several solar cell types were taken into account: thin crystalline silicon, gallium arsenide on germanium, cleft gallium arsenide, copper indium diselenide and amorphous silicon. The crystalline silicone one was chosen than the more performing but less technologically developed amorphous silicone and copper indium diselenide [63] [55].

Inflatable solar arrays can be used to support the activity of rover vehicles on martian surface. The NASA JPL developed a mars rover inflatable solar array in

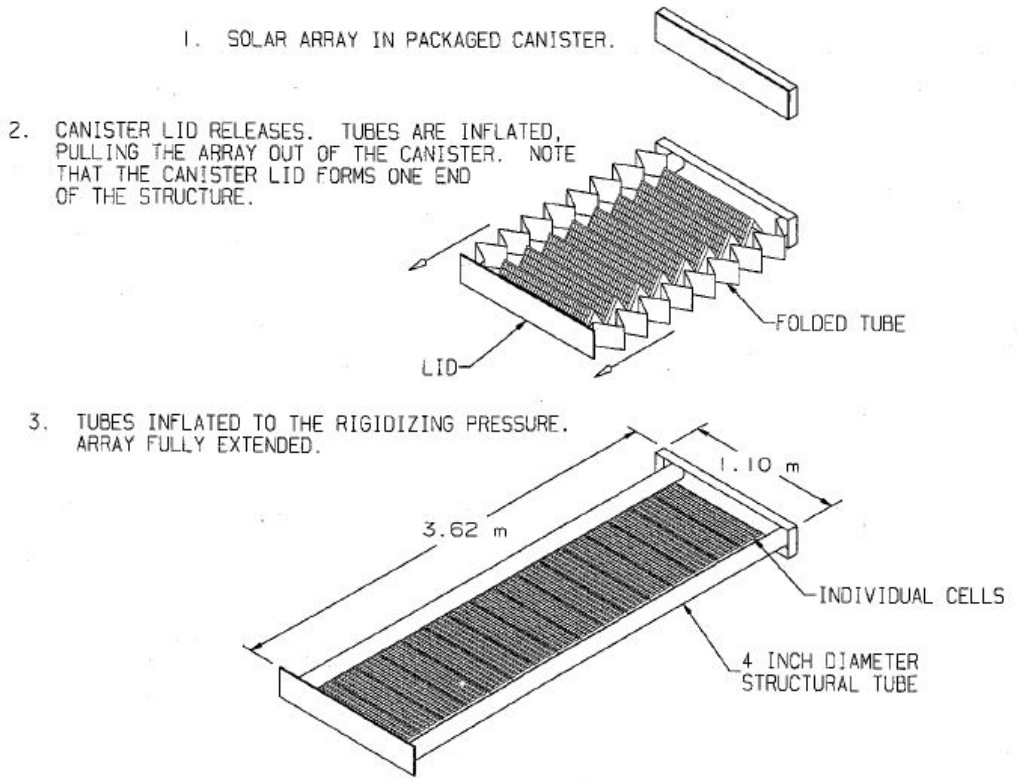

Figure 4.2. ITSAT inflatable solar array design

order to produce the necessary power levels for rover activities.
This array had a parasol shape and was made of four components: the canopy, the inflatable torus, the inflatable column and 16 solar modules (figure **??**). The modules were supported by the torus and the column. The torus was made of aluminized Mylar, while the column was made of laminated Kapton and aluminized Mylar. The solar cells consisted of amorphous silicon deposited on a thick layer of polymide. The solar panels were covered with an encapsulant polyester layer [10].

4.1.1 Structural design of advanced solar array program (ESA)

The purpose for future solar array applications is to improve packing and deployment technologies as well as find better and cheaper power-to-weights and power-to-size solutions. In order to do that, the European Space Agency (ESA) started the "Structural Design of Advanced Solar Array" program (2003).
The program had the following objectives: to find advanced solar cell and flexible blanket technologies, to find a proper deployable support structure design and to

demonstrate the feasibility of an inflatable solar array structure. The program involved the combined use of thin film solar cells and a deployable flexible blanket in order to reduce masses and costs.

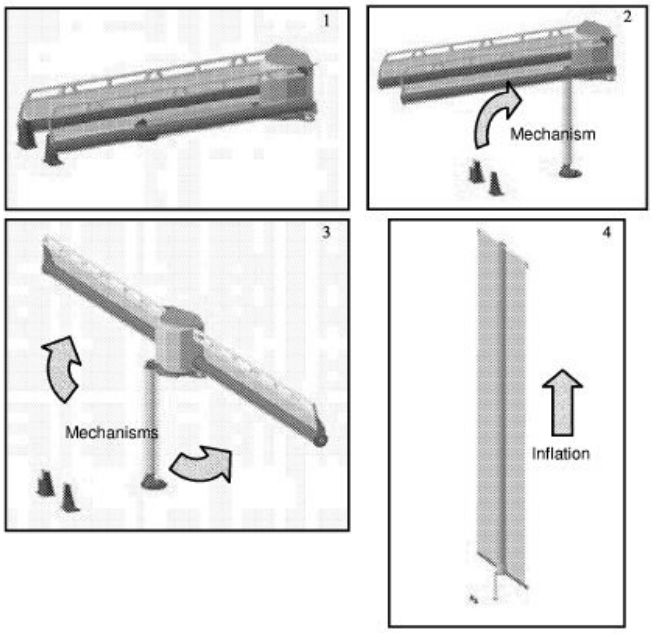

Figure 4.3. Subsequential deployment process of the solar array in two different directions

An inflatable central mast system with two subsequential deployment in two different directions seemed to be a great configuration in terms of mass and manufacturing costs (figure 4.3).
As concerns the thin film solar cells, an amorphous silicone deposited on a polymer rather than a copper indium diselenide was chosen. The copper indium deselenide seemed to have better parameters for solar array applications but the technology involving it wasn't already well developed.
The TADECS system is located inside the accordion-folded boom. Its aim was to control the deployment mechanism. Once deployed, the boom underwent a rigidization process.
The boom was made of three layers: an internal polymide bladder layer, a photocurable resin and glass fibres structural layer and a polymide external layer that works as space environment protection.
A series of tests and structural analyses were made to demonstrate the feasibility of the deployment sequence and of the rigidization process. The test results were very encouraging and paved the way for future inflatable solar array applications [75].

4.2 Dynamic model of space inflatable booms

In order to develop an inflatable solar array design, it is necessary to better understand the dynamic model of inflatable booms that act like supporting tubes (central mast) from which the deployment then takes place.
All the stages of the inflation have to be known in order to ensure stability and controllability of the deployment process. The pressurization (inflation) rate and the initial packed configuration seem to be the main parameters that affect the deployment dynamic.
The inflatable solar arrays boom can be folded in many methods, but the most studied methods are the z-folded and rolled types.

As concern the rolled boom method, the equation of motion for the deployment is shown below:

$$\frac{\mathrm{d}}{\mathrm{d}t}\left\{I\left[s(\alpha)\right]\frac{\mathrm{d}\alpha}{\mathrm{d}t}\right\} = p\left[s(\alpha)\right]\pi R^2 r\left[s(\alpha)\right]$$

where I is the moment of Inertia of the unrolled part of the structure, s is the arc length of the part of the structure enveloped around the hub, R is the radius of the inflated tube, p is the internal pressure, α is the rigid body rotation of the roll and r is the distance between the hub and the bottom of the rolled structure.

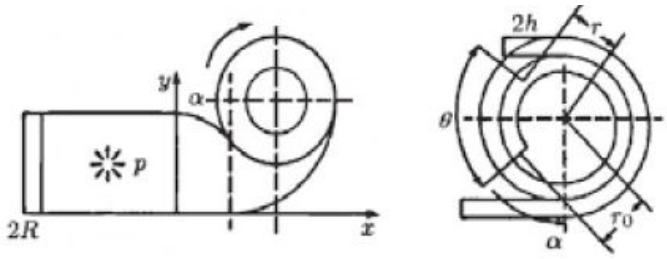

Figure 4.4. Geometry of the rolled structure

In turn, the moment of inertia is defined as:

$$I(s) = I_0(s) - I_1(s) + r^2(s)\rho 2\pi RHS$$

where I_0 is the moment of inertia of the unrolling tube about the center of the hub and I_1 is the transportation momentum that must be added since the center of rotation of the unrolling structure doesn't coincide with the center of mass.
Considering a variable inflation pressure value during boom deployment, some studies found out that the larger the pressure reduction factors, the slower the average deployment velocity. Furthermore, high velocity of deployment can lead to several

problems since at the end of the urolling process the structure is subjected to a shock. The higher the velocity, the greater the shock. Some kind of energy sinks (hook or loop strips) have to be considered to reduce the final velocity.
Another primary problem is buckling. A vertical hub force has to be applied in order to avoid buckling [86] [21].

The Z-folded is another important folding method widely studied in the recent years (figure 4.5). Several models were developed in order to solve its dynamic deployment: nonlinear hinge model, energy and momentum conservation model, fluid-structure integration model and control volume model.

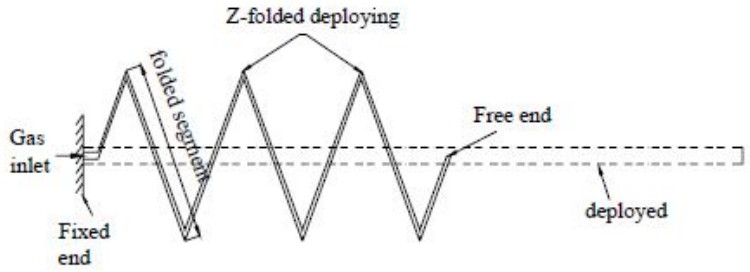

Figure 4.5. Deployment of a Z-folded solar array

In the following subsections, the control volume model and the non-linear hinge model of a z-folded boom are discussed.

4.2.1 Control volume model

An example of Z-folded, control volume model deployment method is described below.
The model consists of a rigid central blanket and two inflatable lateral booms (similar to ITSAT design). The inflatable booms are modeled as isotropic elastic material, while the blankets as rigid bodies. The lower support of the structure is fixed ($u = 0$, $v = 0$, $w = 0$) and the inflation velocity is constant. The booms are inflated thanks to inflow gas (figure 4.6).

The model adopted consists of discretization of the total volume into smaller finite volumes: the boom is separated into n gas chambers connected by $n - 1$ orifices. The chambers are divided into master and slave chambers (respectively MC and SC). The MC receives the gas pressure directly from the gas inlet. The Sc receives gas pressure from the previous gas chambers (figure 4.7).

Gas pressure inside a chamber is controlled by adjacent orifices. The gas flow is considered quasi-statics. The increase in volume for every chamber depends on the difference between outgoing and incoming mass flow. The equations in figure

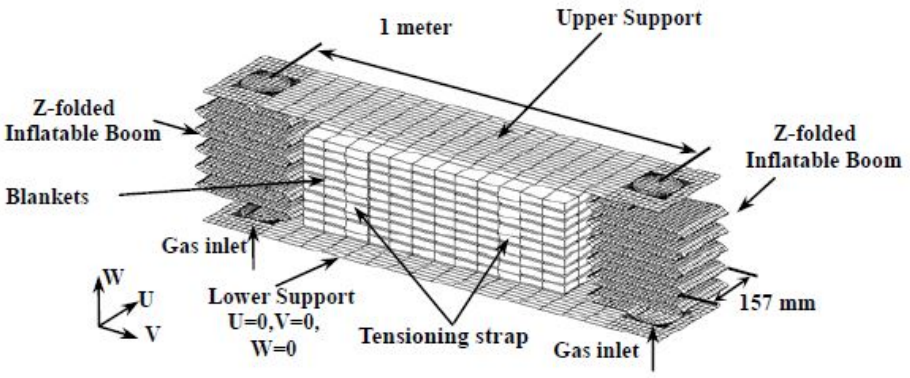

Figure 4.6. Model of the Z-folded solar array

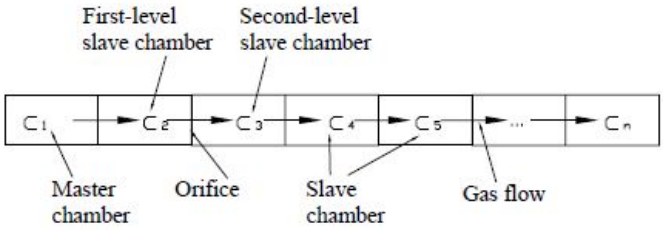

Figure 4.7. Control volume deployment model of the Z-folded solar array

4.8 can be used: O and A represent respectively the orifices and its areas, p_e is the external pressure out of the chamber, p_n and T_n are the internal pressure and temperature in the n chamber.

Knowing the mass in input and output, the gas energy E, mass density ρ and pressure p (through the equation state for an ideal gas) as function of time can be calculated, as shown in figure 4.9.

The pressure is used as input in the FEM analysis in order to determine the structural configuration at a certain time t. The resulting equation of motion is:

$$[M]\left\{\ddot{D}\right\} + [C]\left\{\dot{D}\right\} + [K]\{D\} = \{R^e\}$$

A series of tests show that, without a control restraint, the booms collide with the blanket. This phenomenon can lead to deployment instability, so a control restraint for the booms is needed. Another important result detected is the proportionality between inflation velocity and the impulse force produced by the upper support as soon as the inflation is ended [97].

$$\dot{m}_{in} = O_{n-1}A_{n-1}\frac{p_n}{R\sqrt{T_n}}Q^{1/k}\sqrt{2g_c\left(\frac{kR}{k-1}\right)\left(1-Q^{k-1/k}\right)}$$

$$\dot{m}_{out} = O_nA_n\frac{p_n}{R\sqrt{T_n}}Q^{1/k}\sqrt{2g_c\left(\frac{kR}{k-1}\right)\left(1-Q^{k-1/k}\right)}$$

$$Q = \frac{p_e}{p_n}$$

Figure 4.8. Gas flow equations

$$m_t = m_{t-\Delta t} + \Delta t(\dot{m}_{in} - \dot{m}_{out})$$
$$E_t = E_{t-\Delta t} + \Delta t c_p \dot{m}_t T_n$$
$$\rho_t = [m_{t-\Delta t} + \dot{m}_t \Delta t]/V_{t-\Delta t}$$
$$p_t = (k-1)\rho_t \frac{E_t}{m_t}$$

Figure 4.9. Calculation of mass, density, energy and pressure of the gas

4.2.2 Non-linear hinge model

In dynamic deployment model, the boom (or tube) is divided into k rigid segments connected by hinges provided of linear dampers and rotational, non-linear springs. Those two elements represent respectively damping moments and stiffness due to pressurization during deployment. One of the biggest difficulties of this model is to assign an adequate value of rotational stiffness to the springs.
Basically, this model can be treated as a multibody system with k second-order Lagrange's differential equation:

$$\frac{d}{dt}(\frac{\delta T}{\delta \dot{q}_k}) - \frac{\delta T}{\delta q_k} + \frac{\delta V}{\delta q_k} = Q_k$$

where T is the kinetic energy, V is the potential energy, q_k are the coordinates and Q_k the forces.
In order to solve this problem, the analogies between the deployment of an inflatable boom and the bending of an inflated cantilever structure subjected to an increasing tip load can be exploited. The assumption consists in seeing bending and deployment as opposite processes. In this way it is possible to make use of the

Bernoulli-Euler method, typically used to estimate the bending behaviour of solid elastic beams:

$$\frac{d^2y}{dx^2} = \frac{M + 2\nu pr^3 \sin\phi}{Etr^3[(\pi - \phi) + \sin\phi\cos\phi]}$$

where y is the transverse deflection, x is the longitudinal coordinate, p is the pressure level and ϕ is the half-angle that measures the wrinkling around the inflated structure.
The relationship between the fold angle θ, the restoring moment at an hinge point M and the pressure p is shown below:

$$M = \pi pr^3[1 - exp(\frac{-3.12Et}{p}\tan\frac{\theta}{2})]$$

This equation can be integrated in the Lagrange's system through the principal of virtual works or by calculating an equivalent spring constant function fo all the hinges.
An inflation model which consists in placing an orifice at each spring location and relationship between the orifice diameter and the θ angle are added to the global model.
Integrating the pressure rate equations with the angular displacement equations the problem can be solved [18] [19].

4.3 Structural considerations

The most important structural requirements to keep an eye on in the design of an inflatable solar array boom are: compressive buckling, beam stiffness, natural frequencies (both of the boom and of the blanket), beam bending buckling.
The geometric and material parameters that affects the requirements just shown are: the radius of the tube r, the length L, the elastic modulus E, the material density ρ and the thickness t.
The compressive buckling is divided in: short cylinder compressive, Euler and transitional buckling.
The first is proportional to the thickness and to the elastic modulus, while doesn't depend on the radius

$$P_{sc} = 1.2\gamma_r\gamma_c\pi Et^2$$

where γ_c is the compressive correlation factor andγ_r is the rigidization correlation factor.
The Euler buckling is affected by all the parameters except the material density:

$$P_e = \frac{\pi^3 E t r^3}{L^2}$$

Cylinders with large diameters are more resistant to buckling. This type of buckling strongly depends on the loading condition.
The transitional buckling is generated by the not perfect straightness of the tube once deployed. This phenomenon produces moments that leads to buckling at lower values.
Too high values of L/r lead to transitional or Euler buckling.

The equations used to estimate the stiffness k and natural frequency f_n are shown below:

$$k = \frac{3\pi E t r^3}{L^3}$$

$$f_n = \frac{1}{2}\pi \sqrt{\frac{3\pi E t r^3}{L^3(m_t + 0.23 m_b)}}$$

where m_b is the beam distributed mass and m_t the tip mass. The thickness doesn't affect the natural frequency. Furthermore, an increase in compression tends to lower the natural frequency value.

The bending buckling failure stress is characterized by the following equation:

$$P_b = \frac{0.6 c \gamma_r \gamma_b E t}{r}$$

where γ_b is the bending correlaction factor. Several types of external momentum can lead to bending buckling such as an angular acceleration applied by ACS (attitude control system) and the g-load due to translational maneuvers.
The bending stregth can be obtained equaling the stress due to g-load and the failure stress it obtained:

$$gload_{failure} = \frac{0.6 \gamma_r \gamma_b E t}{2\pi L^2 \rho}$$

The thickness or the elastic modulus have to be increased in order to avoid bending due to high g-load values. Alternatively, a less dense material can be used.

In conclusion, an high radius value is recommended. This lead to a twofold advantage: an increased natural frequency and stiffness, and a decreased possibility of Euler or transitional bending. The length of the boom makes it grow Euler

buckling, natural frequency and bending strength. However, for a larger need of power, long booms are unavoidable.
For those reasons, considering the length fixed, the best strategy seems to be having a larger radius in such a way to reduce the thickness and so the mass of the system [24].

Chapter 5

Inflatable reflectors

There are two types of inflatable reflectors used in space: antennas and solar concentrators. The two configurations have similar shapes, but have different applications. The former are charaterized by a RF transparency material (such as polymids), while the latter should be made of transparent materials in the infrared and visible range [14]. First of all, a typical parabolic reflector design will be described.

5.1 Parabolic reflectors

A typical inflatable reflector (figure 5.1) is composed by a thin reflecting-coated parabolic membrane and a specular transparent canopy. They are joined together with a flexible ring, in such a way as to form a parabolic lenticular structure. Thanks to radiative exchanges with the reflective membrane, the canopy has the task of reducing thermal gradients.

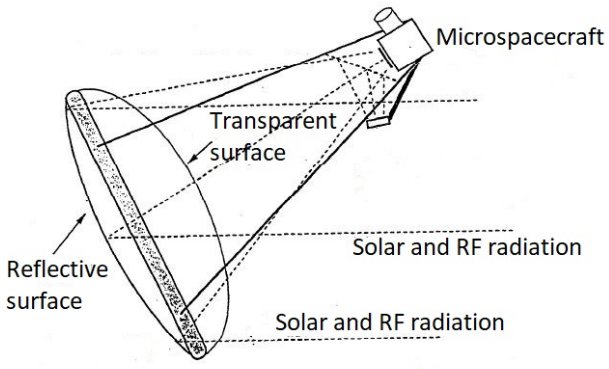

Figure 5.1. Concept of solar reflector

The lenticular structure is supported by a bending-resistant elliptical torus with

a circular cross section. The torus has to be rigidized reducing the risk of pressure losses due to punctures. The parabolic structure requires very low inflation pressure, so a rigidization process in not obligatory. Three inflatable trusses, usually made of thin aluminum shell, link the torus to the spacecraft.
A control system is needed to point the reflector in the direction of the sun (solar concentrator) or in direction of other space objects (antenna) during spacecraft motion [36].

As already mentioned, the reflective membrane of an inflatable parabolic reflector doesn't need rigidization since the inflation pressure is very low. However, some concepts involve a rigidization material for the reflector in such a way that the canopy can be removed after inflation, so eliminating the losses due to transmissions (figure 5.2). The efficiency of the system will result to be increased.

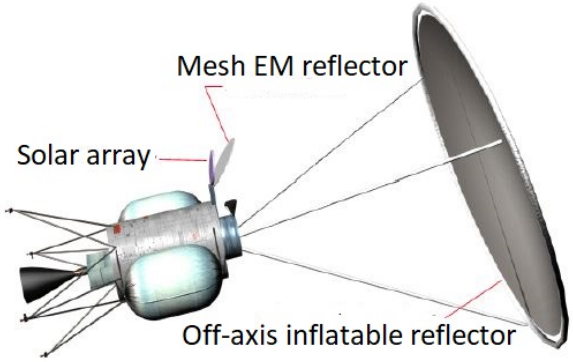

Figure 5.2. Concept of solar reflector without canopy

This choice allows not to carry make-up-gas to maintain inflation due to leaks, since the rigidization happens immediately after the inflation and is kept constant by this special material. So the rigidized reflector can keep its shape without continuos pressure inflation.
Several methods are studied for mechanically removing the canopy. One of them uses voltage-release epoxy adhesive: after inflation, a voltage is applied at the adhesive in order to make it lose its adhesive force. Another method involves the use of a mechanical tear strip [77].

Another alternative configuration involves the removal of the torus (figure 5.3). In this concept, three region are identified: the parabolic caps (operational part), a central parabolic region and a transition zone between them.

The central parabolic region isn't subjected to hoop stresses, and so is characterized by wrinkles. The condition of second-order continuity between the caps and the central region is not respected: there isn't continuity in the curvature ratio $\frac{k}{k_c}$, where k and k_c are the meridional and circumferential curvatures). For this reason,

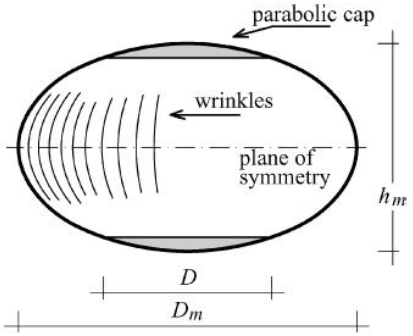

Figure 5.3. Concept of torus-less inflatable reflector

a transition zone is needed since the two parabolic regions are incompatible. In order to have a weight and shape efficient structure, the transition contour have to be short and the the parabolic caps have to be as deep as possible (high $\frac{f}{D}$ ratios) [35].

5.1.1 Paraboloid shape

The shape of the reflecting surface is usually defined by the intersection between a paraboloid and a cylinder, as shown in figure 5.4.

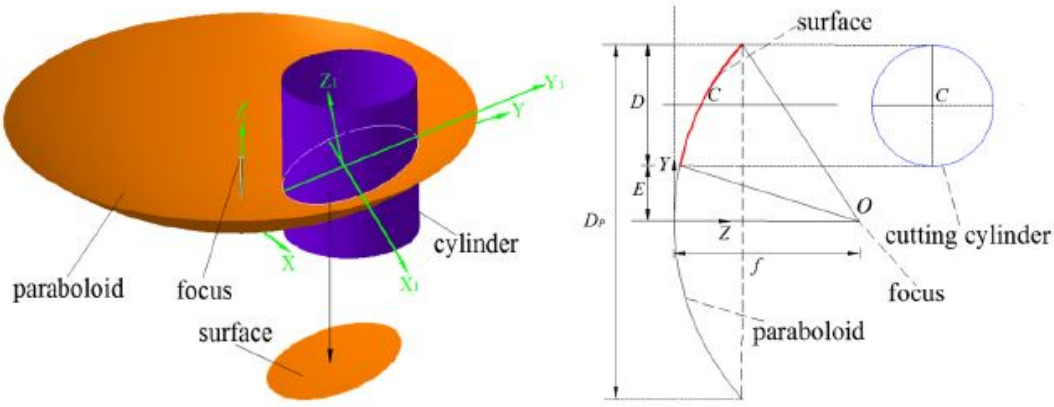

Figure 5.4. Three-dimensional (left) and bidimensional (right) reflector surface

The system of equations characterizing the paraboloid is the following:

$$z = \frac{x^2 + y^2}{4f}$$

$$x^2 + [y - (E + \frac{D}{2})]^2 \leq \frac{D^2}{4}$$

where f is the focal length, D is the diameter of the cylinder [93].

5.1.2 Reflector membranes

A reflector membrane must have a surface as accurate as possible in order to reach high radiation concentration levels. An accurate design of the reflector based on patterns (gores) and seams have to be developed, so that, once inflated, the reflector has exactly the three-dimensional parabolic shape expected.

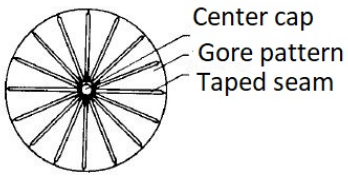

Figure 5.5. View of gore and seam pattern

The seamed gores (made of flat, thin plastic sheet), once pressurized, are subject to an elastic deformation that brings them to take the designed paraboloid shape. Even small errors in the initial gore shaping can lead to an improper shape of the membrane. Determining the initial shape (uninflated) of the gore is complicated: the deformation is a function of the material, inflation pressure and geometry. In particular, in a membrane structure, the elastic modulus is not constant in the entire structure, but varies with the stress levels. This leads to a difficult predictation of the expansion of the gores and so to surface distorsions [88].

Remembering that the gores are identical and usually pie-shaped, a first approximation calculation in order to estimate the uninflated shape of the gores is given by the following equations:

$$dc = dc'(1 + \frac{S_H - \nu S_M}{E})$$

$$ds = ds'(1 + \frac{S_M - \nu S_H}{E})$$

$$S_M = \frac{pR_H}{2t}$$

$$S_H = (\frac{pR_H}{2t})(2 - \frac{R_H}{R_M})$$

where dc and ds are the arc element in the circumferential and meridional direction of the pressurized paraboloid, dc' and ds' are the arc element in the uninflated

body, S_H and S_M are the stress in the circumferential and meridional directions, R_H and R_M are the radius of curvature respectively in the circumferential and meridional directions.
Once defined materials, thickness and inflation pressure, the system can be solved.

5.1.3 Surface accuracy of the membrane

Thermal loads, boundary loads and intertial loads can reduce seriously the reflector surface accuracy. A reduction in accuracy leads to reduced performance of the inflatable membrane, so it is important to better understand which parametres affect the accuracy in order to optimize the system.
Shape errors are heavily influenced by thermal gradients. For decreasing thermal gradients, the shape accuracy results to be increased. MLI insulation or emissive coatings can be applied on reflector to avoi large thermal gradients. Alternatively, a material with lower values of thermal expansion coefficient can be considered.
Using very low inflation pressure values can also reduce surface errors: the lower the pressure, the lower the stresses induced, the more accurate the surface (figure 5.6)[20].

Construction	Conditions	$\varepsilon_{RMS}(\Omega_R)$	ε_{RMS} for $p_0 = 10.0$ Pa	ε_{RMS} for $p_0 = 12.5$ Pa	ε_{RMS} for $p_0 = 25.0$ Pa
Gores	14 Gores	4.6484	2.7030	2.5675	1.7947
	16 Gores	3.6082	2.0223	1.9020	1.2119
	18 Gores	2.8808	1.4564	1.3342	0.7590

Figure 5.6. Influence of inflation pressure on surface accuracy

Other two parameters that heavily affect the shape error are material film thickness and elastic modulus, as shown in figure 5.7.
As concerns the latter, materials with higher elastic modulus show better surface performance (figure **??**). However, increasing too much the module could affect the packagability and the thoughness of the reflector. Increasing the material thickness, the surface accuracy can be improved (figure 5.7). However, increasing too much the thickness leads to lower membrane stresses and lower first mode frequencies, given by the following expression:

$$f = \frac{0.766}{D}\sqrt{\frac{\sigma}{\rho}}$$

where D is the diameter, σ is the stress and ρ is the material density.
The membrane reflector needs to provide stiffness. The resulting stiffness of the reflector will be reduced with the increase of the thickness [74].

Film Thickness mm (mil)	RMS Error (mm)	Peak-to-Valley Distance (mm)
0.025 (1)	0.49	2.60
0.050 (2)	0.35	2.07
0.076 (3)	0.28	1.73
0.101 (4)	0.23	1.47
0.127 (5)	0.20	1.27

Modulus of Elasticity, E Mpa (ksi)	RMS Error (mm)	Peak-to-Valley Distance (mm)
793 (115)	0.36	2.09
1,482 (215)	0.25	1.58
2,172 (315)	0.20	1.27
3,447 (500)	0.14	0.96

Figure 5.7. Influence of material thickness (left) and material modulus (right) on surface accuracy

An important parameter to evaluate the accuracy level of the surface is the slope error. It is defined as the difference angle between the vector normal to the reflector surface and that normal to the designed paraboloid. The less this angle, the more accurate the shape of the surface (compared to the designed one). Furthermore the surface precision (RMS slope error) is related directly to the number of gores: the more the gores, the less the surface error, as shown in figure 5.8.

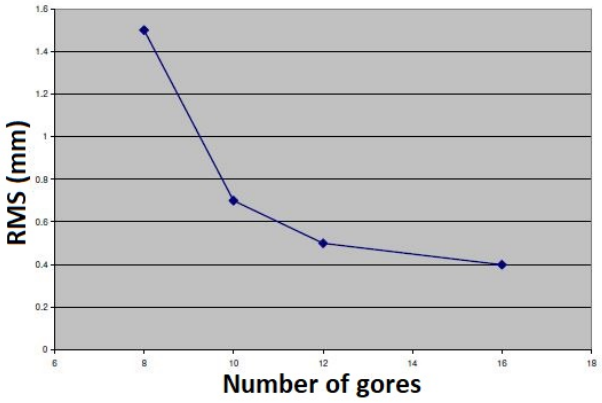

Figure 5.8. Slope error as function of the number of gores

The desired RMS accuracy is often set at the beginning of the design, so, also considering the effect of manufacturing errors, the minumum number of gores that ensures the desired accuracy is chosen [77] [36].

5.1.4 Rim-supporting torus

The pressure over the parabolic reflector and the canopy produces a load that is sustained by the torus shape rim-support. The torus has to be characterized by high rigidity, since it has to withstand deformations. Thanks to the torus, the reflector membrane maintain its shape.

The torus, having an elliptical shape, is submitted to non-uniform loads that can lead to bending in its plane.

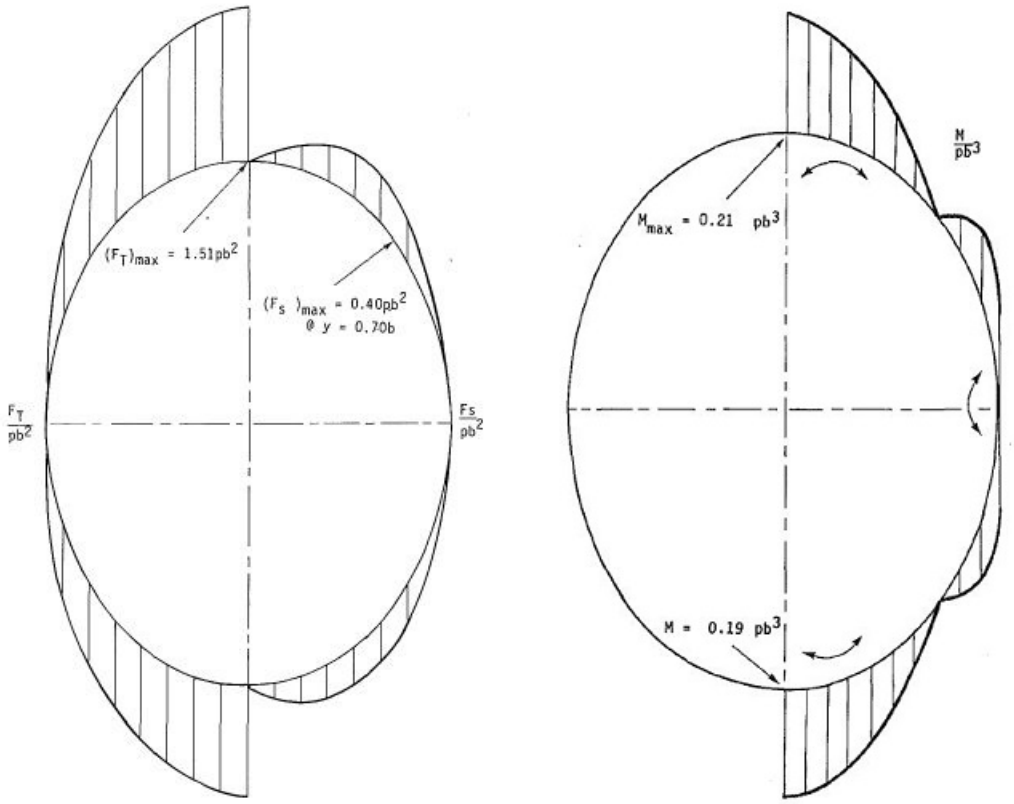

Figure 5.9. Distribution of shear forces and compression forces (left) and internal moments (right) along an elliptical ring

Some studies demonstrate that the tension caused by the membrane reflector on the torus is directly proportional to the product between reflector inflation pressure p and semi-major axis of the torus ($\propto pb$). Since the reflector is designed to maintain a certain value of tension so as to reduce wrinkles, we can assume that designing larger reflectors leads to a reduction in the inflation pressure. However, at the same time, increasing the size, forces and moments transmitted to the torus increase. Indeed, the former are proportional to $\propto pb^2$, while the latter are porportional to $\propto pb^3$.
The compression loads result prevaling on the shear loads and can cause extremely danger bending moments. Furthermore the part at the top end of the elliptical configuration is the most stressed and is therefore the most subjected to bending moments (figure 5.9).
Once established material, torus cross section and all the forces and moments at play, a deformation analysis is needed.

Primarily the bending moment and secondly the compression load cause a change in torus length and radius. The deformations are proportional to $\propto \frac{pb^5}{EI}$ and the maximum is at the top end.
The deformation values have to be minimal in order not to distort the reflector surface, so an accurate evaluation of dimensions, materials and inflation pressure have to be done [36].

5.1.5 Dynamic behaviour

During a preliminary design, the use of an analytical model with adequate approximations is of crucial importance for the study of a thin membrane.
Studying the dynamic behaviour with a classical finite-element method means falling back into an excessive amount of storage capacity and run time to obtain solutions. Indeed, the extremely low thickness, that characterizes thin polymide films used for inflatable structures, can cause a non-convergence of the non-linear static analysis (material non-linearity due to the variation of the elstic modulus as function of inflation pressure, temperature and frequency). [84] [53].
In this section an analytical method to evaluate the dynamic behaviour (natural frequencies and modal shapes) of a classical lenticular inflatable reflector supported by a torus is described. Several simplifications are assumed: constant pressure, small vibrations and absence of interaction between the inflation pressure gas and the membrane.

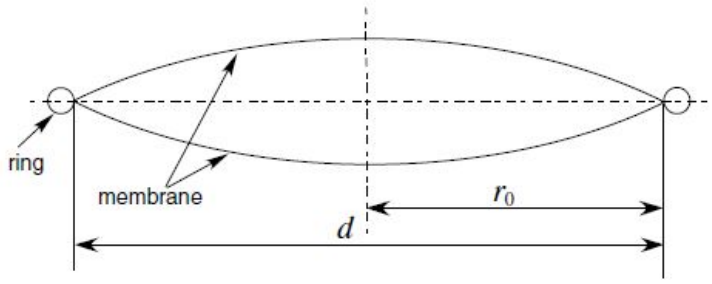

Figure 5.10. Mechanical model of the inflatable concentrator

Firstly, the prestresses of the inflated membrane have to be calculated.
Applying the membrane theory of shallow shells, the static equilibrium equations can be written:

$$\frac{d}{dr}(rN_1^0) - N_2^0 = 0$$

$$\frac{N_1^0}{R_1} + \frac{N_2^0}{R_2} + p = 0$$

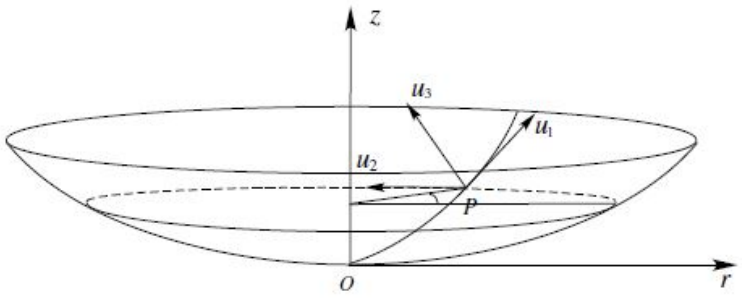

Figure 5.11. Coordinate system of the paraboloid membrane

where N_1^0 and N_2^0 are respectively the inflation pre-tension forces in the meridional and circumferential directions, R_1 and R_2 are the radii of curvature in the two directions. If the shape of the paraboloid is known, the values of the two radii of curvature can be calculated and, then, substituted in the static equations. Thus, the values of the pre-tension forces and stresses can be calculated:

$$N_1^0 = N_2^0 = N^0 = -pf$$

$$\sigma_0 = -\frac{pf}{h}$$

where p is the inflation pressure, f is the focal length of the paraboloid and h is the thickness of the membrane.
For evaluating the dynamic stability, since the parabolic membrane is a geometric non-linear problem, the prestress values have to be incorporated into a set of non-linear equations together with compatibility equations. Applying a linearization, considering the assumptions initially made (small vibrations), the equations of motion for transverse free vibration turn out to be the following:

$$N^0 \nabla^2 u_3 + \frac{1}{2f} \nabla^2 \phi = \rho h u_{3,tt}$$

$$\frac{1}{Eh} \nabla^4 \phi + \frac{1}{2f} \nabla^2 u_3 = 0$$

$$\nabla^2 = \frac{\delta^2}{\delta r^2} + \frac{1}{r} \frac{\delta}{\delta r} + \frac{1}{r^2} \frac{\delta^2}{\delta \theta^2}$$

where E is the Young modulus, ρ is the mass density, u_3 is the membrane normal displace component, ϕ is the Airy stress function and ∇^2 is the Laplacian operator. Applying the boundary conditions the system of equations can be solved, thus obtaining the normal displacement u_3 and the Airy stress function ϕ.
The meridional and circumferential displacements, respectively u_1 and u_2 can be calculated starting from the strain components ϵ_1 and ϵ_2, given by Hooke's law:

$$\epsilon_1 = \frac{1}{Eh}(N_1 - \nu N_2)$$

$$\epsilon_2 = \frac{1}{Eh}(N_2 - \nu N_1)$$

whit

$$N_1 = \frac{1}{r}\frac{\delta\phi}{\delta r} + \frac{1}{r^2}\frac{\delta^2\phi}{\delta\theta^2}$$

$$N_2 = \frac{\delta^2\phi}{\delta r^2}$$

Substituting the ϵ_1 and ϵ_2 values just calculated, the meridional and circumferential displacements u_1 and u_2 are determined through the following geometric expressions:

$$\epsilon_1 = \frac{\delta u_1}{\delta r} - \frac{u_3}{R_1}$$

$$\epsilon_2 = \frac{u_1}{r} + \frac{1}{r}\frac{\delta u_2}{\delta\theta} - \frac{u_3}{R_2}$$

All the displacements determined are in the following form:

$$u_1 = U_1(r)\cos n(\theta - \psi)e^{j\omega t}$$

$$u_2 = U_2(r)\sin n(\theta - \psi)e^{j\omega t}$$

$$u_3 = U_3(r)\cos n(\theta - \psi)e^{j\omega t}$$

Once the paraboloid displacement and stresses are calculated, the torus behaviour has to be studied. Indeed, the forces acting on the paraboloid membrane cause a deformation of the torus.
The interaction forces between the membrane and the torus, that are functions of the paraboloid internal force N_1, cause a radial distributed load q_r and a transverse distributed load q_z on the torus. The former causes an in plane vibration, while the latter an out of plane vibration of the torus.

The torus displacements can be calculated and have the following form:

$$u = U\cos n\theta e^{j\omega t}$$

$$v = V\sin n\theta e^{j\omega t}$$

$$w = W\cos n\theta e^{j\omega t}$$

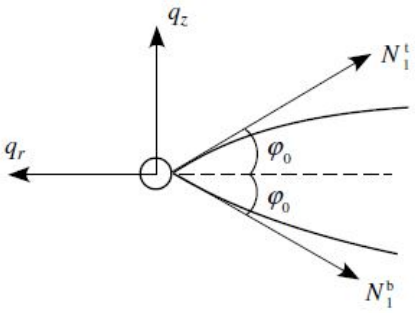

Figure 5.12. Force balance between the paraboloid and the torus

Substituting the found displacement both of the torus and the paraboloid into the boundary condition generates a system of homogeneous equations. The roots of this system represent the natural frequencies of the structure. Doing a backward substitution the modal shapes can be determined.
The values calculated with this analytical method and the FEM analysis are very similar. The level of accuracy results to be proportional to the ratio between the focal length and the aperture of the paraboloid ($\propto \frac{f}{d}$) [61].

5.2 Solar concentrators applications

The aim of a solar reflector is to focus solar radiation, so as to increase energy density.
An application of inflatable solar reflectors is solar thermal propulsion: solar radiation is collected and focused into the absorbers of the thruster whose propellant (generally hydrogen) is heated and then expanded through a nozzle without ignition or combustion. Hydrogen engines need a large amount of energy, but, thanks to their high specific impulse, allow to save mass in comparison with chemical propulsion. The effectiveness of this application increases for long-term missions [53]. Another application involves to focus solar radiation on a conversion device such as a photovoltaic array in order to generate high power levels. Conventional photovoltaics have low efficiences, so they require large surfaces to collect high energy levels. That increase the spacecraft drag and weight. [16]

Solar reflectors become of fundamental importance when the distance from the sun increases, for example for a Mars mission. Indeed, the quantity of incident solar radiation decrease rapidly with the distance from the sun ($\propto 1/d^2$), as shown in figure 5.13.

For a mission in proximity of the Earth, the incident radiation is about $1.2kW/m^2$.

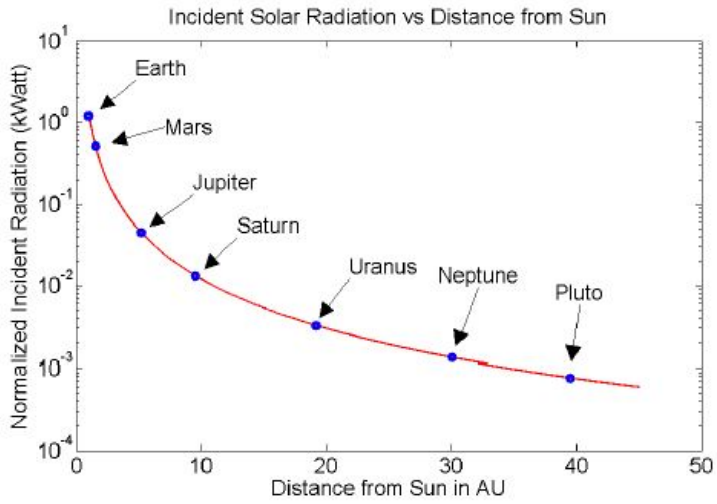

Figure 5.13. Incident solar radiation as function of distance from the sun

On Mars, the incident radiation falls to about $0.52kW/m^2$. This means that, in order to capture the same power, the photovoltaics of a spacecraft sent to Mars should be doubled in size.
In order to minimize masses and costs a solar reflector is needed for missions which involve moving away from the sun [25].

5.3 Antenna applications

The need to design large (high gain), lightweight, low-cost antennas for Radio Frequence (RF) applications brought to the development of inflatable refeclor antennas. Indeed, classical antenna concepts, especially large ones, are mechanically very complex, expensive and have low reliability.
Almost all the applications require a large antenna size: mobile communication (L-band, $1.5GHz$ with aperture of 10-20 metres or Ka-band, $20-30GHz$ with aperture of 4-8 meters), earth observation ($6-20GHz$ with aperture of 20-40 metres), active microwave sensing, orbiting very long baseline interferometry ($43-60GHz$ with aperture of 20-25 metres), DoD space based radar ($1.5-2.5GHz$ with aperture of 20-30 metres).
Using inflatables, large antenna dimensions with low costs, low weights and low storage volume can be developed. However, the higher the antenna band frequency, the higher the surface accuracy must be. In order to use inflatable antennas for higher frequencies applications, several efforts to improve surface accuracy of inflatable antennas have to be done [43].

The first inflatable reflector antenna concept in space is the Inflatable Antenna Experiment (IAE), developed by L'Garde in the late nineties. It was composed of a reflector membrane and a canopy (lenticular structure) joined to a torus, as described on previous paragraphs.

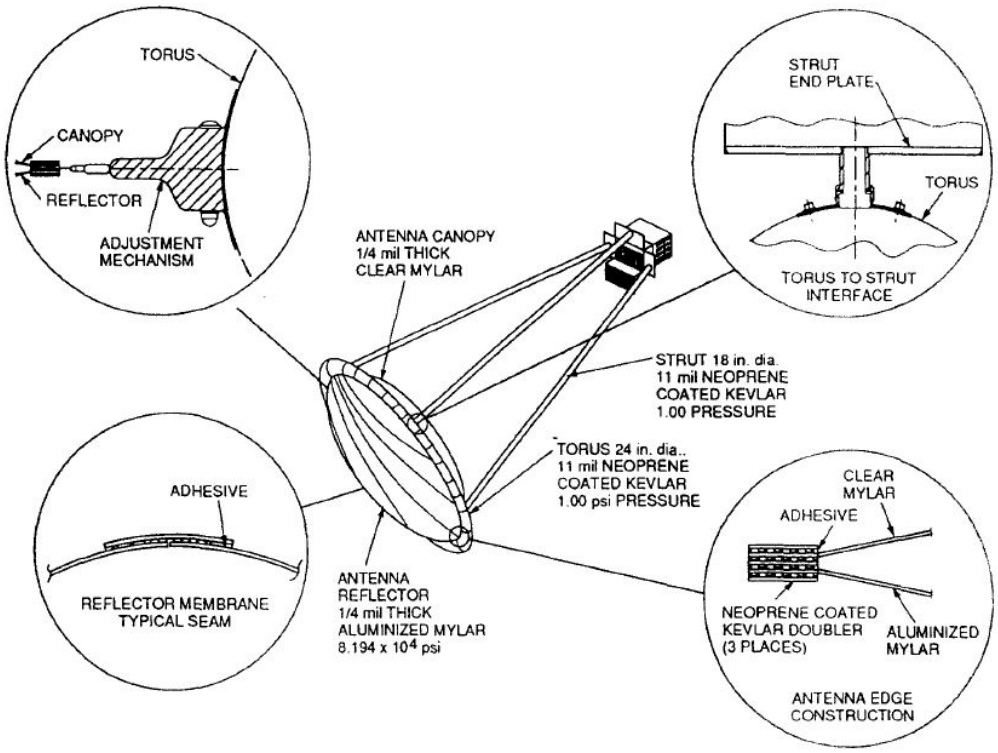

Figure 5.14. Design of the IAE antenna

The canopy was made of clear Mylar, while the membrane of aluminized Mylar. The two bodies were connected through neoprene coated Kevlar. This material is also used for the torus (figure 5.14) [32] [91]. The IAE was a great historic milestone, since it was the first inflatable structure put into orbit. It demonstrated that new technologies based on inflation and deployment mechanisms were feasible.

In the early 2000, an hybrid inflatable dish antenna (HIA) concept was developed by ILC Dover (figure 5.15). The HIA is a mix between the traditional rigid parabolic and the innovative inflatable reflector technologies. It consisted of a central rigid antenna and a inflatable rigidizable reflector annulus.

In case of deployment system failure, the rigid antenna would have worked the same way. In other words, the rigid central antenna behaved like a backup system. Once inflated, the system didn't need a make-up gas to keep its shape. An inflatable and rigidizable torus was used to keep the annulus tensioned [34] [100].

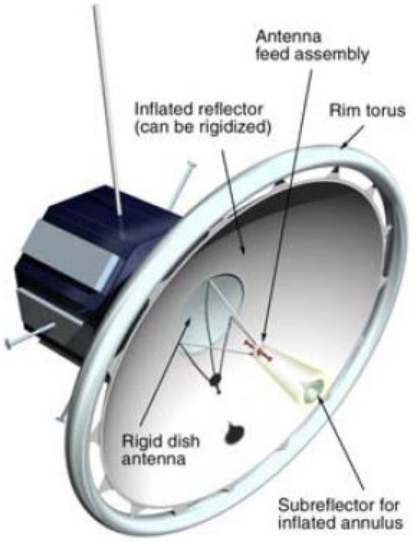

Figure 5.15. Design of the HIA

Other concepts involve the use of reflectarray antennas: they provide wider angle beam scanning, but shorter bandwidth than parabolic reflectors. For those type of antennas is simplier to maintain an high surface accuracy rather than for parabolic ones. Reflectarray antennas are made of inflated torus tubes supporting and tensioning a flat thin-membrane reflective surface. The two elements are linked by tension cords and attachment points.

Some concepts, as ILC Dover and L'Garde L-Band SAR arrays for remote sensing, involve a rectangular frame. The ILC Dover tubes are made of urethane coated Kevlar compared to rigidizable stretched aluminum of L'Garde ones. The membrane are, in both cases, made of a clopper cladding on Kepton.
Another similar concept, the JPL and ILC 3-meters Ka-Band reflectarray for telecom applications, involve a horse-shoe shape frame made of urethane coated Kevlar and a membrane made of Uplex (polymide). The horse-shoe shape reduced wrinkles of the membrane [40].

Other 3-meters Ka-Band reflectarray antennas were developed, such as the "Movie Screen" (figure 5.16). In the undeployed configuration, the flattened booms of the "Movie Screen" are rolled up on two mandrels, while the membrane was rolled up on a composite cylinder.

The deployment process (figure 5.17) is made of two phases: the unrolling phase and the pressurization phase. The feed of the system is placed near the spacecraft in order to reduce thermal gradients. The inflatable booms of "Movie Scream"

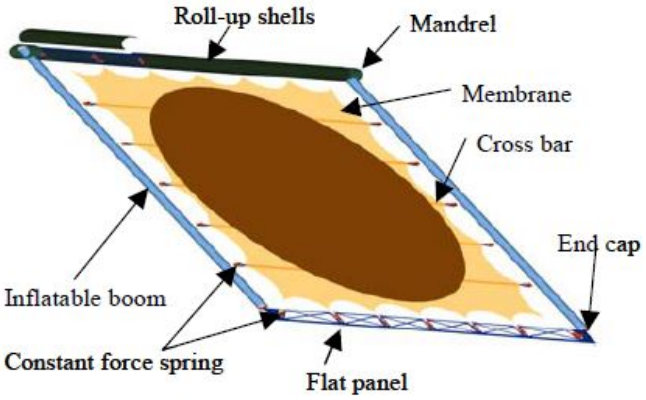

Figure 5.16. "Movie Screen" reflectarray antenna concept

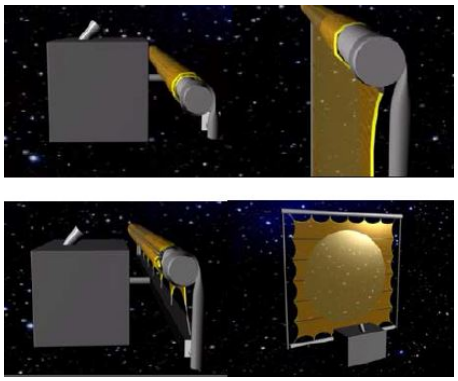

Figure 5.17. Deployment process of "Movie Screen"

were self-rigidized through the Spring Tape Reinforced (STR) aluminum laminate method in such a way that no make-up gas were needed [41].

More advanced concepts involve the development of a annular ring 10 meters X/Ka dual-band reflectarray antenna (figure 5.18). The X-band is used for uplink signals, while the Ka-band for high data rate downlink.
The membrane is made of three layers: an outer layer of X-band elements and a layer of Ka-Band elements (figure 5.19).
The spacing between the layers is fundamental for the performance of the double antenna: the layers are kept some distance with a single side foam and a Kapton spacer. The former avoids the excessive approach of the membranes, while the latter avoids the excessive separation.

The STR aluminum laminate concept has been used to reinforce the booms of the dual-band antenna. The antenna is folded through a Z-folding method.
An innovative type of catenary system to tension the membrane was developed:

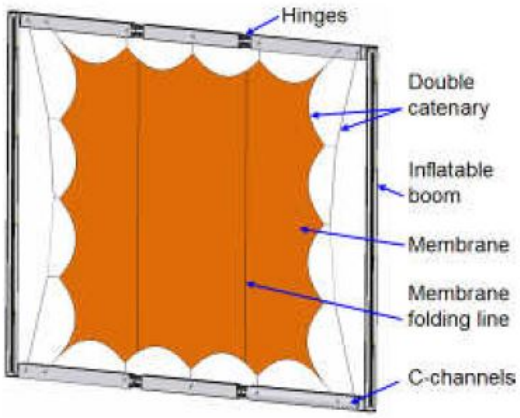

Figure 5.18. Dual-band reflectarray antenna concept

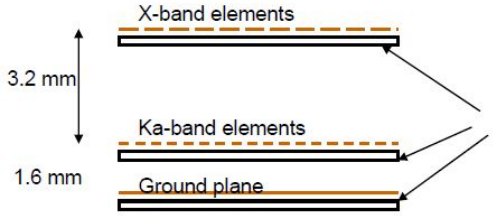

Figure 5.19. Dual-band reflectarray antenna lineup

the classical, difficult to fold, cross bars, were replaced by a double catenary system consisting of outer and inner catenaries [29] [30].

Most recent application involve using inflatable antennas for Cubesats. The antennas actually implemented in Cubesats (such as dipole or patch antennas) has a very low gain and low data rates. For this reason, they can't be used in orbits except for LEO orbit. Inflatable antennas enables higher gain, higher data rates and would require low storage volume, making the Cubesat usable even in GEO and deep space.

The antenna gain is related to the diameter through this equation:

$$G = \frac{\pi^2 D^2 \eta}{\lambda^2}$$

Furthermore the antenna gain is closely related to data rates, so, the high aperture that can be reached with inflatable antennas will increase data rates. As can be seen in figure 5.20, a 1-meter inflatable parabolic dish antenna provides very high data rates than a classical 1-meter microstrip antenna.

An inflatable parabolic dish antenna concept made of two parabolic membranes was developed for Cubesat applications. The reflective membrane is made of Mylar

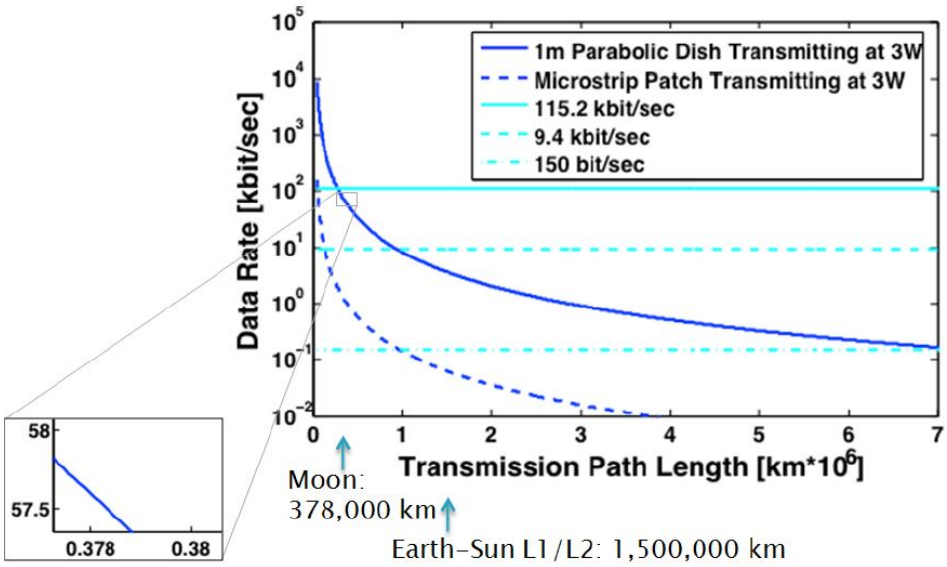

Figure 5.20. Data rate as function of path length comparison

coated with vapor aluminum (conductive coating) and the canopy is a RF transparent Mylar membrane connected to the Cubesat bus. The canopy and the reflective membrane form a lenticular structure. A circular metal wire hoop structure is positioned between the two paraboloids in order to provide structural integrity and shape accuracy.

Other alternative concepts that involves a cylindrical or a conical canopy were studied. The cylindrical shape seemed to have the highest peak gain.
Sublimating powder provides the inflation and continues to maintain the desired pressure inside the antenna.
This concept was thought for a S-band antenna, but can be extended to a X-band antenna. Indeed, for interplanetary explorations, higher frequencies are requested [4] [5].

5.4 Critical aspects

The most critical aspects involving inflatable antennas are buckling, deployment method and thermal loads, other than the already named surface accuracy.
According to the STR aluminum laminate self-rigidize method, four spring tapes are attacched in axial direction to the booms, increasing their modulus of elasticity. Therefore, this method increase significantly the buckling capability, allowing to design longer booms without running into buckling.

Thermal loads and buckling are closely related.
A structural analysis to evaluate structural integrity (static and dynamic), deformations and surface distorsions of the antenna is needed. In particular, a non-linear dynamic analysis (static, modal and response analysis) to evaluate the response of the structure under thermal and mechanic loads (inflation pressure, pretension loads and wrinkling) has to be considered. Problems related to vibrations, and so damping, have to be studied [41].

5.4.1 Thermal loads

The booms used to sustain an antenna structure are usually made of a self-rigidizable aluminum laminate (a layer of aluminum between two layers of Kapton). The extreme thermal loads encountered in the space environment can cause the distorsion of the booms and vibrations. Since solar rays often radiate only a side of the structure, the boom are subjected to hard bending that can lead to a loss of buckling strength.
It is important to estimate the thermal distribution on the boom and to study the consequent deflection due to bending. At the end, a buckling analysis should be done. A finite element model with solar heat flow and material properties as input have to be developed to analyze the temperature distribution, followed by a static analysis to calculate deformations. At the end a buckling analysis of the deformed booms is requested to confirm the integrity of the structure.

As concerns an antenna application, the RF behaviour of the reflective membrane under thermal (rather than mechanical) loads has to be studied. Indeed, the membrane tensioning (due to pressure inflation), induces much less deformations on the boom with respect to thermal loads. Thermal deformations on the booms cause the deflection of the reflective surface that lead to the antenna malfunction [31].

5.5 Materials used

Considering the paraboloid shape of an inflatable reflector presented in the previous paragraphs, both the torus and the lenticular structure are usually made of Kapton polymide films. A layer of Silicon-backed Kapton is used to bound the canopy to the reflective membrane. Kapton is often chosen since it can effectively shield the reflector from atomic oxigen and from UV.
A particular reflective coating is used to collect radio waves (in the case of an antenna) and to collect solar energy (in the case of the concentrator) [84].

As concerns the antennas, several methods are studied to make the polymide

materials reflective to RF in the past: Vacuum Depositing Aluminum (VCA), reflective RF paintings, electroless silver coating. The former is the best one but is very expensive and not effective on large reflectors, while the other two techniques have poor durability.
In the recent years other methods have been evaluating such as incorporating a wire mesh reflector material into the polyimide during the casting process, filling the polyimide with milled metallic material (aluminum or silver) or electroless silver plating. The former option was eliminated since increases the permeability (higher gas losses) and orthotropicity (greater shape unpredictability) of the reflector. The third method has very low costs but there are difficulties to join the polyimide surface. Finally, the second technique results to be the most performing one, with low costs, high scalability, simplier manufacturing and reduced thermal expansion coefficient [74] [43].

For designs that involve removing the canopy, a rigidizable material is needed. The two most used rigidizable materials in this field are: aluminum/plastic laminates and Kevlar/thermoplastic elastomer composites.
The former are made of thin plastic films and aluminum foil. The working principle is as follows: during deployment, the inflation pressure stretches the thin membrane so that the aluminum is in the plastic region and the plastic is in the elastic region. In that way, the aluminum works as a stiff shell.
The latter is rigidized bringing the temperature below the glass transition temperature (T_g) of the material [77].

Chapter 6

Solar sails

Solar sails are a propulsion space method that exploit sunlight radiation pressure in order to obtain thrust and directional changes. Solar photons beat on a large mirror and produce thrust and directional changes through momentum exchange.
The advantage of solar sails is the infinite specific impulse: no propellant is needed (the propellant is the sunlight).
However the forces produced by solar photons are very low ($9N/km^2$ at 1 AU), large mirrors of hundreds of meters are needed to obtain an acceptable thrust. This is where it comes to play inflatables: large dimensions with small costs and weights can be achieved with an inflatable solar sail.
Solar sails can be used for several missions, such as interplanetary missions, where a large amount of propellant should be carried on the spacecraft, or for station-keeping manouvers. Unfortunately, the major drawback of this type of propulsion is the low thrust, and so, the extended mission time. For this reason they can't be used for manned missions.

6.1 Design concepts

One of the first inflatable solar sail concept dates back to the late 90s. An inflatable torus was used for supporting the thin-sheet aluminized plastic material of the sail and inflatable booms were used to connect the torus with the payload (figure 6.1). The torus and the booms provide structural rigidity to the system. Fly swatter vanes are rotated to maneuver the sail through differential solar pressure [33].

Another concept developed by NASA LaRC involved a scalable square sail supported by inflatable booms (figure 6.2). The sail is made of Kapton polymide film, while the boom, sealed between two rigid endcaps, is made of polyethylene.

A striped architecture, achieved attaching periodically the sail to the boom is used. The compressive loads the booms have to withstand, due to tensile stresses

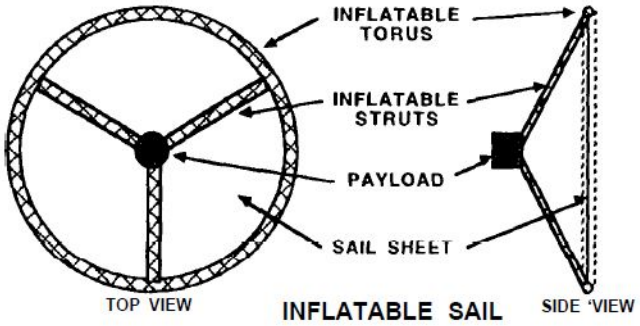

Figure 6.1. Solar sail concept

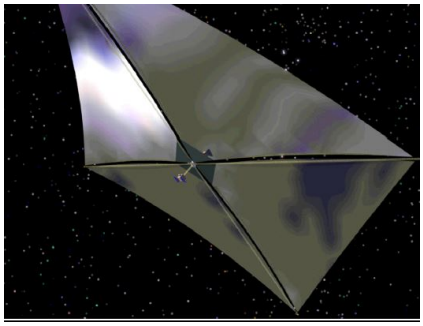

Figure 6.2. NASA LaRC solar sail concept

in the membrane, are applied on the attachments rather than at the global tips of the booms. In that way, the compressive loads are applied on shorter distances so as to reduce Euler buckling problems. Furthermore the bending moments result to be distributed rather than concentrated at the tips of the booms. This design allows to have a thiner cross sections and thus minor weights.
The beam is made of two elements: the inflatable boom and the sun side spreader system. The latter is added to reinforce the boom against bending due to solar flux beating the membrane.
The booms consisted of longitudinal and lateral fibers, forming a grid to withstand compressive and inflation loads.
The booms are rigidized after deployment through the sub-Tg method: fibers are impregnated with a resin that increase its modulus below the glass transition temperature.
A conical inflation deployment is selected for this design. It ensures an higher control and reliability.
The sail is composed of chords suspended between the boom's attachments. A Mylar membrane laids on them. This design stabilizes the sail against solar flux and

maneuvering loads.
The attitude control and force orientation is provided through control vanes integrated in the tips of each boom. The vanes provide 3-axis control rotating around the boom axis [54] [64].

6.2 Aerial density

The principal parameter that characterizes a solar sail is aerial density, that is the weight to surface ratio (g/m^2). The higher the aerial density, the higher the acceleration (solar pressure divided by aerial density). The aerial density depends on the thickness of the sail and the supporting structure.
Values of aerial density for an inflatable solar sails vary from 70 to 8 g/m^2.

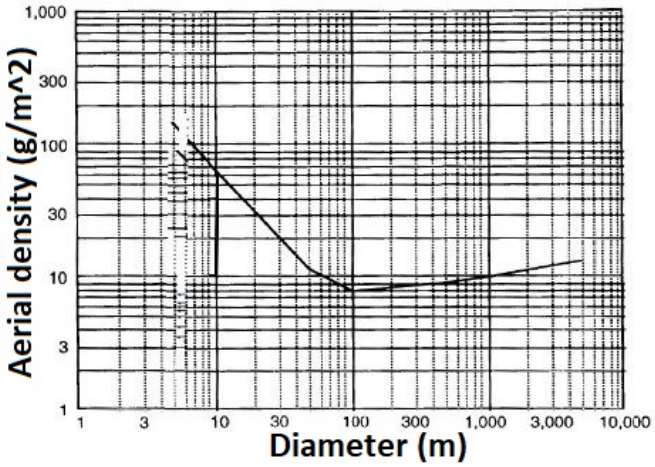

Figure 6.3. Aerial density as function of sail diameter

For small sails the aerial density is very high because of torus manufacturing problems. The minimum aerial density is obtained for sails around 100m in length. For larger sails (order of kilometres) the aerial density increase since the torus has to be reinforced to avoid buckling.
Once established the dimensions of the sail and its aerial density, the acceleration can be calculated. Considering the solar pressure at 1 AU the acceleration can be found as follows:

$$T = 9\mu N/m^2 * Sail_{area} * Reflectivity$$

$$Sail_{mass} = aerialdensity * Sail_{area} + m_{pl}$$

$$A_c = T/Sail_{mass}$$

where m_{pl} is the payload mass.
Once established the acceleration of the system, an approximation of the time mission, based on the trajectory considered, can be calculated. The lower the acceleration (small diameters), the greater the time.

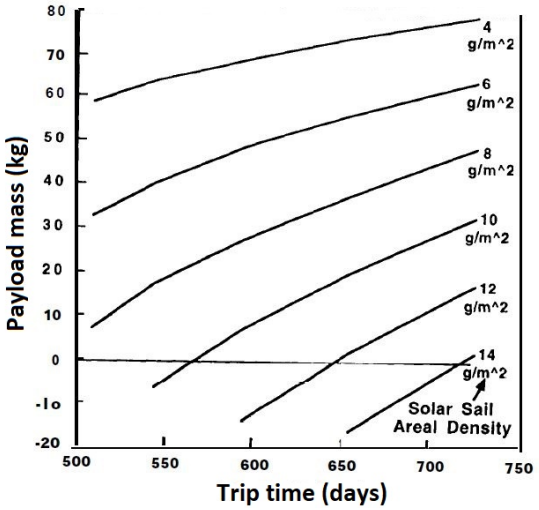

Figure 6.4. Payload mass as function of trip time and aerial density

Furthermore, it can be seen in figure 6.4 that higher aerial density values strongly reduce the payload mass (if considering the same trip time) [33].

The trend for the future is to lower as much as possible the aerial density value for inflatable solar sails.
Last technologies involving the use of sub-Tg rigidizable booms, striped sail architecture and conical deployment can lead to aerial density values of $4.8 g/cm^2$, as shown in figure 6.5.

6.3 Deployment

The deployment of a solar sail has to be as accurate as possible in order to avoid destabilizing effects. Indeed, a wrong deployment, for example due to delays in inflation time of the booms, can lead to asymmetries or vane failures. A geometric asymmetry will cause the shift of the sail center of pressure with respect to the spacecraft center of mass. This shift in turn will cause asimmetry in thrust and therefore a change in the sailcraft attitude. In case of errors in the deployment process, corrective actions have to be taken.
In order to achieve a successful deployment several parameters have to be taken into account. The most important are vane deployment failure, length profile during inflation and asymmetries in boom length.

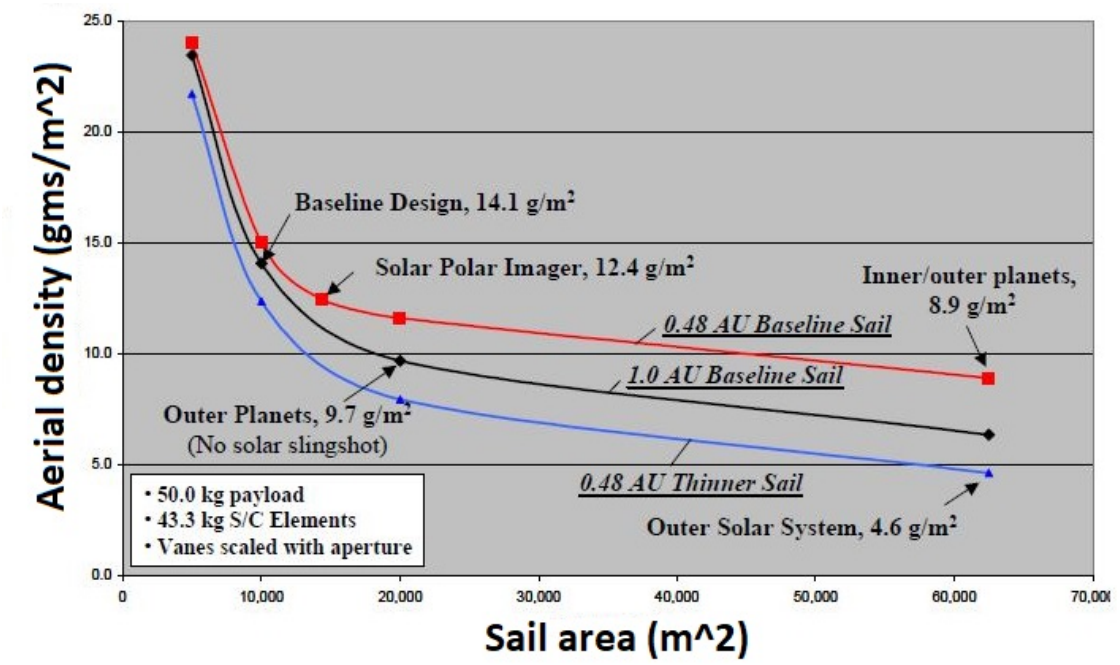

Figure 6.5. Aerial density as function of sail area

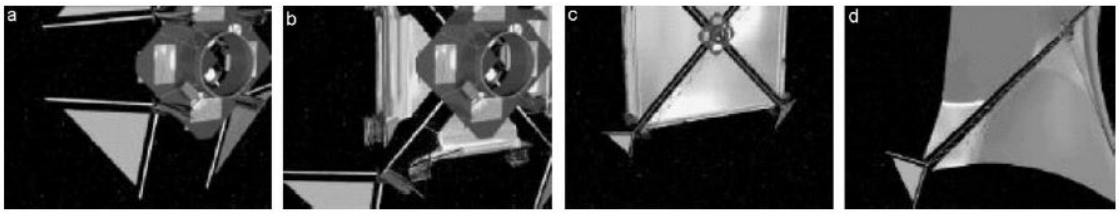

Figure 6.6. Solar sail deployment sequence: a) vane deployment, b)boom deployment, c) partial deployment d) full deployment

The deployment, considering a square sail with inflatable booms, is composed of different steps. Firstly the vane booms are rotated from the stowed position, then the booms are deployed through inflation pressure. In turn, the booms deploy the sails and the spreader. The amount of inflation gas for each boom during inflation process is monitored through a control system: it is important to deploy each boom simmetrically. The control system has to also monitor the length of each boom relative to the length of the other booms. In case one boom is longer than the others, the control system will adjust the problem reducing or stopping the gas inflation rate for that boom. The out-of-plane asymmetries of the booms have to be close to zero.

If asimmetry occurs despite the control system is active, a spin-stabilization

system can be added to the sailcraft in order to increase the stability and safety of deployment. The initial spin (around the axis perpendicular to the sail passing in the center of mass) required to stabilize the sail increases as the asymmetry increases.
Even a little initial spin of 0.01 Hz can stabilize the attitude of the sailcraft, as shown in figure 6.7.

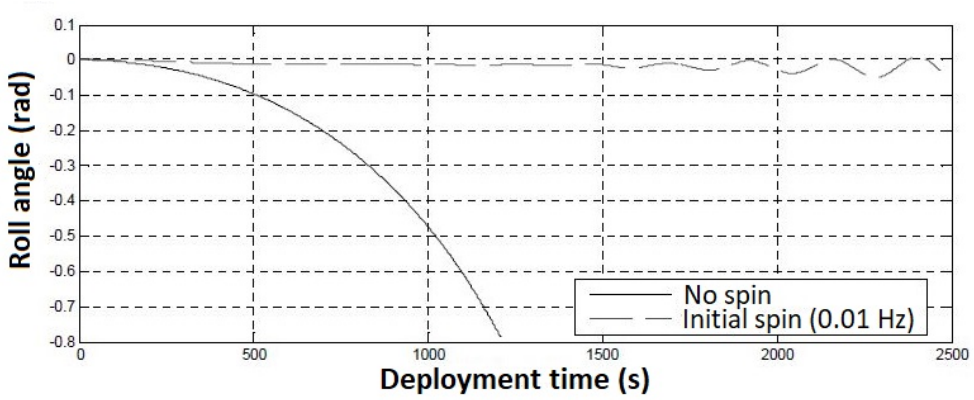

Figure 6.7. Roll angle (attitude) of the sailcraft with a twin asymmetry, with and without initial spin

However, using a spin-stabilization system, not only brings benefit: indeed it can produce dangerous and undesirable moments due to Coriolis forces and body angular momentum that can lead to booms bending failure (figure 6.8).

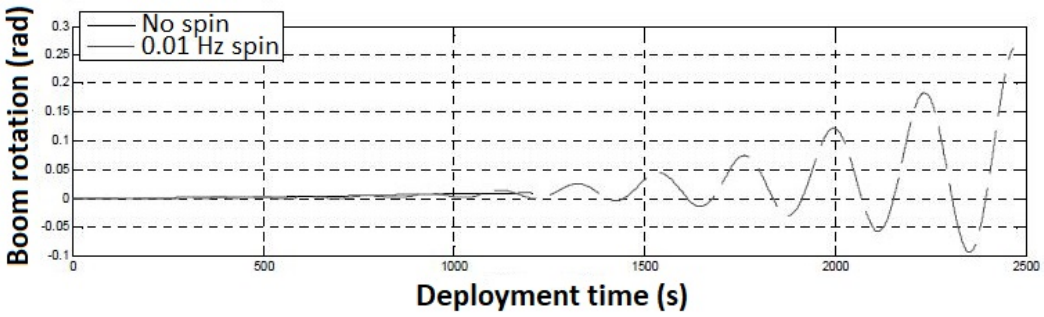

Figure 6.8. Boom deflection considering a twin asymmetry, with and without initial spin

Further analysis have to be done in order to study and solve the negative effects of spin-stabilization [70] [76].

6.4 Thermal loads

Thermal effects due to solar pressure loads have to be studied. Indeed, on orbit attitude control maneuvers can cause a non-uniform thermal distribution on the sail that can produce undesired strains and, consequently, asymmetries. Thrust and torque performances result to be varied by the effects of thermal distributions: the sail can become unstable. Thermal effects of on orbit maneuvers bringing the inflatable sail to a position off-normal to the sun by as much as 35 degrees have to be considered: for high values of solar incidence, large asymmetries due to thermal strains will occur.
A coupled thermal-structure non-linear finite elements analysis has to be done to verify the effects of thermal distribution on the structure and the other way around: sail temperature and solar pressure affect the shape of the sail that affects them in turn. An iterative method between FEM predicted sail shape and temperature distribution is necessary.
Firstly, a thermal radiation model has to be developed. Temperatures for each structural element of the finite element model can be obtained with the following equations:

$$E_{absorbed} = \alpha I \cos\theta$$

$$E_{emitted} = \sigma(\epsilon_f + \epsilon_b)T^4$$

Equaling the energy absorbed and emitted by the sail, the final equilibrium temperature can be obtained:

$$T = [AU \frac{\alpha}{\epsilon_f + \epsilon_b} \frac{1}{\sigma} \cos\theta]^{\frac{1}{4}}$$

where θ is the solar sail structural element incidence with respect to the sun and AU is the distance from the sun.

Once defined the initial temperatures of all the structural elements, thermal loads are calulated and added to the structural loads. In this way, the new sail membrane shape is calculated. If the RMS difference between the initial and new nodal positions is greater than 1% of the initial maximum sail deflection, the model continues to iterate until convergence. Once the iteration converges, the sail performances can be evaluated [6].

6.5 Thermal desorption

An innovative way to produce higher levels of thrust in solar solar sails is thermal desorption (TP): the flat membrane of the solar sail can be coated with heat-sensitive materials that, once heated by solar rays, release atoms at an high speed in order to produce thrust. The acceleration due to thermal desorption will be added to that due to solar radiation pressure. Once the thermal desorption mechanism ends, the solar sail will be accelerated only by solar radiation pressure (SRP).
In order to have better performances, the membrane sail should have an high reflectivity. On the contrary, the coating material should have the highest possible absorptivity.
An inflatable torus-shaped solar sail concept using desorption was recently studied. This particular inflatable solar sail consists of a thin coated reflective membrane kept flat by an inflatable supporting rim-torus. The torus has to carry both the pressure loads due to inflation and the tensile forces due to the stretching of the membrane.

The acceleration due to thermal desorption depends on the initial mass and mass rate of the realeased coating. At the beginning of the desorption the coating mass is M_0. The coating mass varies according to the following equation: $M_c(t) = M_0 - m_0 t$, where $m_0 = -\frac{dM_c(t)}{dt}$ is the rate of desorption. At the end of the desorption $M_c = 0$ (the coating mass is completely released). The force acting on the sail, considering both TP and SRP is:

$$F = \frac{d}{dt}(M(t)v) = (\sigma A + M_t + M_p + M_c)\frac{dv}{dt} + \frac{dM_c}{dt}v$$

where M_t is the mass of the torus (or any other kind of support structure considered), M_p is the mass of the payload, σ is the aerial density and A is the area of the sail membrane.
An alternative way to rewrite the force acting on the sail, considering the Maxwell's electromagnetic theory for solar radiation, is:

$$F = \frac{dM_c}{dt}v_{th} + \frac{k}{r^2}A$$

where $k = \frac{\eta L_s}{2\pi c}$, c is speed of light and L_s is the solar luminosity.
Equaling the two different force expressions, a first-order differential equation for v is obtained. Solving this equation leads to obtain the maximum velocity of the sail:

$$v_{max} = v_p + (v_p - v_{th} + \frac{kA}{r^2 m_0})\frac{M_0}{\sigma A + M_t + M_p}$$

where v_p is the initial sail velocity and v_{th} is the thermal speed of the desorbed atoms that depends on the temperature and the mass of the atoms ($v_{th} = \sqrt{\frac{8k_B T}{\pi m}}$).

The maximum velocity equation is closely related to the ratio between the coating mass M_0 and the mass of the entire sailcraft minus the coating mass. This means that, exploiting the lower masses of an inflatable structure rather than a classical rigid structure, higher velocities can be obtained.

The deflection and vibration of the membrane under accelerations and pressure due to TP and SRP have to be studied. At the beginning of the thermal desorption the pressure acting on the membrane is a combination of solar pressure radiation and desorption pressure:

$$p = \frac{k}{r^2} + \frac{m_0 v_{th}}{A}$$

The maximum deflection results to be:

$$\zeta_{max} = \frac{1}{4q}(\frac{k}{r^2} + \frac{m_0 v_{th}}{A})$$

where q is the in-plane tensile force in the membrane produced by the inflatable pressurized torus.

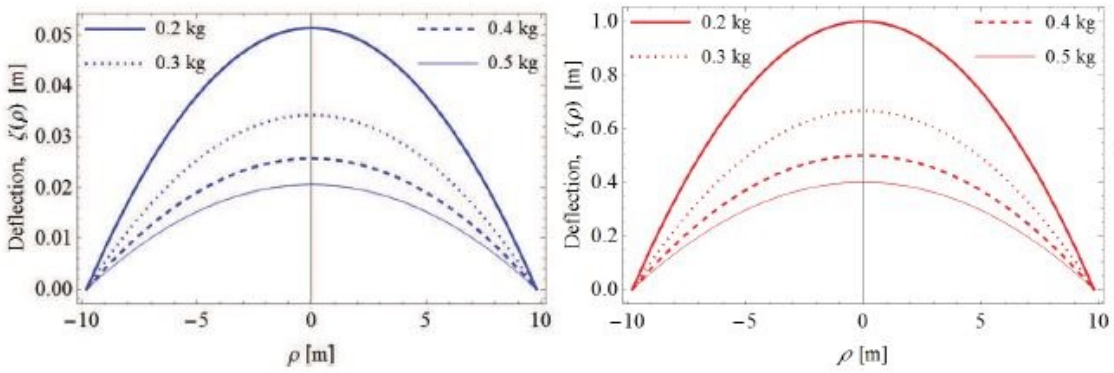

Figure 6.9. Deflection of the membrane due to solar radiation pressure (left) and thermal desorption (right)

At the end of the desorption, the only pressure acting of the membrane is that due to solar rays: the membrane begins to vibrate. The inflatable torus has to be designed to reduce both vibrations and deflection.

The tensile strength applied to the membrane depends on the pressure applied by the internal gas inside the torus. Higher the internal pressure of the torus, higher the tensile strength of the membrane and lower the deflection of the membrane will be. Increasing the mass of the gas (hydrogen), the torus internal pressure will increase and the deflection will decrease.

The deflection due to solar radiation is much less than the deflection due to thermal desorption, as can be seen in the figure above. In both cases the deflection is reduced for higher values of torus internal pressure (higher values of gas mass) [51].

Chapter 7

Packing methods, rigidization techniques and deployment dynamic

Inflatable structures, as described in this thesis work, can be used for a large variety of space applications and show several advantages from the point of view of weights and volumes. Nevertheless, their development has to face the challenges due to packing methods, rigidization techniques and deployment dynamic.

7.1 Packing methods

Primarily, an efficient and reliable packing method is needed in order to ensure a predictable deployment scheme. Two critical aspects have to be considered for the choice of the method: packing efficiency in the launch vehicle and deployment ratio (ratio between unfolded and packed length). Furthermore, each packing method affects the strain energy of the stored and deployed configuration and the deployment dynamics in a different way. The choice of the packing method is based on the role of inflatable structures within the global structure.
The main packing methods for space inflatable cylinder booms will be presented below.

The coil and wrapping packing method involve a flattening of the inflatable boom followed by a coiling or wrapping around a hub, as shown in figure 7.1.

In the coiled configuration the boom is deployed by inflating the gas at the base, while in the wrapped configuration it is deployed by inflating the gas from the hub. The final unrolling velocity is often high for both methods, so a retardation device (often Velcro strips) is added to the system to reduce it. The main drawback for both methods is the possible formation of local buckling and wrinkling in the not

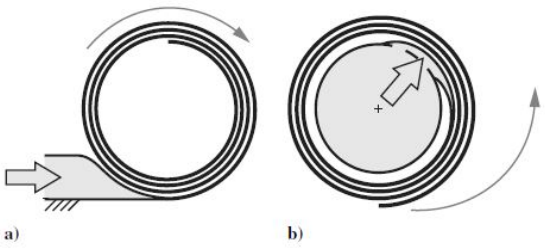

Figure 7.1. a) coiling, b) wrapping packing and deployment methods

deployed configuration. That occurs when the difference between the external and internal coiling/wrapping radius (and for increased diameters) is large. This causes the creation of fold lines that limit the flow of inflation gas, decreasing the chances for a successful deployment. The wrapping configuration is also subject to entanglement during deployment.

The classical z-folding packing method involve the flattening of the inflatable boom followed by a folding scheme at regular spaced intervals. Each interval is delineated by discrete lines or hinges. However, this discrete nature can cause an unpredictable deployment since the inflation air is restricted between sections. Local bending and buckling due to initial folding and deployment make this packing method very hard to develop. A model of non-linear hinges have to be sized properly in order to make the deployment less unstable. A proper value of rotational spring stiffness has to be assigned to each hinge, depending on inflation pressure, fold angle and geometry of the boom.
The classical geometry of z-folding method can be modified in order to reach a more stable deployment: additional folds can be added to improve the inflation pressure and flow rate performances (figure 7.2).

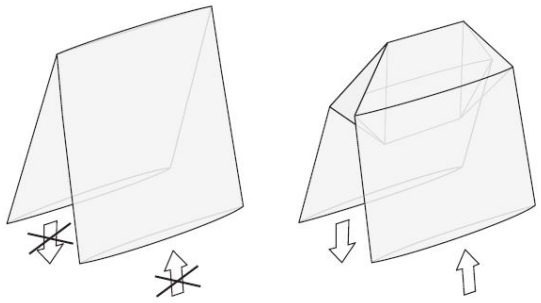

Figure 7.2. Classical (left) and modified (right) z-fold packing method

Despite a more efficient gas flow, the modified z-fold geometry provides a decreased packing efficiency and an increased complexity.

An innovative way to fold inflatable cylindrical booms based on origami patterns is being studied. The origami folding patterns are more intricate than the simple parallel folds of z-folding method. The origami patterns differ according to the number of fold lines that meet a vertex, also called degrees. The greater the number of degrees, the greater the flexibility, but higher are the local strains that can lead to a puncture.

The conical folding method (figure 7.3) introduces a little conicity in order to form a telescopic stowage configuration (concentric packaging). In this way the cross section remains undeformed, contrary to the methods previously described.

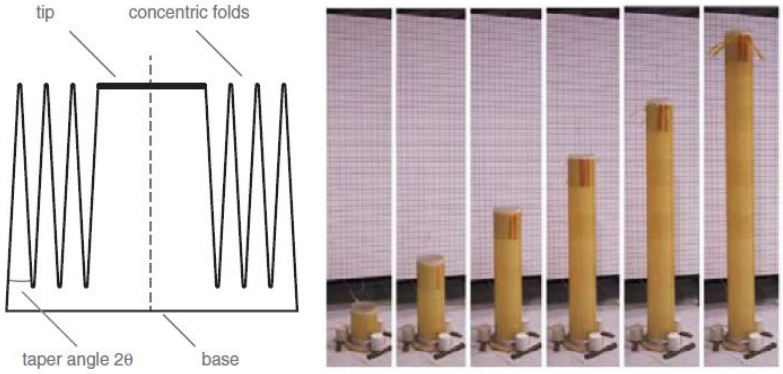

Figure 7.3. Cross sectional view (left) and conical deployment through inflation (right)

The deployment occurs after inflating gas at the base of the conical boom. The inflation pressure pushes the walls towards the outer folds, unfolding them.
A mandrel is used to ensure a straight deployment. The main advantages of this method are high load-carrying capacity, reduced mass (without losses in buckling strength) and stable deployment. The main disadvantage is the presence of friction during deployment that can be solved adopting larger taper [73] [81].

7.2 Rigidization techniques

After the deployment, the inflation gas can leak out of the boom due to manufacturing, folding or deployment imperfections: a method of trapping the gas within the inflatable structure in order to obtain structural rigidity is required.
Generally, the higher the pressure of the gas, the faster the leak. Small structures

are more prone to leaks since they require inflation pressure up to 1 bar. Altough larger structures require low gas pressures, a rigidization method is often required for long-term missions.
The main characteristics that all rigidization techniques should have are: ease of handling and stowage, long storage life, low energy requirement and minimum outgassing. The chosen rigidization technique affects the structural properties of the deployed structure.
Several rigidization techniques are described below.

The UV rigidization consists of impregnating the structure with a resin layer that will be cured through UV radiation (UV setting resins). The UV radiations can come from artificial lamps or solar radiation. The former method has higher accuracy but requires a source of power in order to operate. The latter is a completely passive rigidization method (no power needed), but suffer from lower precision. The main advantages of this technique are low outgassing and long storage life.
The main disadvantage is that the UV radiation doesn't always manage to penetrate all layers of the structure. Some types of fibers used for space applications (such as graphite) or polymers used for the bladder layer don't allow enough UV transmission. Furthermore, the UV rigidization is a irreversible process: this makes ground tests more difficult.

The thermal rigidization consists of impregnating the structure with a resin layer that will be cured through heat (thermosetting resin). The heat can come from the sun (passive rigidization) or from an integrated heating system. In the latter case, the curing process has a very high precision. The advantages of this method are high structure stiffness and strength after rigidization, low outgassing and low thermal expansion coefficients. As opposed to UV rigidization, thermal rigidization is compatible with all the fibers used for space applications. The only drawbacks of this method are heat retention (that can be mitigated using MLI blankets) and the irreversibility of the process (difficulties in handling and ground testing).

The glass transition rigidization method takes advantage of the change of state of some materials (including polymers) that occurs when the temperature drops below the melting point. Polymers are composed of a crystalline and an amorphous part. For temperature values below the glass transition temperature, the crystalline part loses its solid form, while the amorphous part not: the result is a rubbery polymer. Altough less rigid than thermosetting resin, the polymers obtained through glass transition allow a self-rigidization after deployment. Furthermore, the reversibility of the process facilitates ground testing. The polymers have to be heated to avoid unintentional rigidizations during deployment. MLI blankets have to be used in order to shield the structure from solar radiation or other heat sources [73].

The stretched metal laminate rigidization method consists of putting thin layers of ductile metals (in particular aluminum) in layers of polymers (Kapton or Mylar). After the deployment, the increase of internal pressure leads the metal to exceed its yield stress, while the polymer is in its elastic region: a pre-stress condition, where the metal is in compression and the polymer in tension, is formed. The main advantages of this method are low outgassing, long-time storage, process reversibility, high rigidization predictability. The main drawbacks is the reduced load-carrying capacity due to pre-stress conditions: this method can be applied only when the structure has to bear low load conditions [81].

7.3 Deployment dynamic

Numerical simulations are necessary to achieve a successful deployment. Interactions between inflation gas and membrane deformation, wrinkling, self-contact in the membrane and numerical stability are key elements to better understand the deployment mechanism. In this section several examples of deployment simulations are described.

7.3.1 Deployment dynamic of a z-folded tube

A numerical method for the deployment process of a z-folded tube is described below. It takes into account the non-linear deformations of the inflatable membrane caused by inflation gas pressure, but doesn't consider the gas dynamic (slow gas inflation).

Figure 7.4 shows the z-folded tube model. The cylindrical tube is folded in half and is divided into two cells at the fold line. The volume of each cell is in turn divided into sub-cells. The surface of each cell is discretized into finite elements. The inflation occurs from the fixed end of the tube.

The gass flow between two cells can be calculated from the following relation:

$$\frac{1}{2}u^2 = c_p T_i^o - c_p T_j^o + \Delta q$$

where u is the flow velocity, Δq is the applied heat, T_i^o and T_j^o are the initial temperatures of cell i and cell j.
The volume of the flowing gas before and after flowing out the folding line is given by the following equations:

$$\Delta V_i = \frac{\Delta m}{m_i^o} V_i^o$$

$$\Delta V_j = A^o u \Delta t_f$$

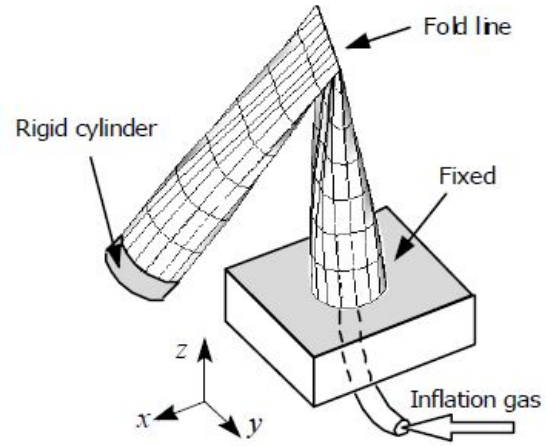

Figure 7.4. Z-folded tube model

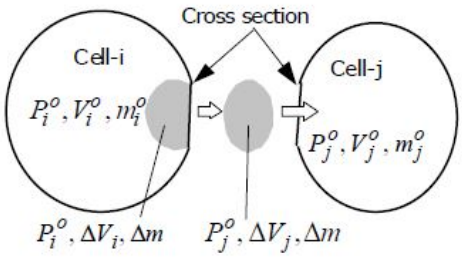

Figure 7.5. Gas flow between two consecutives cells

where Δt_f is the unit time step, A^o is the cross sectional area at the fold. Using the equations written above in conjuction with the thermo-mecanical relation of the gas ($\Delta Q = \Delta H - \bar{V}\Delta P$) and considering the process isothermal, the value of the mass flow can be calculated:

$$\Delta m = A^o \Delta t_f \sqrt{\frac{2m_i^o}{V_i^o} \frac{(P_j^o)^2}{P_i^o} \log \frac{P_i^o}{P_j^o}}$$

Once calculated the mass flow, the cell pressure in the j-cell is recalculated. However, due to deformation of the membrane, the pressure acting on each cell doesn't have a constant value: the pressure is different in each sub-cell. An equivalent value of the cell pressure can be recalculated as follows:

$$P_{cell} = \sum_{k}^{sub-cell} \frac{P_k V_k}{V_{cell}}$$

where P_k and V_k are respectively the pressure and the volume of the k-th sub-cell.
The results obtained through this analytical method are very similar to the results that can be obtained through a micro-gravity experiment (figures 7.6 and 7.7).

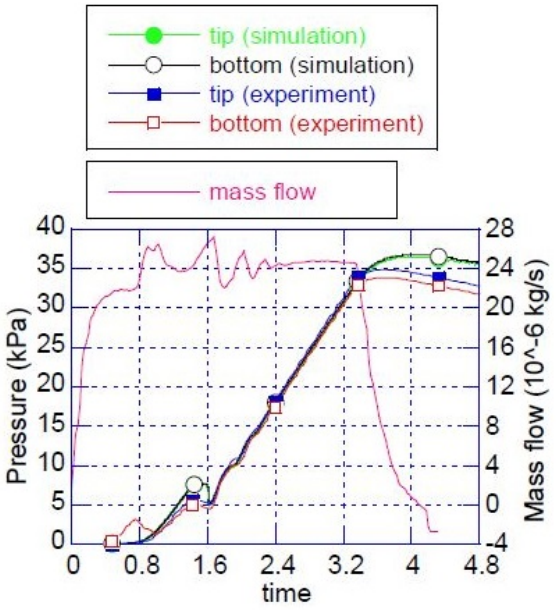

Figure 7.6. Mass flow and gas pressure comparison

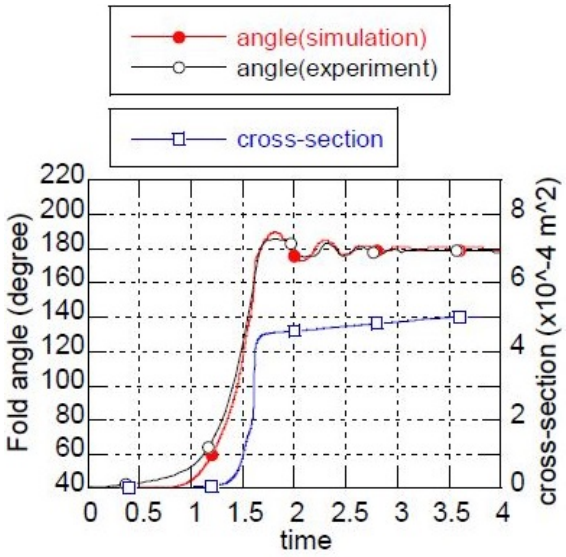

Figure 7.7. Fold angle and cross section comparison

At the beginning of the deployment ($0 < t < 0.9s$), the bottom pressure increases while the top pressure is almost zero: this is due to the folding line that doesn't allow the passage of the gas. Subsequently ($1.5 < t < 1.6s$), the pressure decrease despite the gas flow is constant: this means that the gas is passing through the cross section corresponding to the fold line. About 2 seconds after the start of deployment, the cross section is fully expanded [69].

A parametrical analysis can be performed in order to see the effects of the inflation rate on the deployment process. Slow, medium and fast inflation flow is considered (respectively $0.01lb/s$, $0.1lb/s$ and $1lb/s$).
Adopting a slow inflation rate, the last folded section of the z-folding will not inflate at an early time and, once inflated, it sees a sudden increase in volume and so in pressure. A large amount of inflation gas and an high value of inflation pressure is required in order to fully deploy the structure under slow inflation rates.
A fast inflation rate provides a faster deployment ($0.085s$ versus $1.38s$ of the slow rate inflation) and shows no inflation problems as the slow inflation rate deployment, however the final pressure difference between the control volumes is large.
The medium inflation rate seems to be the best compromise since it shows a good deployment time ($0.19s$), an homogeneous pressure distribution and smaller mass inflation demand [94].

7.3.2 Deployment of a rolled tube

The deployment process of a composite aluminum laminate rolled boom controlled by Velcro strips, taking into account the formation of wrinkles and the interaction between the inflation gas and the membrane structure, is described in this section. The great advantage of using Velcro strips is that the force imposed at the end of the deployment process is zero (rolling brake).

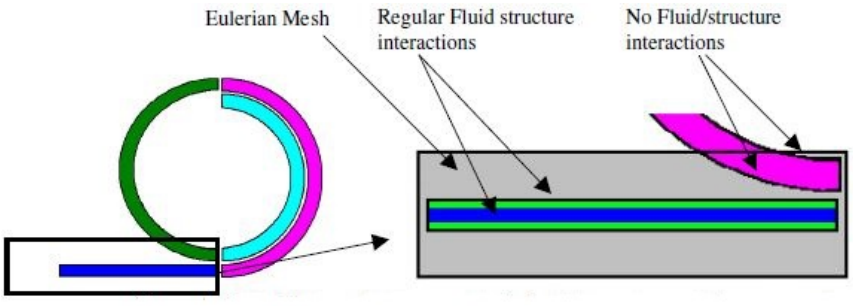

Figure 7.8. Eulerian-Lagrangian interation with multiple gas chamber

A finite element model of the rolled boom can be developed in order to simulate the deployment dynamics. The solid part of the structure (the boom) is described

with a Langrangian model, while the gas can be described with a Eulerian model. The inflatable boom is modeled with four different chamber in order to avoid that the Eulerian mesh interacts with the uninflated sections of the boom.
Each gas chamber has its own mesh so that the mesh of a lower layer doesn't affect an upper layer (figure 7.8). The Velcro strips can be modeled as breakable joints.

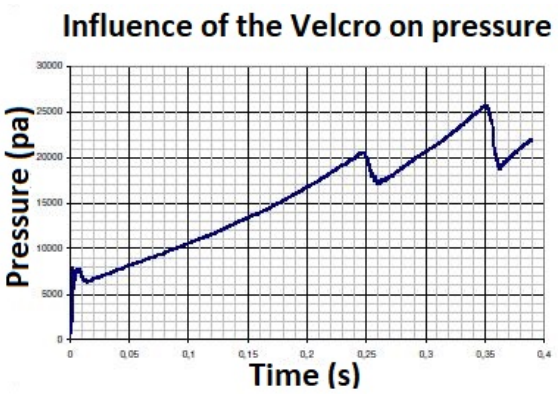

Figure 7.9. Pressure as functions of deployment time

The results of the model shows that the deployment of the boom isn't constant. Indeed, altough the gas is inflated at a constant rate, the gas pressure doesn't increase constantly since the gas meets a resistance until the velcro strip is broken. When the pressure in the chamber is high enough, the force generated by the contact between the almost unfolded part and the rolled part exceeds the yield stress of the Velcro strip, which is then broken. When the Velcro strips is broken, a part of the boom unrolls and the pressure instantly falls (figure 7.9).

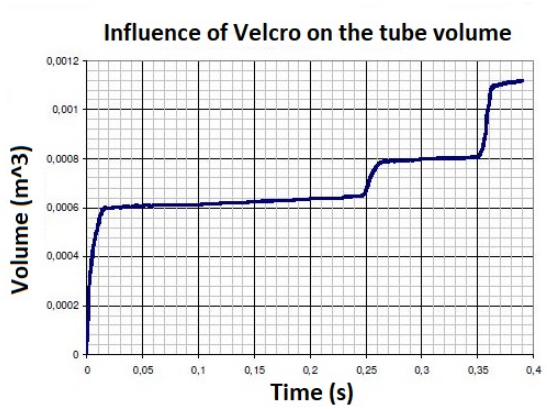

Figure 7.10. Volume as function of deployment time

Also the inflation volume, as the pressure, results to be non linear due to the

presence of Velcro strips (figure 7.10).

The deployment process results to be non-linear, with alternating unrolling and re-inflation phases. Nevertheless, the results of the numerical simulation is quite similar to the results of the experiments done [96] [56].

Chapter 8

Conclusions

Inflatable structures represent a new possibility and a better alternative to rigid space structure. The main advantages are low weights, low costs, high packing efficiency and low system complexity.
Interest in those structures began in the 50s and throughout history several space inflatable configurations has been proposed: from unmanned reflectors, solar arrays, solar sails, re-entry descent technologies, to manned airlock, modules and habitat.
For inflatable applications that require an high surface accuracy (such as reflectors), the harsh space environment (ruled by radiations, large variations in temperature and MMOD impacts) constitutes a great challenge. Indeed, inflatables are more suitable for missions that doesn't involve an high-precision geometry.
As concerns manned configurations, an air pressurization (at least 69 kPa) of the structure is required.
A multi-layered flexible structure is often used to withstand the space environment. It consists of a bladder layer, a restraint layer, a thermal protection layer and a MMOD cover. Each layer is optimized for a particular function. In particular, the bladder is used to retain gas leakage and the restraint to handle internal pressure loads. Most recent developments involve providing intelligence to the structure through adding sensors and self-healing materials in order to increase system reliability.
The most used materials for inflatables space applications are polymers and high strength fibers such as Kevlar, Vectran and Spectra. Thermal insulation is often reached through MLI blankets. The MMOD shield is often made of multiple Kevlar or Nextel shield sin series.
Bending, buckling and wrinkling behaviour of inflatable structures have to be intensely studied. The structure must have an optimized shape in order to reduce global and concentrated stresses and avoid buckling. Inflation pressure and material thickness have to be chosen properly since they affect the static and modal behaviour of the structure.
Several analytical models and analysis have been developed in order to study the

dynamic behaviour of inflatable thin membranes, however, due to the high non-linearity of the problem, only a few configurations have achieved a high TRL level. Another hard challenge that inflatable structures must face is the unpredictability of the deployment process: the study of gas-membrane deformation interaction, wrinkilng, self-contact and numerical stability are fundamental to better understand the deployment mechanism. Numerical methods, finite elements analysis and laboratory tests have to be done to increase the reliability of the deployment and to make the process less unpredictable.
The predictability of the deployment mechanism is hardly affected by the packing method chosen. Furthermore, the packing method affects the packing efficiency in the launch vehicle. The conical telescopic method seems to be the most promising one. Innovative methods involve the use of origami folding patterns.
For long-lasting missions, a rigidization method is required to ensure an efficient structural performance after the deployment. The sub-Tg resins and the metal laminates methods seems to be the most promising one.

In conclusion, inflatable structures certainly offer countless potential benefits (high packing efficiency, low weights, low costs and low system complexity), however several efforts have to be done in order to increase their technology readiness level, so reducing the risk associated with their use.

Bibliography

[1] NASA Content Administrator, ed. *Project Echo*. Aug. 7, 2017. URL: https://www.nasa.gov/centers/langley/about/project-echo.html.

[2] OM Alifanov, VI Outchvatov, and KM Pichkhadze. "Thermal protection of re-entry vehicles with the usage of inflatable systems". In: *Acta Astronautica* 53.4-10 (2003), pp. 541–546.

[3] E Allouis, Alex Ellery, and CS Welch. "Entry descent and landing systems for small planetary missions: Parametric comparison of parachutes and inflatable systems for the proposed Vanguard Mars mission". In: *Acta Astronautica* 59.8-11 (2006), pp. 911–922.

[4] Alessandra Babuscia et al. "Inflatable antenna for cubesat: Motivation for development and initial trade study". In: *iCubeSat*. MIT. 2012.

[5] Alessandra Babuscia et al. "Inflatable antenna for cubesats: Motivation for development and antenna design". In: *Acta Astronautica* 91 (2013), pp. 322–332.

[6] Jeremy A Banik et al. "Solar sail topology variations due to on-orbit thermal effects". In: *Journal of Spacecraft and Rockets* 44.3 (2007), pp. 558–570.

[7] Robert T Bigelow. *Orbital debris shield*. US Patent 7,309,049. 2007.

[8] Andrew J Brune et al. "Thermal protection system response uncertainty of a hypersonic inflatable aerodynamic decelerator". In: *Journal of Spacecraft and Rockets* 54.1 (2017), pp. 141–154.

[9] EP Buslov et al. "Protection of inflatable modules of orbital stations against impacts of particles of space debris". In: *Acta Astronautica* 163 (2019), pp. 54–61.

[10] David Cadogan and John Lin. "Inflatable solar array technology". In: *37th Aerospace Sciences Meeting and Exhibit*. 1999, p. 1075.

[11] David Cadogan, J Stein, and Mark Grahne. "Inflatable composite habitat structures for lunar and mars exploration". In: *Acta Astronautica* 44.7-12 (1999), pp. 399–406.

[12] David Cadogan et al. "Intelligent flexible materials for deployable space structures (InFlex)". In: *47th AIAA/ASME/ASCE/AHS/ASC Structures, Structural Dynamics, and Materials Conference 14th AIAA/ASME/AHS Adaptive Structures Conference 7th*. 2006, p. 1897.

[13] Anthony Campbell et al. *Advanced inflatable airlock system for EVA*. Tech. rep. SAE Technical Paper, 2002.

[14] Costa Cassapakis and Mitch Thomas. "Inflatable structures technology development overview". In: *Space programs and technologies conference*. 1995, p. 3738.

[15] Aman Chandra, Jekanthan Thangavelautham, and Alessandra Babuscia. "Modular inflatable space structures". In: *2018 IEEE Aerospace Conference*. IEEE. 2018, pp. 1–9.

[16] AB Chmielewski. "Overview of gossamer structures". In: *Progress in Astronautics and Aeronautics*. 191 (2001), pp. 1–33.

[17] AB Chmielewski and CHM Jenkins. "Gossamer spacecraft". In: *WIT Transactions on State-of-the-art in Science and Engineering* 20 (2005).

[18] A Clem, S Smith, and J Main. "A pressurized deployment model for inflatable space structures". In: *41st Structures, Structural Dynamics, and Materials Conference and Exhibit*. 2000, p. 1808.

[19] A Clem, S Smith, and J Main. "Deployment dynamics of an inflatable solar array". In: *40th Structures, Structural Dynamics, and Materials Conference and Exhibit*. 1999, p. 1520.

[20] Michael Coleman and Frank Baginski. "A shape deformation study of large aperture inflatable elastic parabolic antenna reflectors". In: *51st AIAA/ASME/ASCE/AHS/A Structures, Structural Dynamics, and Materials Conference 18th AIAA/ASME/AHS Adaptive Structures Conference 12th*. 2010, p. 2501.

[21] Delin Cui et al. "An overview of dynamics modeling of inflatable solar array". In: *Energy Procedia* 14 (2012), pp. 1967–1972.

[22] Joseph Del Corso et al. "Advanced high-temperature flexible TPS for inflatable aerodynamic decelerators". In: *21st AIAA Aerodynamic Decelerator Systems Technology Conference and Seminar*. 2011, p. 2510.

[23] Joseph A DelCorso et al. "Flexible Thermal Protection System Development for Hypersonic Inflatable Aerodynamic Decelerators". In: (2012).

[24] Billy Derbes. "Case studies in inflatable rigidizable structural concepts for space power". In: *37th Aerospace Sciences Meeting and Exhibit*. 1999, p. 1089.

[25] Travis Deyle. "Inflatable Membrane Solar Concentration Systems for Space-Based Applications". In: *Term Paper, ECE* (2007).

[26] Robert Dillman et al. “Flight performance of the inflatable reentry vehicle experiment 3”. In: (2013).

[27] William R Doggett et al. “Non-Axisymmetric Inflatable Pressure Structure (NAIPS) Concept that Enables Mass Efficient Packageable Pressure Vessels with Openings”. In: *3rd AIAA Spacecraft Structures Conference*. 2016, p. 1475.

[28] The Editors of Encyclopaedia Britannica, ed. *Echo*. August 07, 2019. URL: https://www.britannica.com/topic/Echo-satellite.

[29] Houfei Fang et al. “Design and technologies development for an eight-meter inflatable reflectarray antenna”. In: *47th AIAA/ASME/ASCE/AHS/ASC Structures, Structural Dynamics, and Materials Conference 14th AIAA/ASME/AHS Adaptive Structures Conference 7th*. 2006, p. 2230.

[30] Houfei Fang et al. “In-space deployable reflectarray antenna: Current and future”. In: *49th AIAA/ASME/ASCE/AHS/ASC Structures, Structural Dynamics, and Materials Conference, 16th AIAA/ASME/AHS Adaptive Structures Conference, 10th AIAA Non-Deterministic Approaches Conference, 9th AIAA Gossamer Spacecraft Forum, 4th AIAA Multidisciplinary Design Optimization Specialists Conference*. 2008, p. 2209.

[31] Houfei Fang et al. “Thermal distortion analyses of a three-meter inflatable reflectarray antenna”. In: *44th AIAA/ASME/ASCE/AHS/ASC Structures, Structural Dynamics, and Materials Conference*. 2003, p. 1650.

[32] RE Freeland and G Bilyeu. “In-step inflatable antenna experiment”. In: *Acta Astronautica* 30 (1993), pp. 29–40.

[33] Robert Frisbee et al. “Inflatable solar sails for low-cost robotic Mars missions”. In: *33rd Joint Propulsion Conference and Exhibit*. 1997, p. 2762.

[34] James Gaspar et al. “Structural test and analysis of a hybrid inflatable antenna”. In: *48th AIAA/ASME/ASCE/AHS/ASC Structures, Structural Dynamics, and Materials Conference*. 2007, p. 1832.

[35] G Greschik, MM Mikulas, and Art Palisoc. “Torus-less inflated membrane reflector with an exact parabolic center”. In: *AIAA journal* 42.12 (2004), pp. 2579–2584.

[36] G Grossman and G Williams. “Inflatable concentrators for solar propulsion and dynamic space power”. In: (1990).

[37] S Haeuplik-Meusburger and K Ozdemir. “Deployable lunar habitation design”. In: *Moon*. Springer, 2012, pp. 469–502.

[38] Jonathan Hinkle et al. “Design development and testing for an expandable lunar habitat”. In: *AIAA SPACE 2008 Conference & Exposition*. 2008, p. 7634.

[39] A Scott Howe et al. “A Dual-Chamber Hybrid Inflatable Suitlock (DCIS) for Planetary Surfaces or Deep Space”. In: *41st International Conference on Environmental Systems*. 2011, p. 5064.

[40] John Huang. “The development of inflatable array antennas”. In: *IEEE Antennas and Propagation Magazine* 43.4 (2001), pp. 44–50.

[41] John Huang et al. “The Development of Large Flat Inflatable Antennna for Deep-Space Communications”. In: *Space 2004 Conference and Exhibit*. 2004, p. 6112.

[42] Stephen Hughes et al. “Inflatable re-entry vehicle experiment (IRVE) design overview”. In: *18th AIAA Aerodynamic Decelerator Systems Technology Conference and Seminar*. 2005, p. 1636.

[43] Eastwood Im et al. “Prospects of large deployable reflector antennas for a new generation of geostationary Doppler weather radar satellites”. In: *AIAA SPACE 2007 Conference & Exposition*. 2007, p. 9917.

[44] John Iovine and William Walker. “Comparison of Analysis to the On-Orbit Thermal Performance of the Bigelow Expandable Activity Module”. In: 47th International Conference on Environmental Systems. 2017.

[45] Alexander M Jablonski and Kelly A Ogden. “Technical requirements for lunar structures”. In: *Journal of Aerospace Engineering* 21.2 (2008), pp. 72–90.

[46] Robert T Kendall and Arthur R Maddox. *The use of inflatable structures for re-entry of orbiting vehicles*. Tech. rep. SAE Technical Paper, 1990.

[47] Kriss Kennedy. “Lessons from TransHAB: An Architect’s Experience”. In: *AIAA Space Architecture Symposium*. 2002, p. 6105.

[48] Kriss J Kennedy. *ISS TransHab: Architecture Description*. Tech. rep. SAE Technical Paper, 1999.

[49] Kriss J Kennedy et al. “Inflatable habitats”. In: *Progress in Astronautics and Aeronautics*. 191 (2001), pp. 527–552.

[50] Scott Kenner. “Long term displacement data of woven fabric webbings under constant load for inflatable structures”. In: *55th AIAA/ASMe/ASCE/AHS/SC Structures, Structural Dynamics, and Materials Conference*. 2014, p. 0352.

[51] Roman Ya Kezerashvili et al. “Inflation deployed torus-shaped solar sail accelerated via thermal desorption of coating”. In: *arXiv preprint arXiv:1908.06761* (2019).

[52] Jan Kozicki and Joanna Kozicka. “Human friendly architectural design for a small Martian base”. In: *Advances in Space Research* 48.12 (2011), pp. 1997–2004.

[53] Larry M Leigh and Michael L Tinker. "Dynamic characterization of an inflatable concentrator for solar thermal propulsion". In: *Journal of spacecraft and rockets* 40.1 (2003), pp. 24–27.

[54] David Lichodziejewski et al. "Development and ground testing of a compactly stowed inflatably deployed solar sail". In: *45th AIAA/ASME/ASCE/AHS/ASC Structures, Structural Dynamics & Materials Conference*. 2004, p. 1507.

[55] David Lichodziejewski et al. "Inflatable rigidizable solar array for small satellites". In: *44th AIAA/ASME/ASCE/AHS/ASC Structures, Structural Dynamics, and Materials Conference*. 2003, p. 1898.

[56] Sébastien Lienard and Yves Lefevre. "Modeling and analysis of the deployment of a rolled inflatable beam using MSC-DYTRAN". In: *46th AIAA/ASME/ASCE/AHS/A Structures, Structural Dynamics and Materials Conference*. 2005, p. 1968.

[57] Michael Lindell et al. "Structural analysis and testing of the Inflatable Reentry Vehicle Experiment (IRVE)". In: *47th AIAA/ASME/ASCE/AHS/ASC Structures, Structural Dynamics, and Materials Conference 14th AIAA/ASME/AHS Adaptive Structures Conference 7th*. 2006, p. 1699.

[58] Doug Litteken and Thomas Jones. "Development of an Inflatable Airlock for Deep Space Exploration". In: *2018 AIAA SPACE and Astronautics Forum and Exposition*. 2018, p. 5247.

[59] Douglas Litteken et al. "Design of a Microgravity Hybrid Inflatable Airlock". In: *2020 IEEE Aerospace Conference*. IEEE. 2020, pp. 1–17.

[60] Douglas A Litteken. "Inflatable technology: using flexible materials to make large structures". In: *Electroactive Polymer Actuators and Devices (EAPAD) XXI*. Vol. 10966. International Society for Optics and Photonics. 2019, p. 1096603.

[61] Fushou Liu and Dongping Jin. "Analytical Investigation of dynamics of inflatable parabolic membrane reflector". In: *Journal of Spacecraft and Rockets* 52.1 (2015), pp. 285–294.

[62] Karen H Lyle and Gregory J Vassilakos. "Modeling of Local BEAM Structure for Evaluation of MMOD Impacts to Support Development of a Health Monitoring System". In: (2015).

[63] Patrick K Malone and Geoffrey T Williams. "Lightweight inflatable solar array". In: *Journal of Propulsion and Power* 12.5 (1996), pp. 866–872.

[64] Troy Mann et al. "Ground testing a 20-meter inflation deployed solar sail". In: *47th AIAA/ASME/ASCE/AHS/ASC Structures, Structural Dynamics, and Materials Conference 14th AIAA/ASME/AHS Adaptive Structures Conference 7th*. 2006, p. 1707.

[65] L Marraffa et al. “Inflatable re-entry technologies: flight demonstration and future prospects”. In: *ESA bulletin* (2000), pp. 78–85.

[66] L. Marraffa et al. “IRDT - Inflatable Re-entry and Descent Technology”. In: 521 (Mar. 2003), p. 19.

[67] L. Marraffa et al. “IRDT - Inflatable Re-entry and Descent Technology”. In: *Hot Structures and Thermal Protection Systems for Space Vehicles*. Ed. by A. Wilson. Vol. 521. ESA Special Publication. Apr. 2003, p. 19.

[68] L Marraffa et al. “IRDT-Inflatable Re-entry and Descent Technology”. In: *Hot Structures and Thermal Protection Systems for Space Vehicles*. Vol. 521. 2003, p. 19.

[69] Yasuyuki Miyazaki and Michiharu Uchiki. “Deployment dynamics of inflatable tube”. In: *43rd AIAA/ASME/ASCE/AHS/ASC Structures, Structural Dynamics, and Materials Conference*, p. 1254.

[70] WG Nathan and IC James. “Deployment modeling of an inflatable solar sail spacecraft”. In: *AIAA* 6336.2006 (2006), pp. 1–15.

[71] PAUL NOWAK, WILLY SADEH, and Jeffrey Janakus. “Inflatable structures for a lunar base habitat”. In: *Aerospace Design Conference*. 1992, p. 1031.

[72] Paul S Nowak, Willy Z Sadeh, and Jeffrey Janakus. “Feasibility study of inflatable structures for a lunar base”. In: *Journal of Spacecraft and Rockets* 31.3 (1994), pp. 453–457.

[73] Arthur L Palisoc, Frederick H Redell, and Geoff Andersen. “Deployment and structural support of space membrane optics system using rigidizable conical booms”. In: *Engineering, Construction, and Operations in Challenging Environments: Earth and Space 2004*. 2004, pp. 946–953.

[74] James Pearson, James Moore, and Houfei Fang. “Large and high precision inflatable membrane reflector”. In: *51st AIAA/ASME/ASCE/AHS/ASC Structures, Structural Dynamics, and Materials Conference 18th AIAA/ASME/AHS Adaptive Structures Conference 12th*. 2010, p. 2500.

[75] Vincent Peypoudat et al. “Development of a 3.2 m-long inflatable and rigidizable solar array breadboard”. In: *Spacecraft Structures, Materials and Mechanical Testing 2005*. Vol. 581. 2005.

[76] Marco B Quadrelli and John West. “Sensitivity studies of the deployment of a square inflatable solar sail with vanes”. In: *Acta Astronautica* 65.7-8 (2009), pp. 1007–1027.

[77] Frederick Redell et al. “Inflatable-rigidizable solar concentrators for space power applications”. In: *46th AIAA/ASME/ASCE/AHS/ASC Structures, Structural Dynamics and Materials Conference*. 2005, p. 1879.

[78] M Roberts. "Inflatable habitation for the lunar base". In: *Lunar Bases and Space Activities of the 21st Century*. 1992, p. 249.

[79] Florian Ruess, J Schaenzlin, and H Benaroya. "Structural design of a lunar habitat". In: *Journal of Aerospace Engineering* 19.3 (2006), pp. 133–157.

[80] Eligar Sadeh et al. "Inflatable habitats for lunar base development". In: *Living in Space* (2009), p. 165.

[81] Mark Schenk et al. "Review of inflatable booms for deployable space structures: packing and rigidization". In: *Journal of Spacecraft and Rockets* 51.3 (2014), pp. 762–778.

[82] Molly M Selig et al. "Creep Burst Testing of a Woven Inflatable Module". In: *2nd AIAA Spacecraft Structures Conference*. 2015, p. 1625.

[83] Khadijah I Shariff. "Inflatable Airlock: Seaming Techniques of Highly Loaded Fabrics". In: *4th AIAA Spacecraft Structures Conference*. 2017, p. 0855.

[84] Kurt Smalley, Michael Tinker, and W Taylor. "Structural modeling of a five-meter thin film inflatable antenna/concentrator with rigidized support struts". In: *19th AIAA Applied Aerodynamics Conference*. 2001, p. 1412.

[85] Brandon P Smith et al. "A historical review of inflatable aerodynamic decelerator technology development". In: *2010 IEEE Aerospace Conference*. IEEE. 2010, pp. 1–18.

[86] S Weaver Smith and J Main. "Modeling the deployment of inflatable space structures". In: *Progress in Astronautics and Aeronautics*. 191 (2001), pp. 203–241.

[87] Yusuke Takahashi and Kazuhiko Yamada. "Aerodynamic heating of inflatable aeroshell in orbital reentry". In: *Acta Astronautica* 152 (2018), pp. 437–448.

[88] Mitchell Thomas and Gordon Veal. *Scaling characteristics of inflatable paraboloid concentrators*. Tech. rep. AIR FORCE RESEARCH LAB WRIGHT-PATTERSON AFB OH PROPULSION DIRECTORATE, 1991.

[89] Gerard Valle and Nathan Wells. "Bigelow Expandable Activity Module (BEAM) ISS Year-One". In: (2017).

[90] Gerard D Valle, Doug Litteken, and Thomas C Jones. "Review of Habitable Softgoods Inflatable Design, Analysis, Testing, and Potential Space Applications". In: *AIAA Scitech 2019 Forum*. 2019, p. 1018.

[91] Gordon Veal and Robert Freeland. "In step inflatable antenna description". In: *Space Programs and Technologies Conference*. 1995, p. 3739.

[92] SL Veldman and CAJR Vermeeren. "Inflatable structures in aerospace engineering-an overview". In: *Spacecraft Structures, Materials and Mechanical Testing*. Vol. 468. 2001, p. 93.

[93] CG Wang, ZM Xia, and HF Tan. "Initial shape design and stability analysis of rib for inflatable deployable reflector". In: *AIAA Journal* 53.2 (2015), pp. 486–492.

[94] John Wang and Arthur Johnson. "Deployment simulation of ultra-lightweight inflatable structures". In: *43rd AIAA/ASME/ASCE/AHS/ASC Structures, Structural Dynamics, and Materials Conference*. 2002, p. 1261.

[95] Rui Wang, Anping Hou, and Yonghong Niu. "The optimal design and analysis of the IRDT system based on two-dimensional ballistic trajectory in atmosphere reentry". In: *20th AIAA International Space Planes and Hypersonic Systems and Technologies Conference*. 2015, p. 3672.

[96] Jian-zheng Wei et al. "Simulation and experiment for inflatable control deployment of rolled booms". In: *51st AIAA/ASME/ASCE/AHS/ASC Structures, Structural Dynamics, and Materials Conference 18th AIAA/ASME/AHS Adaptive Structures Conference 12th*. 2010, p. 2580.

[97] Jianzheng Wei et al. "Numerical Simulation for Deployment Dynamics of Lightweight Inflatable Solar Array". In: *52nd AIAA/ASME/ASCE/AHS/ASC Structures, Structural Dynamics and Materials Conference 19th AIAA/ASME/AHS Adaptive Structures Conference 13t*. 2011, p. 1969.

[98] Detlef Wilde, Matthias Tausche, and Matthias Orth. "Inflatable Re-entry Technoloqies-IRT". In: *54 th International Astronautical Congress*. 2003.

[99] Detlef Wilde et al. "Inflatable re-entry and descent technology (IRDT)-further developments". In: *2nd International Symposium of Atmospheric Re-entry Vehicles and Systems, Arcachon, France*. 2001.

[100] Cliff Willey et al. "Hybrid inflatable dish antenna system for spacecraft". In: *19th AIAA Applied Aerodynamics Conference*. 2001, p. 1258.

[101] Jie Wu et al. "Nonlinear Structural Dynamics of the Inflatable Re-entry Vehicle Experiment (IRVE)". In: *22nd AIAA International Space Planes and Hypersonics Systems and Technologies Conference*. 2018, p. 5204.